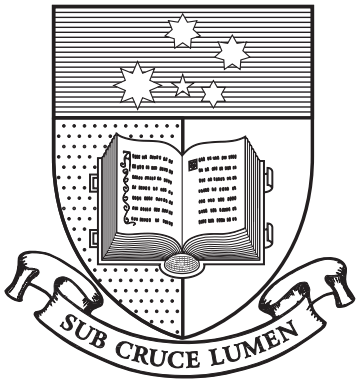

Laplace-Domain Analysis of Fluid Line Networks with Applications to Time-Domain Simulation and System Parameter Identification

by
Aaron C. Zecchin
B.E. (Civil) (Hons), B.Sc.

Thesis submitted to The University of Adelaide
School of Civil, Environmental & Mining
Engineering in fulfilment of the requirements for
the degree of
Doctor of Philosophy

Chapter 6

Parameter Identification of Hydraulic Networks

6.1 Introduction

In addition to design and analysis of real world systems, an important application of theoretical models is the inverse modelling, or parameter identification, of real systems [*Ljung*, 1999]. Inverse modelling aims to map from the system behavioural space (data space) to the system's parameter space, which is the opposite of standard *forward modelling* which maps a system's design to its behavioural responses. Statistically, parameter identification (or inverse modelling) aims to answer the question *what are the most likely parameter values of the system given the observed data?*. In the context of pipeline networks, many authors have proposed answers to this question, particularly in the application of leak detection.

Within this chapter, two novel approaches, based on the Laplace-domain network admittance matrix, are proposed. The first approach involves the derivation of a system relating the measured nodal variables that is decoupled from the unmeasured variables through the use of an oblique filter. This decoupled system is then used as the base model for a maximum likelihood estimation (MLE) parameter identification approach [*Schoukens and Pintelon*, 1991]. The second method is based on the expectation-maximisation (EM) algorithm [*Watanabe and Yamaguchi*, 2004], where the full system dynamics are retained, and the unmeasured states are dealt with in a statistical framework.

This chapter is structured as follows. In Section 6.2, the prominent network parameter identification methodologies are surveyed, with their relative merits and limitations discussed. Section 6.3 presents the model framework for the two proposed parameter identification methods, where the issues of node partitioning and

frequency-domain statistical methods are discussed. In section 6.4, the MLE decoupling method is derived, and discussed with numerical experiments. Section 6.5 derives the EM approach with a discussion and numerical experiments. Conclusions and future directions are discussed in Section 6.6.

6.2 Background

The broad area of interest within this chapter is the *identification of hydraulic networks* based on *fluid state measurements*. There are two key components, first the term *identification of hydraulic networks* generically means the mapping from the data space (measurements of state variables) to a system information space, where, the term information space connotates the inclusion of a broader class of methods that aim to determine different levels of information about the physical characteristics of the system. Second, the emphasis on *fluid state measurements* means that the system identification process is based on measurements of the fluid states of pressure and flow[1]. This distinction is important for the restriction of this literature review as, particularly in the system identification area of leak detection, there exist numerous methods whose diagnostic process is based on other system properties[2].

The different classes of hydraulic network identification methodologies are presented and discussed here. For the sake of continuity, a more detailed discussion of the methodologies with respect to their key differentiating properties is deferred until Appendix C.

The class of the identification methodology refers to the *a priori* assumptions that are made about the hydraulic system, and the nature of the system information space that the data is mapped to. The methods can be classed in the following three classes.

1. *Parameter identification.* The system structure is assumed to be known (*i.e.* the topology of a network's components is completely known), and the information of interest is the actual parameter values of the system's components

[1] Additionally, temperature measurements have been used by some authors (*e.g. Thompson and Skogman* [1983] for applications to multi-product petroleum lines).

[2] The area of leak detection is a huge research area spanning over 70 years, and a detailed treatment is not undertaken here. Examples of methods not addressed within the scope of this chapter are visual inspection methods [*Lee et al.*, 2005a], the use of tracer gases, odorant and radioactive tracers, earth sensitivity changes [*Emara-Shabaik et al.*, 2002], use of robotic pigs [*Furness and Reet*, 1998], use of a correlation methods of acoustic signals in the pipe wall [*Fuchs and Riehle*, 1991; *Tafuri*, 2000], magnetic resonance imaging , and statistical methods based on material age and properties. For an overview and comparison of leak detection methods, the reader is referred to *Cole* [1979]; *Black* [1992]; *Fuchs and Riehle* [1991]; *Furness and Reet* [1998]; *Tafuri* [2000].

(*e.g.* wavespeed, friction factor, leakage rate). For this class, the diagnostic space consists of the parameter space of the model's components, and hence the mapping is simply a parameter estimation process [*Ljung*, 1999].

2. *System detection.* A nominal system structure is assumed (the parameters may or may not be known), and the information of interest is whether the data has arisen from this nominal model. The most common example of this class are fault sensitive filters [*Willsky*, 1976] or fault detection methods [*Venkatasubramanian et al.*, 2003] where the nominal model is the fault free model, and the aim is to detect the point at which a fault occurs within the system.

3. *System detection and identification.* For this case, the system structure is not exactly known but is assumed to be one of a set of candidate system structures, and the information of interest is the most likely of these candidates that the data has arisen from. So not only are some system parameters estimated, but the actual configuration of the system is also identified. A common example of this class are fault model filters [*Willsky*, 1976] or fault detection and identification (FDI) methods [*Venkatasubramanian et al.*, 2003], where the aim is not only to determine when the system is operating in a faulty state, but also the nature of the faults requires determination.

Examples of these methods are outlined below. The emphasis of classes 2 and 3 is not on accurate physical modelling, but on the robust detection of faults amidst parametric, system and measurement uncertainties. The control engineering literature has dealt with methods from classes 2 and 3.

6.2.1 Class 1: Parameter identification

The emphasis within the methods of this class has been on the use of process based models to estimate or calibrate system parameters. Typically, issues associated with system uncertainties are not directly addressed as most methods in this category implicitly assume that the system structure is known, the system is adequately described by the process based mathematical model and the system measurements are not significantly corrupted by noise. The hydraulic and acoustic engineering literature has typically dealt exclusively with methods of this class.

Methods of this class can be divided into two categories, namely, analytic fault signature studies, and numerical parameter estimation. Despite the fact that these methods are often referred to as detection methods, they are not in classes 2 and 3 as no consideration of alternate model structures is undertaken.

Analytic fault signature studies

Analytic fault signature studies deal with systems of a known configuration except for an unknown anomaly, which is either a leak [*Lee et al.*, 2005a], a block [*Wang et al.*, 2005b], a section of pipe wall degradation, or an air pocket [*Stephens*, 2008]. These methods involve a model of the anomalies dynamic behaviour (either analytical [*Lee et al.*, 2005a], statistical [*Isermann*, 1984] or based on a heuristic [*Liou and Tian*, 1995]) and assess the data for the presence of this pattern. Selected methods from the literature are outlined below.

The most basic form of analytic signature matching methods of pipeline systems are the pressure wave reflection methods [*Jönsson and Larson*, 1992; *Silva et al.*, 1996; *Brunone*, 1999; *Covas and Ramos*, 1999; *Brunone and Ferrante*, 2001; *Stephens*, 2008]. These methods directly exploit the phenomena, as noted in *Contractor* [1965], that any minor loss element[3] will reflect a fraction of an incident pressure wave. As an anomaly causes a change in the impedance of a pipe, it partially reflects energy from the incident wave, which is seen in the pressure response as an uncharacteristic change in pressure. For a given step input, leaks and degraded sections cause a negative reflection [*Brunone*, 1999; *Stephens*, 2008], blocks cause a positive reflection, and air pockets cause an oscillatory reflection *Stephens* [2008]. The delay of this reflected wave is determined from the trace, and combined with knowledge of the wavespeed, the location of the reflection's origin can be determined [*Brunone*, 1999]. Under varying assumptions, various authors have derived different expressions from which the reflected wave magnitude is related to the anomaly size [*Jönsson and Larson*, 1992; *Brunone*, 1999; *Covas and Ramos*, 1999]. The limitation of these methods is that they are mainly only applicable to reaches of single lines, as the methods cannot deal with the superposition of multiple higher order reflections resulting from multiple components [*Covas and Ramos*, 1999].

An interesting extension to the single wave reflection methods is the acoustic pulse reflectometry work of *Sharp* [1996]. Based on a discontinuities reflection and transmission coefficients, *Sharp* [1996] determined the impulse response at the end of a tube containing multiple discontinuities. This was applied to the identification of holes in wood wind instruments [*Sharp and Campbell*, 1997], and bore reconstruction [*Sharp*, 1998].

An alternative approach to determining the relationship between a system's behavioural response and anomaly properties has been to analytically solve the system equations with the inclusion of the anomaly dynamics. Based on a trigonometric series solution to the waterhammer equations, *Wang et al.* [2002a] developed a novel

[3] A minor loss element is defined as a localised element within a fluid line model that causes a step change in the pressure or flow.

technique to estimate the parameters of a lumped anomaly. *Wang et al.* [2002a] determined that an anomaly uniquely influenced the damping rate of the trigonometric spatial modes, and that this pattern of influence was dependent on the anomaly size and location. Using a time gating method to determine the damping rate of the modes, this method was applied to single pipelines with leaks [*Wang et al.*, 2002b], blocks [*Wang et al.*, 2005b] and dead end laterals [*Wang et al.*, 2005a]. This work was studied and extended to a 2-D unsteady friction model in *Nixon et al.* [2006].

Considering an acoustic duct, *Wu and Fricke* [1989] demonstrated that the presence of distributed blocks served to shift the eigenfrequencies of the duct. Based on the wave equation, analytic expressions were derived relating the blockage properties to the duct's eigenfrequency shifts. This was extended to ducts with multiple blocks [*Wu and Fricke*, 1990], and ducts with a single measurement point [*Wu*, 1994]. This work was further extended in *De Salis and Oldham* [1999] and *de Salis and Oldham* [2001] to increase the method's noise immunity, which was also applied to ducts with leaks [*de Salis et al.*, 2002]. Considering higher order acoustic wave modes, *Muggleton et al.* [2002] developed a wavenumber based method to determine leak properties in an elastic pipe.

The frequency-domain behaviour of transient hydraulic pipes with anomalies has been extensively studied. Given the convenient analytic framework of the transfer matrix method [*Chaudhry*, 1970], there are different derivations of the anomaly induced patterns in the system's frequency response. Two main philosophies exist in the literature, (i) the anomaly induces an additional resonant frequency, and (ii) the anomaly induces oscillation in the magnitudes of the energies of the fluid line's harmonics.

The existence of an additional resonant frequency for a pipeline with a leak was first hypothesised by *Jönsson and Larson* [1992], who presented limited numerical results confirming this, but their experimental results were inconclusive. This idea was then developed further in a series of papers [*Mpesha et al.*, 2001, 2002] where estimates for the leak properties were derived semi-analytically (*i.e.* heuristic scaling factors were used) based on the frequency and the magnitude of the new leak associated harmonic in the frequency response [4].

[4]Despite the reported success with numerical studies in [*Mpesha et al.*, 2001, 2002], a discussion paper *Lee et al.* [2003b] brought serious doubt as to the validity of these results. Amongst other criticisms by Lee *et al.* (*i.e.* harmonics of frequency response were not located at the theoretically expected locations, violations of the linearity requirement by extreme valve movements, and the improper extraction of the frequency response), in reproducing the frequency response for one of the case studies *Mpesha et al.* [2002], (using a Fourier Transform of the method of characteristics (MOC) time history of pressure and the transfer-matrix method), no additional peaks were noticed. This discrepancy could not be explained by Mpesha *et al.* in their response to *Lee et al.* [2003b]. The assertion of *Lee et al.* [2003b] as to the nonexistence of an additional leak related harmonic was also made clear in a series of papers [*Ferrante et al.*, 2001; *Ferrante and Brunone*, 2003a]. In this

Ferrante et al. [2001] and *Ferrante and Brunone* [2003a] noted that the presence of the leak altered the magnitude of the original harmonics. *Covas et al.* [2002] observed that the leak pattern on the harmonics was oscillatory and that the period of these oscillations was indicative of the leak location. In a series of papers [*Lee et al.*, 2003a, 2004, 2005a], Lee *et al.* developed a frequency-domain estimation method based on the patterned influence of the leak on the magnitude of the harmonics of the frequency response. *Lee et al.* [2005a] showed analytically that the leak induced an inverted sinusoidal pattern in the harmonics, and further that the period and phase of this sinusoid indicated the leak location and the magnitude of this sinusoid indicated the leak magnitude. A similar approach was adopted in *Sattar and Chaudhry* [2008], and *Mohapatra et al.* [2006a,b] applied a similar technique to estimate the parameters of a block for single and branched pipes.

Numerical parameter estimation

Within many applications, system behavioural features cannot be analytically related to system parameters. In such cases, the parameter estimates are defined as those that minimise an adopted error function between the measured data and the model predictions [*Ljung*, 1999], and are generally computed using numerical optimisation routines. Within the hydraulics literature, the parameter identification methods have tended to focus on the estimation of pipe friction parameters and the sizing of leaks. Within this category, many steady state methods exist (*e.g.* weighted least squares methods [*Pudar and Liggett*, 1992; *Datta and Sridharan*, 1994; *Reddy et al.*, 1996; *Greco and Del Giudice*, 1999], Kalman filtering [*Todini*, 1999], systems identification theory [*Andersen and Powell*, 2000], generalised likelihood ratio test methods [*Mukherjee and Narasimhan*, 1996], and Bayesian methods [*Kapelan et al.*, 2007]), but are not covered here as the focus is on transient methods.

The foundational work of *Liggett and Chen* [1994] is widely considered as the first attempt to use transient techniques for leak detection within a generalised network. Within this work, the inverse transient method (ITM) was proposed which, essentially, involved a coupling between a hydraulic MOC network model and the Levenberg-Marquardt minimisation algorithm to iteratively compute the network

rigorous work, based on the frequency-domain representation of the linearised frictionless standard water hammer equations, Ferrante *et al.* showed quite conclusively that for smaller leaks no new leak-related harmonic would appear in the frequency response. They showed that additional peaks would appear for larger leaks where, in effect, a new smaller reservoir-pipe-valve (R-P-V) system is created due to the size of the leak. However, in this instance, the original harmonics would disappear such that the original and leak related harmonics would never co-exist in the frequency response. The explanation for this behaviour was given by the Laplace-domain analysis of *Zecchin et al.* [2006], where the leak size was observed to shift the systems poles along an arc in the complex plane.

parameters that minimise the l_2-norm of the difference between the model predictions and the observed data. Formulated as a leak detection method, *Liggett and Chen* [1994] estimated the leak sizes, assumed to occur at specified nodes, and the pipe roughnesses.

The ITM has been applied by other authors of which the focus has been either: the analytic determination of the error surface gradients for a special network instance (*i.e.* series pipeline) [*Nash and Karney*, 1999]; the implementation of an alternate optimisation engine to drive the inverse calibration (*e.g.* standard and hybrid genetic algorithms [*Vítkovský et al.*, 2000; *Kapelan et al.*, 2003], or shuffled complex evolution [*Vítkovský*, 2001]); the laboratory testing of the method [*Vítkovský*, 2001; *Covas and Ramos*, 2001; *Wang et al.*, 2002a; *Vítkovský et al.*, 2007]; field application of the method [*Stephens*, 2008]; or analysis of practical issues such as identifiability [*Vítkovský et al.*, 2003a] and parameter and model uncertainties [*Vítkovský et al.*, 2007; *Jung and Karney*, 2008].

There has been limited and only moderate success in the application of the ITM to experimental and field networks. *Vítkovský* [2001] identified the main limitation of the method as being the inability of the transient network model to accurately predict the long time[5] behaviour of the system. In addition to the system structural uncertainties, this limitation arises from the unmodelled physical processes within the system (*i.e.* unmodelled fluid dynamic processes such as transient turbulence, and dissolved oxygen, and unmodelled fluid structure interactions such as pipe wall and pipe restraint dynamics). As to be expected, these issues have been observed to be greatly compounded in the field [*Stephens*, 2008]. Additionally, due to the typically large number of parameters involved in networks, it has been found that the ITM tended to attribute the behaviour of a system with only a single leak to that containing a number of leaks [*Liggett and Chen*, 1994].

The development of an ITM based on frequency-domain models, either directly [*Lee et al.*, 2005a] or indirectly [*Kim*, 2007, 2008], has also been studied. *Lee et al.* [2005a] developed an inverse method that utilised on a frequency-domain model to select the set of parameters that yielded the best fit of the model power spectrum to the measured power spectrum. In contrast, *Kim* [2007] used a frequency-domain model as the basis of a time-domain model (by way of impulse response method (IPREM) *Suo and Wylie* [1989]) for which the prediction errors were minimised to produce parameter estimates. Aside from computational benefit in comparison to discrete methods, the major advantage with frequency-domain models is that wavespeed and leak location can be estimated as continuous variables (which is not possible with the discrete methods) and thus eliminating the nonphysical model

[5]Long time being in the order of seconds.

fitting of restricting leaks to occur at network nodes.

With regard to leak detection, an alternative to parameter estimation is state estimation. *Benkherouf and Allidina* [1988] developed a single model approach that assumed multiple leaks at a number of locations, where a Kalman filter was used to estimate the leak quantities at these locations. Using a steady-state assumption, a relationship was derived to determine the properties of an equivalent single leak based on the multiple leak locations and values. In a similar vain to the ITM, *Reddy et al.* [2006] formulated a state estimation method for a gas pipeline network. By adopting the lumped transfer function model from *Kralik et al.* [1984a], the method was based on minimising a constrained least squares problem, for which, under certain observability criteria, an analytic expression for the optimal state measurements was derived. This method was applied to the estimation of unknown nodal demands.

6.2.2 Class 2: System detection

The focus of the detection methods of class 2 is on the reliable and robust detection of faulty hydraulic systems based on measurements of the dynamic fluid behaviour, amidst measurement and system uncertainties. These methods do not attempt to determine the type of fault (*i.e.* block or leak), but rely on detecting the presence of the fault based on deviations from nominal behaviour via some heuristic [*Liou and Tian*, 1995] or statistical [*Isermann*, 1984; *Billmann and Isermann*, 1987; *Wang et al.*, 1993] analysis. Clearly an underlying assumption, fundamental to these methods, is that the nominal behaviour can be well described by a known model with known parameters.

Liou and Tian [1995] presented two algorithms based on assessing the residuals between the measurements and model predictions for *leak discrepancy patterns*. Based on a heuristic reasoning, *Liou and Tian* [1995] formulated a discrepancy measure, as a function of the data, and deduced the onset of a leak based on this measure. Based on the *fault sensitive filter* framework proposed in *Willsky* [1976][6], *Candy and Rosza* [1980] proposed a transient fault detection scheme for a plutonium

[6]Fault sensitive filters [*Willsky*, 1976; *Isermann*, 1984] assess the discrepancy (residuals or innovations) between the measured data and the model describing the nominal faultless system. Given that the model is adequate and calibrated, the innovations between the system measurements and the model's prediction based on past data (typically involving a Kalman filter estimator), should consist entirely of random fluctuations (typically modelled as an uncorrelated, zero mean, and constant variance Gaussian sequence [*Pintelon et al.*, 1994]). In this sense, the model acts as a whitening filter, as it is used to extract the white noise sequence from the raw (correlated and biased) data sequence. The innovation sequence is then subjected to a statistical test to determine its significance, *i.e.* whether it is within the accepted level of random fluctuations or is indicative of a behavioural deviation from the nominal state.

nitrate concentrator.In this method, a simplified model of the process was developed coupled with an extended Kalman filter to estimate the state of the process. The error between the state estimate and the measured data was subjected to hypothesis tests based on Chi-squared and likelihood-ratio statistics to detect significant deviations from the nominal state. *Wang et al.* [1993] formulated an auto-regressive model of a leaking and a non-leaking pipeline. A Kullback information approach was used to determine similarity between models based on the estimated hydraulic grade line slope. When the similarity exceeded certain bounds, a leak was concluded to be present.

6.2.3 Class 3: System detection and identification

The detection and identification methods of class 3 build on the purely detection class 2 methods by not only detecting when the hydraulic system is operating in a faulty operational state, but also identifying the particular faulty operational state that the system is in [*Willsky*, 1976]. To undertake the identification process, these methods typically adopt a multiple model framework using either filters [*Digernes*, 1980; *Emara-Shabaik et al.*, 2002], diagnostic observers [*Verde*, 2001], or residual generators [*Shields et al.*, 2001], each typically associated with a particular model, and implement either thresholding [*Verde*, 2001], or statistical [*Emara-Shabaik et al.*, 2002] methods to determine the most likely operational model in real time. The majority of the methods in this class are leak detection methods where the multiple models consist of a leak-free model, and a bank of models associated with a leak in a specific spatial domain.

Some of the earliest fault detection and identification developments for leak detection within a pipeline was given by *Digernes* [1980]. In this work, *Digernes* [1980] proposed a multiple model framework consisting of a bank of parallel Kalman filters, one for the nominal model, and one for each model corresponding to a leak at a specific spatial location. The innovations sequences from the filters were tested to determine the most likely operating model, where three different statistical tests were used, a windowed Chi-squared, a log-likelihood ratio, and a semi-Markovian test based on estimating the underlying hypothesis probabilities.

A Markovian structure was also adopted by [*Loparo et al.*, 1991] in the development of a multiple model non-linear filtering algorithm applied to leakage detection of a heat exchanger. The identification process involved the estimation of models' conditional probabilities (which involved solving a stochastic differential equation), and a threshold was applied to determine when a specific probability was significant.

Emara-Shabaik et al. [2002] and *Khulief and Emara-Shabaik* [2006] developed

a leak detection and identification method for a single line based on a non-linear multiple-model state estimation scheme. In this approach, the system fluid equations where discretised (using a backward-time/centred-space finite difference scheme) and formulated as a nonlinear state space model. Similar to *Digernes* [1980], modified extended Kalman filters were used to generate model residuals, and a thresholding technique was used to determine the onset of a leak.

Based on the development of a FDI for bilinear systems, *Shields et al.* [2001]; *Ashton and Shields* [1999] developed a method for detecting the onset of restrictions or blockages in petroleum lines. Using a finite-dimensional, nonlinear state-space model, a method was proposed to construct a robust nonlinear fault detection residual generator for each fault location (under certain conditions, proof of the existence of such a generator was also given [*Ashton and Shields*, 1999]). The residuals are tracked on line to determine the onset of the fault.

Motivated by analytic redundancy FDI methods, *Verde* [2001] developed a methodology for the detection and isolation of multiple leaks, at predefined locations within a single pipeline, based on end measurements of pressure and flow. Using the work of *Hou and Muller* [1994], *Verde* [2001] derived a bank of functional observers, each designed to be robust to the influence of a respective leak[7]. The combined diagnosis of the residuals generated by the observers provides a strategy for detecting and isolating multiple leaks. A simplified approach for pipelines with at most two leaks was presented in *Verde* [2004, 2005]. This involved a two stage process that first detected the onset of a leak and then estimated the leak location using two independent residual generators.

Based on a frequency-domain model for a reservoir-pipe-valve system, *Zecchin et al.* [2005] proposed a simple M-ary hypothesis testing method to determine the existence and location of a leak. This method involved the estimation of pipeline parameters for the nominal and faulty models and used the generalised likelihood ratio framework to determine the most likely model.

In contrast to the process based models, *Chen et al.* [2006] proposed a FDI method based on an empirical feature extraction for vibrational modes within a hydraulic motor. The vibrational modes were characterised by wavelet coefficients with which a support vector machines approach was used to detect their presence (or otherwise) within a measured data trace.

In contrast to the multiple model methods, probably one of the simplest leak detection methods in this class are the cross correlation methods of *Isermann* [1984]; *Billmann and Isermann* [1987]. These methods do not use a process based model

[7]That is, an observer is formulated for a subsystem that decouples the influence of a particular leak from that of the other leaks.

of the system, but simply monitor a time averaged correlation function of end flow measurements of a single fluid line. Over a certain time period, end flow measurements would be expected to be reasonably correlated. However, just after the onset of a leak, the upstream flow increases and the downstream flow decreases, thus causing a negative correlation in the flow. Therefore, comparing the correlation to a threshold provides a means by which a leak can be detected.

6.3 Framework for Detection and Identification

The remainder of this chapter focuses on the development of statistically based frequency-domain parameter identification methodologies for general hydraulic networks. In this sense, the proposed methodologies can be classified as numerically based class 1 methods. However, in comparison to the existing methods, the proposed methods distinguish themselves as they possess the advantages of frequency-domain methods (in comparison to discrete based methods), without the limitations that existing frequency-domain methods have to only simple first order looped systems.

Frequency-domain based methods have the advantages that the spatially related parameters (such as leak location and wavespeed) can be represented in a continuous sense, and the computational efficiency of the model makes them well suited for combination with iterative optimisation algorithms that typically are required to compute the parameter estimates. The discrete nature of parameter estimation methods such as the ITM means that they do not possess these advantages. However, the strength that methods such as the ITM have possessed is that they can be applied to a broad class of hydraulic network types, since the majority of frequency-domain methods have been formulated to deal only with R-P-V systems. Based on utilising the general network models from Chapters 3 and 4, the proposed methodologies present a frequency-domain approach to parameter identification that can be applied to hydraulic networks of an arbitrary structure.

The detection and identification problem types presented in Section 6.2 are defined below within the context of the network concepts and notation used within this thesis. Despite the fact that only problems of the class 1 type are considered, the problem types of all three classes are presented with additional preliminary material. Firstly, a new general network type is defined that encompasses both the network structures of Chapters 3 and 4. This facilitates a more general discussion of the detection and identification problems. In Section 6.3.2 the three different class problems are defined with examples. Section 6.3.3 outlines a nodal partitioning framework used in later sections to derive measurement state models

required for parameter identification, and Section 6.3.4 outlines background material for frequency-domain identification.

6.3.1 The $\mathscr{M}$-network and element parameterisation

To more easily deal with the network structures from both Chapters 3 and 4, a general network type is defined here. This network type is termed a $\mathscr{M}$-network, as it is a network of interlinking multinode elements, which are defined below.

Definition 6.1. *A* linear multinode element *is defined as an arbitrary hydraulic element interlinking n nodes with the admittance relationship*

$$\begin{bmatrix} q_1(t) \\ \vdots \\ q_n(t) \end{bmatrix} = \int_0^t \begin{bmatrix} \mathcal{Y}_{11}(t-\tau) & \cdots & \mathcal{Y}_{1n}(t-\tau) \\ \vdots & \ddots & \vdots \\ \mathcal{Y}_{n1}(t-\tau) & \cdots & \mathcal{Y}_{nn}(t-\tau) \end{bmatrix} \begin{bmatrix} p_1(\tau) \\ \vdots \\ p_n(\tau) \end{bmatrix} \mathrm{d}\tau \tag{6.1}$$

where $\mathcal{Y}_{ij}(t)$ are the impulse response functions of the nodal flow at node i from the pressure at node j.

Clearly, both pipelines and compound nodes are special cases of multinode elements. A more detailed discussion and examples of multinode elements are given in Appendix B.2, but are not included here for brevity. Given the definition of a multinode element, a $\mathscr{M}$-network can be defined.

Definition 6.2. *A* multinode element network *($\mathscr{M}$-network) is a network consisting of the pair*

$$(\mathcal{G}(\mathcal{N}, \Xi), \mathcal{M})$$

which is comprised of

1. *the multi-link graph $\mathcal{G}(\mathcal{N}, \Xi)$ ($\mathcal{N}$ is the set of nodes, Ξ is the set of multi-links, each associated with a $\mathscr{M}$-element) combined with*
2. *the set of $\mathscr{M}$-element admittance impulse response functions $\mathcal{M} = \{\boldsymbol{\mathcal{Y}}_\xi : \xi \in \Xi\}$.*

The link end flow properties are related to the nodal flows and pressures by the simple node relations from Definition 3.4.

A more detailed definition along with examples is given in Appendix B.2, but the important point to note is that both a simple node network $(\mathcal{G}(\mathcal{N}, \Lambda), \mathcal{P})$ and a compound node network $(\mathcal{G}(\mathcal{N}, \Lambda), \mathcal{P}, \mathcal{C})$ are both special cases of the $\mathscr{M}$-network.

The $\mathscr{M}$-network $(\mathcal{G}(\mathcal{N}, \Xi), \mathcal{M})$ with component dynamics $\mathcal{M} = \{\boldsymbol{\mathcal{Y}}_\xi : \xi \in \Xi\}$ is parameterised by the set

$$\boldsymbol{\vartheta} = \{\boldsymbol{\vartheta}_\xi : \xi \in \Xi\}$$

where each $\boldsymbol{\vartheta}_\xi$ is the parameter set of the element admittance matrix $\boldsymbol{\mathcal{Y}}_\xi$ (*i.e.* $\boldsymbol{\mathcal{Y}}_\xi(t) = \boldsymbol{\mathcal{Y}}_\xi(\boldsymbol{\vartheta}_\xi, t)$), consisting of the physical parameters such as diameter, length, roughness height, *etc.*, for a pipe, or degree of closure, valve loss coefficient, *etc.*, for a valve. For the problems defined below, some or all of the parameters require identification, but this set is always symbolised by $\boldsymbol{\vartheta}$.

Due to parametric reasons, the set $\boldsymbol{\vartheta}$ is not always the set of physical parameters, as not all the physical parameters are always identifiable (*i.e.* there exists a unique map from the data space to the parameter space). In these cases, a reduced set of identifiable parameters (which are functions of the physical parameters) are adopted for $\boldsymbol{\vartheta}$. This is explained in the following examples for the $\mathscr{L}$approximations of the turbulent-steady-friction (TSF) and turbulent-unsteady-friction (TUF) pipe types.

Example 6.1. *As discussed in Section 2.4, the dynamics for a $\mathscr{L}$-line are completely described by the propagation operator Γ and the characteristic impedance Z_c. For the TSF model from Example 2.4, these functions are given by*[8]

$$\Gamma(s) = \Gamma_o \sqrt{s\,(s + r_o)}, \quad Z_c(s) = Z_{co}\sqrt{\frac{s + r_o}{s}}$$

where

$$\Gamma_o = \frac{l_o}{c_o}, \quad Z_{co} = \rho_o \frac{c_o}{A_o}, \quad r_o = \frac{f_o v_o}{D_o} \tag{6.2}$$

where c_o is the wavespeed, D_o is the diameter, l_o is the length, f_o is the Darcy-Weisbach friction factor, A_o is the cross-sectional area, v_o is the operating point velocity for the linearisation and ρ_o is the fluid density. The functions Γ and Z_c are dependent on five parameters c_o, D_o, l_o, f_o and $v_o \neq 0$ (assuming that the density is known), however they only appear as the three terms (6.2)*. Therefore, the nature of the functions Γ and Z_c is completely described by the values of these three terms. The fact that there is not a unique mapping from these three terms to the five original parameters means that the five parameters cannot be used for the purposes of identification. However, an identifiable parameter set for the TSF pipe is $\boldsymbol{\vartheta} = \{\Gamma_o, Z_{co}, r_o\}$.*

Example 6.2. *For the TUF model from Example 2.7, the propagation operator and characteristic impedance are given by*

$$\Gamma(s) = \Gamma_o \sqrt{s\,(s + r_o)}, \quad Z_c(s) = Z_{co}\sqrt{\frac{s + r_o + r(s)}{s}}$$

[8] With reference to Example 2.4 $\Gamma_o = \sqrt{R_o C_o}$ and $Z_{co} = \sqrt{R_o / C_o}$.

where Γ_o, Z_{co}, and r_o are as defined above, but with f_o as a function of ϵ_o, D_o, $v_o \neq 0$ and the kinematic viscosity ν_o, and r is the unsteady resistive function that is also dependent on ϵ_o, D_o, v_o and ν_o. Given that the density and viscosity are known, Γ and Z_c are dependent on the five parameters c_o, D_o, l_o, ϵ_o and v_o. Unlike the simpler expressions for the TSF pipes, these parameters do not appear in these functions consistently in a reduced number of terms, and hence an identifiable parameter set for the TUF pipes is $\boldsymbol{\vartheta} = \{c_o, D_o, l_o, \epsilon_o, v_o\}$.

Remarks:

1. The organisations of the parameter sets in Examples 6.1 and 6.2 are not unique, for example, the set $\{R_o, C_o, r_o\}$ is also a valid identifiable parameter set for the TSF pipe. In fact, computational studies demonstrated that a better parameterisation for the TUF pipes is

$$\boldsymbol{\vartheta} = \{c_o, D_o, l_o, C_\epsilon, C_{\mathbb{R}_e}\}$$

   where the new parameters C_ϵ and $C_{\mathbb{R}_e}$ are given by

$$C_\epsilon = \log_{10}\left(\frac{\epsilon_o}{D_o}\right), \quad C_{\mathbb{R}_e} = \log_{10}\mathbb{R}_{eo} \tag{6.3}$$

   where $\mathbb{R}_{eo}$ is the steady-state Reynolds number. This parameterisation is valid as there is a unique mapping from this parameterisation to $\{c_o, D_o, l_o, \epsilon_o, v_o\}$.

2. The term identifiability here is used loosely in a deterministic sense to mean that the minimal parameter set that uniquely parameterises the operators Γ and Z_c. The ability to accurately map to a parameter estimate from system behavioural observations is discussed in the examples for Sections 6.4 and 6.5.

6.3.2 Problem definitions

Given the notation of the $\mathscr{M}$-network, the class 1, 2, and 3 problem types discussed in Section 6.2 can now be defined for an arbitrary hydraulic network. The detection and identification problem type (class 3) is defined first, from which the parameter identification problem (class 1) and the model detection problem (class 2) are presented as special cases.

Definition 6.3. *The $\mathscr{M}$-*network detection and identification problem *is defined as identifying the most likely model structure $\{\mathcal{G}(\mathcal{N}, \Xi_{\widehat{\alpha}}), \mathcal{M}_{\widehat{\alpha}}\}$, and associated parameter estimates $\widehat{\boldsymbol{\vartheta}}_{\widehat{\alpha}}$ from the measurements $\left\{\tilde{\boldsymbol{\psi}}_m(t), \tilde{\boldsymbol{\theta}}_m(t) : t \in \mathcal{T}\right\}$ where $\widehat{\alpha} \in$*

$[0, 1, \ldots, N]$ *uniquely identifies a component set such that*

$$\{\Xi_{\widehat{\alpha}}, \mathcal{M}_{\widehat{\alpha}}\} \in \boldsymbol{\Xi} \times \boldsymbol{\mathcal{M}},$$

where $\boldsymbol{\Xi}$ *is a finite set of possible component sets and* $\boldsymbol{\mathcal{M}}$ *is the set of associated dynamic functions, and*

$$\widehat{\boldsymbol{\vartheta}}_{\widehat{\alpha}} \in \boldsymbol{\Upsilon}_{\widehat{\alpha}} \tag{6.4}$$

where $\boldsymbol{\Upsilon}_{\widehat{\alpha}}$ *is the set of component parameters for the* $\widehat{\alpha}$ *model, and the measurements at sample points* $t \in \mathcal{T}$ *are given by*

$$\begin{bmatrix} \tilde{\boldsymbol{\psi}}_m(t) \\ \hdashline \tilde{\boldsymbol{\theta}}_m(t) \end{bmatrix} = \begin{bmatrix} \boldsymbol{\psi}_m(t) \\ \hdashline \boldsymbol{\theta}_m(t) \end{bmatrix} + \begin{bmatrix} \boldsymbol{e}_\psi(t) \\ \hdashline \boldsymbol{e}_\theta(t) \end{bmatrix} \tag{6.5}$$

where $\boldsymbol{\psi}_m$ *and* $\boldsymbol{\theta}_m$ *are the actual values of the measured states and* $\boldsymbol{e}_\psi$ *and* $\boldsymbol{e}_\theta$ *are the error terms. The actual measured states are related to the state vectors* $\boldsymbol{\psi}$ *and* $\boldsymbol{\theta}$ *by*

$$\begin{bmatrix} \boldsymbol{\psi}_m(t) \\ \hdashline \boldsymbol{\theta}_m(t) \end{bmatrix} = \left[\begin{array}{c:c} \boldsymbol{A}_\psi & \boldsymbol{0} \\ \hdashline \boldsymbol{0} & \boldsymbol{A}_\theta \end{array}\right] \begin{bmatrix} \boldsymbol{\psi}(t) \\ \hdashline \boldsymbol{\theta}(t) \end{bmatrix} \tag{6.6}$$

where $\boldsymbol{A}_\psi$ *and* $\boldsymbol{A}_\theta$ *are binary matrices that pick out the relevant measured nodes from the state vectors, which are related by the admittance relationship*

$$\boldsymbol{\theta}(t) = \int_0^t \boldsymbol{\mathcal{Y}}_{\alpha^*}(\boldsymbol{\vartheta}^*_{\alpha^*}, t-\tau)\boldsymbol{\psi}(\tau)\mathrm{d}\tau \tag{6.7}$$

where $\boldsymbol{\mathcal{Y}}_{\alpha^*}(\boldsymbol{\vartheta}^*_{\alpha^*}, \cdot)$ *is the impulse response admittance matrix for the actual unknown* α^* *network* $\mathcal{G}(\mathcal{N}_{\alpha^*}, \Xi_{\alpha^*})$.

Remarks:

1. The term *most likely* is not explicitly defined here, but the definition is given by an adopted statistical diagnostic process, where the form of the process is based on the properties of the measurement errors $\boldsymbol{e}_\psi$, $\boldsymbol{e}_\theta$. Note that a solution to this problem, essentially involves using statistical reasoning to define a map from the measurements $\left\{\widetilde{\boldsymbol{\psi}}_m(t), \widetilde{\boldsymbol{\theta}}_m(t) : t \in \mathcal{T}\right\}$ to the identification and estimation outcome $\left\{\widehat{\alpha}, \widehat{\vartheta}_{\widehat{\alpha}}\right\}$.

2. The problem above says that the configuration of the network $\mathcal{G}(\mathcal{N}, \Xi)$ is known down to the nodal structure $\mathcal{N}$ of the network, but that the form of the component set Ξ is uncertain. The component set is known to be one of a finite number of sets within $\boldsymbol{\Xi}$, which, for convenience, are labelled by the integer $\widehat{\alpha}$. For FDI methods, one set within $\Xi_0 \in \boldsymbol{\Xi}$ corresponds to the

nominal model, and the other sets $\Xi_{\widehat{\alpha}}, \widehat{\alpha} \in [1, \ldots, N]$ correspond to one of N potential fault models, see the example below.

3. Equations (6.5) and (6.7) say that the measurements are assumed to be corrupted measurements from the nodal state variables of the linear system defined by the admittance matrix $\boldsymbol{\mathcal{Y}}_{\widehat{\alpha}}$. For problems where the modelling errors are insignificant, $\boldsymbol{e}_{\psi}$, $\boldsymbol{e}_{\theta}$ correspond to measurement errors only. However, in the case where the true system dynamics are given by the nodal state relationship

$$[\boldsymbol{I} + \boldsymbol{\Delta}](\boldsymbol{\theta}) = [\boldsymbol{\mathcal{Y}} + \boldsymbol{\Delta}\boldsymbol{\mathcal{Y}}](\boldsymbol{\psi})$$

where $\boldsymbol{\Delta}$ and $\boldsymbol{\Delta}\boldsymbol{\mathcal{Y}}$ are dynamic operators that symbolise the unmodelled features in the network dynamics, then the errors also include modelling errors.

The following example demonstrates the form of the multiple models used in the detection and identification problem, and a more comprehensive example, encompassing more aspects of the problem is given later.

Example 6.3. *Consider the case of a FDI problem where it is known that there is one leaking pipe within a network, and the problem is to determine which pipe is leaking. Given the network topology $\mathcal{G}(\mathcal{N}, \Lambda)$, the nominal model is the fault free $\mathscr{L}$-line network $(\mathcal{G}(\mathcal{N}, \Lambda), \mathcal{P})$, and the potential fault models are the $\mathscr{M}$-networks $(\mathcal{G}(\mathcal{N}, \Lambda), \mathcal{P}_{\lambda}), \lambda \in \Lambda$ where $\mathcal{P}_{\lambda}$ is the set of system dynamics but with the normal model for pipe λ replaced by the leaking model, that is*

$$\mathcal{P}_{\lambda} = \mathcal{P} \cup \left\{\widetilde{\mathcal{Y}}_{\lambda}\right\} / \{\mathcal{Y}_{\lambda}\}$$

where $\widetilde{\mathcal{Y}}_{\lambda}$ represents the pipeline dynamics for pipe λ with a leak. Therefore for this problem $\boldsymbol{\Xi} = \{\Lambda\}$ and $\boldsymbol{\mathcal{M}} = \{\mathcal{P}, \mathcal{P}_{\lambda} : \lambda \in \Lambda\}$.

Given the definition of the detection and identification problem, the parameter identification problem can be defined as follows.

Definition 6.4. *The* $\mathscr{M}$-network parameter identification problem *is defined as a special case of definition 6.3 where $\boldsymbol{\Xi}$ and $\boldsymbol{\mathcal{M}}$ are the singletons $\boldsymbol{\Xi} = \{\Xi\}$ and $\boldsymbol{\mathcal{M}} = \{\mathcal{M}\}$.*

Remark: Definition 6.4 essentially states that the framework for $\mathscr{M}$-network detection and identification problem holds for the parameter identification problem, but where the model structure is assumed to be known to be $\mathcal{G}(\mathcal{N}, \Xi)$. That is, as there is no uncertainty concerning the model structure, the solution to the problem in Definition 6.4 is essentially to define the map from the measurements to the

parameter estimate

$$\left\{\widetilde{\boldsymbol{\psi}}_m(t), \widetilde{\boldsymbol{\theta}}_m(t) : t \in \mathcal{T}\right\} \longmapsto \widehat{\boldsymbol{\vartheta}}. \tag{6.8}$$

An example of the elements of the identification problem in Definition 6.4 are given below.

Example 6.4. *Consider the problem of estimating the pipeline parameters of the $\mathscr{L}$-line network $(\mathcal{G}(\mathcal{N}, \Lambda), \mathcal{P})$. Assuming that, for each pipe, only the wavespeed, diameter, and steady-state friction factor require estimation, the parameter space is given by $\Upsilon = \cup_{\lambda_j \in \Lambda} \Upsilon_j$ where Υ_j is the parameter set for pipe j and is given by*

$$\Upsilon_j = [c_{j,min}, c_{j,max}] \times [d_{j,min}, d_{j,max}] \times [f_{j,min}, f_{j,max}]$$

where the intervals correspond to the maximum and minimum values for the wavespeed, diameter, and friction factor respectively. Given that a digital acquisition system is used with sampling period Δt, then the measurement points are $\mathcal{T} = \{0, \Delta t, \ldots, N\Delta t\}$. Assuming that the model error is negligible, the error terms $\boldsymbol{e}_\psi$ and $\boldsymbol{e}_\theta$ are purely measurement errors, which can be described as the independent normal variates

$$\begin{bmatrix} \boldsymbol{e}_\psi(t) \\ \hdashline \boldsymbol{e}_\theta(t) \end{bmatrix} \sim \mathcal{N}\left(\begin{bmatrix} \mathbf{0} \\ \hdashline \mathbf{0} \end{bmatrix}, \begin{bmatrix} \Sigma_\psi & \mathbf{0} \\ \hdashline \mathbf{0} & \Sigma_\theta \end{bmatrix} \right), \quad t \in \mathcal{T}.$$

For completeness, the detection problem is now defined

Definition 6.5. *The $\mathscr{M}$-*network detection problem *is defined as a special case of definition 6.3 where $\widehat{\alpha} \in \{0, 1\}$, $\boldsymbol{\Xi} = \{\Xi_o, \Xi_o^c\}$, $\boldsymbol{\mathcal{M}} = \{\mathcal{M}_o, \mathcal{M}_o^c\}$ and $\boldsymbol{\Upsilon} = \{\boldsymbol{\vartheta}_o, \emptyset\}$ where $\hat{\alpha} = 0$ implies the nominal model $(\mathcal{G}(\mathcal{N}, \Xi), \mathcal{M}_o)$ with parameterisation $\boldsymbol{\vartheta}_o$, and $\hat{\alpha} = 1$ implies not the nominal model.*

Remark: Simply put, the detection problem assesses the likelihood that the data arose from the nominal network $(\mathcal{G}(\mathcal{N}, \Xi_o), \mathcal{M}_o)$ model. This definition is purely conceptual as the sets Ξ_o^c and $\mathcal{M}_o^c$ are countably infinite and the network $(\mathcal{G}(\mathcal{N}, \Xi_o^c), \mathcal{M}_o^c)$ cannot be constructed.

6.3.3 Nodal partitioning and measurement state model

The treatment of the parameter estimation problem from Definition 6.4 is the main focus of this chapter, as it is fundamental to all problem types. This problem can be summarised as the estimation of the parameter set $\boldsymbol{\vartheta}$ from the model defined by

the admittance relationship $\boldsymbol{\mathcal{Y}}$ between the nodal pressures $\boldsymbol{\psi}$ and flows $\boldsymbol{\theta}$

$$\boldsymbol{\theta}(t) = \int_0^t \boldsymbol{\mathcal{Y}}(\boldsymbol{\vartheta}, t-\tau)\boldsymbol{\psi}(\tau)\mathrm{d}\tau \tag{6.9}$$

where the estimation is based on the limited state measurements

$$\begin{bmatrix} \widetilde{\boldsymbol{\psi}}_m(t) \\ \hdashline \widetilde{\boldsymbol{\theta}}_m(t) \end{bmatrix} = \left[\begin{array}{c:c} \boldsymbol{A}_\psi & \mathbf{0} \\ \hdashline \mathbf{0} & \boldsymbol{A}_\theta \end{array}\right] \begin{bmatrix} \boldsymbol{\psi}(t) \\ \hdashline \boldsymbol{\theta}(t) \end{bmatrix} + \begin{bmatrix} \boldsymbol{e}_\psi(t) \\ \hdashline \boldsymbol{e}_\theta(t) \end{bmatrix} \tag{6.10}$$

at time points $t \in \mathcal{T}$. From this summary, it is clear that Definition 6.4 represents an errors in variables problem [*Pintelon et al.*, 1994; *Ljung*, 1999] as there exists no distinction between the input and output variables as all the measurements are assumed to be corrupted by errors. A natural approach to the treatment of this problem is to combine the measurements with the model structure to formulate an error function between the predicted and observed variables, for which the parameter estimates are the minimisers [*Pintelon et al.*, 1994]. However, the complications are immediate, namely as

1. the model (6.9) relates the actual error free states $\boldsymbol{\psi}$ and $\boldsymbol{\theta}$, but only the corrupted states $\widetilde{\boldsymbol{\psi}}_m$ and $\widetilde{\boldsymbol{\theta}}_m$ are known, and
2. the model (6.9) relates the entire states $\boldsymbol{\psi}$ and $\boldsymbol{\theta}$, however only a limited number of these states $\boldsymbol{\psi}_m$ and $\boldsymbol{\theta}_m$ are measured.

The first point is treated in later in the chapter in the context of frequency-domain estimation, and the second point is discussed here. To expand on this point, as only a limited number of the states are observed, the network model (6.9) cannot be used directly, as it relates the entire state, not just the measured variables. This presents two options, either state estimation methods must be implemented to compensate for the unmeasured states and allow for the model to be used, or a subsystem that is robust to the unmeasured variables must be derived. Techniques addressing these issues are developed in Sections 6.4 and 6.5, but a framework for the manipulation of the state model (6.9) required for these sections, based on a nodal partitioning, is presented below.

To enable the development of a usable model for the measured variables from the complete model (6.9), it is useful to categorise the nodes of $\mathcal{N}$ into disjoint node sets depending on whether the nodal variables are known, measured or unknown. This leads to the following definition.

Definition 6.6. *For a given $\mathscr{M}$-network $(\mathcal{G}(\mathcal{N}, \Xi), \mathcal{M})$, a* network nodal partitioning *is defined as a partitioning of the nodal set $\mathcal{N}$ into three disjoint subsets*

Table 6.1: The $\mathscr{M}$-network nodal partitioning and associated state classifications from Definition 6.6

Nodal set	Nodal state classification		
	Known	Measured	Unknown/unmeasured
$\mathcal{A}_1$	-	ψ, θ	-
$\mathcal{A}_2$	-	ψ	θ
$\mathcal{A}_3$	-	θ	ψ
$\mathcal{A}_4$	-	-	ψ, θ
$\mathcal{B}_1$	θ	ψ	–
$\mathcal{B}_2$	θ	-	ψ
$\mathcal{C}_1$	ψ	θ	-
$\mathcal{C}_2$	ψ	-	θ

1. *$\mathcal{A}$, the set of nodes for which neither of the variables of pressure and flow are known,*

2. *$\mathcal{B}$, the set of nodes for which the nodal flow is known, and*

3. *$\mathcal{C}$, the set of nodes for which the nodal pressure is known.*

This partitioning can be further refined by considering combinations for which the nodal states are either measured or unmeasured. This results in the 8 unique sets that are tabulated in Table 6.1. Note that the following relations hold, $\mathcal{A} = \mathcal{A}_1 \cup \mathcal{A}_2 \cup \mathcal{A}_3 \cup \mathcal{A}_4$, $\mathcal{B} = \mathcal{B}_1 \cup \mathcal{B}_2$, and $\mathcal{C} = \mathcal{C}_1 \cup \mathcal{C}_2$.

Remark: These 8 sets do not represent an enumeration of the possible combinations of known, measured, and unknown nodal properties, but rather they represent a complete partitioning covering all realistic combinations for which the nodal variables are simultaneously known and unknown. The only omission is the case of known pressure and known flow, which is an unrealistic case as only one of these variables can be controlled and hence known (*i.e.* at a junction the outflow can be controlled, and hence it is known to be zero, but the pressure must be measured, and at a reservoir, the pressure can be controlled and is known, but the outflow must be measured).

Given the sets in Table 6.1 from Definition 6.6, the network nodal state space can be partitioned as

$$\boldsymbol{\psi}(t) = \begin{bmatrix} \boldsymbol{\psi}_{\mathcal{A}_1}(t) \\ \boldsymbol{\psi}_{\mathcal{A}_2}(t) \\ \boldsymbol{\psi}_{\mathcal{A}_3}(t) \\ \boldsymbol{\psi}_{\mathcal{A}_4}(t) \\ \boldsymbol{\psi}_{\mathcal{B}_1}(t) \\ \boldsymbol{\psi}_{\mathcal{B}_2}(t) \\ \boldsymbol{\psi}_{\mathcal{C}_1}(t) \\ \boldsymbol{\psi}_{\mathcal{C}_2}(t) \end{bmatrix}, \qquad \boldsymbol{\theta}(t) = \begin{bmatrix} \boldsymbol{\theta}_{\mathcal{A}_1}(t) \\ \boldsymbol{\theta}_{\mathcal{A}_2}(t) \\ \boldsymbol{\theta}_{\mathcal{A}_3}(t) \\ \boldsymbol{\theta}_{\mathcal{A}_4}(t) \\ \boldsymbol{\theta}_{\mathcal{B}_1}(t) \\ \boldsymbol{\theta}_{\mathcal{B}_2}(t) \\ \boldsymbol{\theta}_{\mathcal{C}_1}(t) \\ \boldsymbol{\theta}_{\mathcal{C}_2}(t) \end{bmatrix}$$

where, similarly, the network admittance matrix from (6.7) can be partitioned as follows

$$\begin{bmatrix} \boldsymbol{\mathcal{Y}}_{\mathcal{A}_1\mathcal{A}_1}(t) & \boldsymbol{\mathcal{Y}}_{\mathcal{A}_1\mathcal{A}_2}(t) & \boldsymbol{\mathcal{Y}}_{\mathcal{A}_1\mathcal{A}_3}(t) & \boldsymbol{\mathcal{Y}}_{\mathcal{A}_1\mathcal{A}_4}(t) & \boldsymbol{\mathcal{Y}}_{\mathcal{A}_1\mathcal{B}_1}(t) & \boldsymbol{\mathcal{Y}}_{\mathcal{A}_1\mathcal{B}_2}(t) & \boldsymbol{\mathcal{Y}}_{\mathcal{A}_1\mathcal{C}_1}(t) & \boldsymbol{\mathcal{Y}}_{\mathcal{A}_1\mathcal{C}_2}(t) \\ \boldsymbol{\mathcal{Y}}_{\mathcal{A}_2\mathcal{A}_1}(t) & \boldsymbol{\mathcal{Y}}_{\mathcal{A}_2\mathcal{A}_2}(t) & \boldsymbol{\mathcal{Y}}_{\mathcal{A}_2\mathcal{A}_3}(t) & \boldsymbol{\mathcal{Y}}_{\mathcal{A}_2\mathcal{A}_4}(t) & \boldsymbol{\mathcal{Y}}_{\mathcal{A}_2\mathcal{B}_1}(t) & \boldsymbol{\mathcal{Y}}_{\mathcal{A}_2\mathcal{B}_2}(t) & \boldsymbol{\mathcal{Y}}_{\mathcal{A}_2\mathcal{C}_1}(t) & \boldsymbol{\mathcal{Y}}_{\mathcal{A}_2\mathcal{C}_2}(t) \\ \boldsymbol{\mathcal{Y}}_{\mathcal{A}_3\mathcal{A}_1}(t) & \boldsymbol{\mathcal{Y}}_{\mathcal{A}_3\mathcal{A}_2}(t) & \boldsymbol{\mathcal{Y}}_{\mathcal{A}_3\mathcal{A}_3}(t) & \boldsymbol{\mathcal{Y}}_{\mathcal{A}_3\mathcal{A}_4}(t) & \boldsymbol{\mathcal{Y}}_{\mathcal{A}_3\mathcal{B}_1}(t) & \boldsymbol{\mathcal{Y}}_{\mathcal{A}_3\mathcal{B}_2}(t) & \boldsymbol{\mathcal{Y}}_{\mathcal{A}_3\mathcal{C}_1}(t) & \boldsymbol{\mathcal{Y}}_{\mathcal{A}_3\mathcal{C}_2}(t) \\ \boldsymbol{\mathcal{Y}}_{\mathcal{A}_4\mathcal{A}_1}(t) & \boldsymbol{\mathcal{Y}}_{\mathcal{A}_4\mathcal{A}_2}(t) & \boldsymbol{\mathcal{Y}}_{\mathcal{A}_4\mathcal{A}_3}(t) & \boldsymbol{\mathcal{Y}}_{\mathcal{A}_4\mathcal{A}_4}(t) & \boldsymbol{\mathcal{Y}}_{\mathcal{A}_4\mathcal{B}_1}(t) & \boldsymbol{\mathcal{Y}}_{\mathcal{A}_4\mathcal{B}_2}(t) & \boldsymbol{\mathcal{Y}}_{\mathcal{A}_4\mathcal{C}_1}(t) & \boldsymbol{\mathcal{Y}}_{\mathcal{A}_4\mathcal{C}_2}(t) \\ \boldsymbol{\mathcal{Y}}_{\mathcal{B}_1\mathcal{A}_1}(t) & \boldsymbol{\mathcal{Y}}_{\mathcal{B}_1\mathcal{A}_2}(t) & \boldsymbol{\mathcal{Y}}_{\mathcal{B}_1\mathcal{A}_3}(t) & \boldsymbol{\mathcal{Y}}_{\mathcal{B}_1\mathcal{A}_4}(t) & \boldsymbol{\mathcal{Y}}_{\mathcal{B}_1\mathcal{B}_1}(t) & \boldsymbol{\mathcal{Y}}_{\mathcal{B}_1\mathcal{B}_2}(t) & \boldsymbol{\mathcal{Y}}_{\mathcal{B}_1\mathcal{C}_1}(t) & \boldsymbol{\mathcal{Y}}_{\mathcal{B}_1\mathcal{C}_2}(t) \\ \boldsymbol{\mathcal{Y}}_{\mathcal{B}_2\mathcal{A}_1}(t) & \boldsymbol{\mathcal{Y}}_{\mathcal{B}_2\mathcal{A}_2}(t) & \boldsymbol{\mathcal{Y}}_{\mathcal{B}_2\mathcal{A}_3}(t) & \boldsymbol{\mathcal{Y}}_{\mathcal{B}_2\mathcal{A}_4}(t) & \boldsymbol{\mathcal{Y}}_{\mathcal{B}_2\mathcal{B}_1}(t) & \boldsymbol{\mathcal{Y}}_{\mathcal{B}_2\mathcal{B}_2}(t) & \boldsymbol{\mathcal{Y}}_{\mathcal{B}_2\mathcal{C}_1}(t) & \boldsymbol{\mathcal{Y}}_{\mathcal{B}_2\mathcal{C}_2}(t) \\ \boldsymbol{\mathcal{Y}}_{\mathcal{C}_1\mathcal{A}_1}(t) & \boldsymbol{\mathcal{Y}}_{\mathcal{C}_1\mathcal{A}_2}(t) & \boldsymbol{\mathcal{Y}}_{\mathcal{C}_1\mathcal{A}_3}(t) & \boldsymbol{\mathcal{Y}}_{\mathcal{C}_1\mathcal{A}_4}(t) & \boldsymbol{\mathcal{Y}}_{\mathcal{C}_1\mathcal{B}_1}(t) & \boldsymbol{\mathcal{Y}}_{\mathcal{C}_1\mathcal{B}_2}(t) & \boldsymbol{\mathcal{Y}}_{\mathcal{C}_1\mathcal{C}_1}(t) & \boldsymbol{\mathcal{Y}}_{\mathcal{C}_1\mathcal{C}_2}(t) \\ \boldsymbol{\mathcal{Y}}_{\mathcal{C}_2\mathcal{A}_1}(t) & \boldsymbol{\mathcal{Y}}_{\mathcal{C}_2\mathcal{A}_2}(t) & \boldsymbol{\mathcal{Y}}_{\mathcal{C}_2\mathcal{A}_3}(t) & \boldsymbol{\mathcal{Y}}_{\mathcal{C}_2\mathcal{A}_4}(t) & \boldsymbol{\mathcal{Y}}_{\mathcal{C}_2\mathcal{B}_1}(t) & \boldsymbol{\mathcal{Y}}_{\mathcal{C}_2\mathcal{B}_2}(t) & \boldsymbol{\mathcal{Y}}_{\mathcal{C}_2\mathcal{C}_1}(t) & \boldsymbol{\mathcal{Y}}_{\mathcal{C}_2\mathcal{C}_2}(t) \end{bmatrix}$$

where the matrices $\boldsymbol{\mathcal{Y}}_{AB}$ can be interpreted to be the admittance mapping from the nodal pressures from set B to the nodal flows for the nodes in set A. The known, measured and unmeasured variables are

$$\boldsymbol{\psi}_k(t) = \begin{bmatrix} \boldsymbol{\psi}_{\mathcal{C}_1}(t) \\ \boldsymbol{\psi}_{\mathcal{C}_2}(t) \end{bmatrix}, \quad \boldsymbol{\psi}_m(t) = \begin{bmatrix} \boldsymbol{\psi}_{\mathcal{A}_1}(t) \\ \boldsymbol{\psi}_{\mathcal{A}_2}(t) \\ \boldsymbol{\psi}_{\mathcal{B}_1}(t) \end{bmatrix}, \quad \boldsymbol{\psi}_u(t) = \begin{bmatrix} \boldsymbol{\psi}_{\mathcal{A}_3}(t) \\ \boldsymbol{\psi}_{\mathcal{A}_4}(t) \\ \boldsymbol{\psi}_{\mathcal{B}_2}(t) \end{bmatrix} \tag{6.11}$$

for pressure, respectively, and

$$\boldsymbol{\theta}_k(t) = \begin{bmatrix} \boldsymbol{\theta}_{\mathcal{B}_1}(t) \\ \boldsymbol{\theta}_{\mathcal{B}_2}(t) \end{bmatrix}, \quad \boldsymbol{\theta}_m(t) = \begin{bmatrix} \boldsymbol{\theta}_{\mathcal{A}_1}(t) \\ \boldsymbol{\theta}_{\mathcal{A}_3}(t) \\ \boldsymbol{\theta}_{\mathcal{C}_1}(t) \end{bmatrix}, \quad \boldsymbol{\theta}_u(t) = \begin{bmatrix} \boldsymbol{\theta}_{\mathcal{A}_2}(t) \\ \boldsymbol{\theta}_{\mathcal{A}_4}(t) \\ \boldsymbol{\theta}_{\mathcal{C}_2}(t) \end{bmatrix} \tag{6.12}$$

for the nodal flows, respectively. Considering these divisions, the admittance functions can be written as in (6.13), which, by reorganising the block rows, can be more

$$
\begin{aligned}
&\left(\left[\begin{array}{c|c}
\boldsymbol{\mathcal{Y}}_{\mathcal{A}_1\mathcal{C}_1} & \boldsymbol{\mathcal{Y}}_{\mathcal{A}_1\mathcal{C}_2} \\
\boldsymbol{\mathcal{Y}}_{\mathcal{A}_2\mathcal{C}_1} & \boldsymbol{\mathcal{Y}}_{\mathcal{A}_2\mathcal{C}_2} \\
\boldsymbol{\mathcal{Y}}_{\mathcal{A}_3\mathcal{C}_1} & \boldsymbol{\mathcal{Y}}_{\mathcal{A}_3\mathcal{C}_2} \\
\boldsymbol{\mathcal{Y}}_{\mathcal{A}_4\mathcal{C}_1} & \boldsymbol{\mathcal{Y}}_{\mathcal{A}_4\mathcal{C}_2} \\
\boldsymbol{\mathcal{Y}}_{\mathcal{B}_1\mathcal{C}_1} & \boldsymbol{\mathcal{Y}}_{\mathcal{B}_1\mathcal{C}_2} \\
\boldsymbol{\mathcal{Y}}_{\mathcal{B}_2\mathcal{C}_1} & \boldsymbol{\mathcal{Y}}_{\mathcal{B}_2\mathcal{C}_2} \\
\boldsymbol{\mathcal{Y}}_{\mathcal{C}_1\mathcal{C}_1} & \boldsymbol{\mathcal{Y}}_{\mathcal{C}_1\mathcal{C}_2} \\
\boldsymbol{\mathcal{Y}}_{\mathcal{C}_2\mathcal{C}_1} & \boldsymbol{\mathcal{Y}}_{\mathcal{C}_2\mathcal{C}_2}
\end{array}\right] * \left[\begin{array}{c} \boldsymbol{\psi}_{\mathcal{C}_1} \\ \boldsymbol{\psi}_{\mathcal{C}_2} \end{array}\right]\right)(t) \\
&+\left(\left[\begin{array}{c|c|c}
\boldsymbol{\mathcal{Y}}_{\mathcal{A}_1\mathcal{A}_1} & \boldsymbol{\mathcal{Y}}_{\mathcal{A}_1\mathcal{A}_2} & \boldsymbol{\mathcal{Y}}_{\mathcal{A}_1\mathcal{B}_1} \\
\boldsymbol{\mathcal{Y}}_{\mathcal{A}_2\mathcal{A}_1} & \boldsymbol{\mathcal{Y}}_{\mathcal{A}_2\mathcal{A}_2} & \boldsymbol{\mathcal{Y}}_{\mathcal{A}_2\mathcal{B}_1} \\
\boldsymbol{\mathcal{Y}}_{\mathcal{A}_3\mathcal{A}_1} & \boldsymbol{\mathcal{Y}}_{\mathcal{A}_3\mathcal{A}_2} & \boldsymbol{\mathcal{Y}}_{\mathcal{A}_3\mathcal{B}_1} \\
\boldsymbol{\mathcal{Y}}_{\mathcal{A}_4\mathcal{A}_1} & \boldsymbol{\mathcal{Y}}_{\mathcal{A}_4\mathcal{A}_2} & \boldsymbol{\mathcal{Y}}_{\mathcal{A}_4\mathcal{B}_1} \\
\boldsymbol{\mathcal{Y}}_{\mathcal{B}_1\mathcal{A}_1} & \boldsymbol{\mathcal{Y}}_{\mathcal{B}_1\mathcal{A}_2} & \boldsymbol{\mathcal{Y}}_{\mathcal{B}_1\mathcal{B}_1} \\
\boldsymbol{\mathcal{Y}}_{\mathcal{B}_2\mathcal{A}_1} & \boldsymbol{\mathcal{Y}}_{\mathcal{B}_2\mathcal{A}_2} & \boldsymbol{\mathcal{Y}}_{\mathcal{B}_2\mathcal{B}_1} \\
\boldsymbol{\mathcal{Y}}_{\mathcal{C}_1\mathcal{A}_1} & \boldsymbol{\mathcal{Y}}_{\mathcal{C}_1\mathcal{A}_2} & \boldsymbol{\mathcal{Y}}_{\mathcal{C}_1\mathcal{B}_1} \\
\boldsymbol{\mathcal{Y}}_{\mathcal{C}_2\mathcal{A}_1} & \boldsymbol{\mathcal{Y}}_{\mathcal{C}_2\mathcal{A}_2} & \boldsymbol{\mathcal{Y}}_{\mathcal{C}_2\mathcal{B}_1}
\end{array}\right] * \left[\begin{array}{c} \boldsymbol{\psi}_{\mathcal{A}_1} \\ \boldsymbol{\psi}_{\mathcal{A}_2} \\ \boldsymbol{\psi}_{\mathcal{B}_1} \end{array}\right]\right)(t) \\
&+\left(\left[\begin{array}{c|c|c}
\boldsymbol{\mathcal{Y}}_{\mathcal{A}_1\mathcal{A}_3} & \boldsymbol{\mathcal{Y}}_{\mathcal{A}_1\mathcal{A}_4} & \boldsymbol{\mathcal{Y}}_{\mathcal{A}_1\mathcal{B}_2} \\
\boldsymbol{\mathcal{Y}}_{\mathcal{A}_2\mathcal{A}_3} & \boldsymbol{\mathcal{Y}}_{\mathcal{A}_2\mathcal{A}_4} & \boldsymbol{\mathcal{Y}}_{\mathcal{A}_2\mathcal{B}_2} \\
\boldsymbol{\mathcal{Y}}_{\mathcal{A}_3\mathcal{A}_3} & \boldsymbol{\mathcal{Y}}_{\mathcal{A}_3\mathcal{A}_4} & \boldsymbol{\mathcal{Y}}_{\mathcal{A}_3\mathcal{B}_2} \\
\boldsymbol{\mathcal{Y}}_{\mathcal{A}_4\mathcal{A}_3} & \boldsymbol{\mathcal{Y}}_{\mathcal{A}_4\mathcal{A}_4} & \boldsymbol{\mathcal{Y}}_{\mathcal{A}_4\mathcal{B}_2} \\
\boldsymbol{\mathcal{Y}}_{\mathcal{B}_1\mathcal{A}_3} & \boldsymbol{\mathcal{Y}}_{\mathcal{B}_1\mathcal{A}_4} & \boldsymbol{\mathcal{Y}}_{\mathcal{B}_1\mathcal{B}_2} \\
\boldsymbol{\mathcal{Y}}_{\mathcal{B}_2\mathcal{A}_3} & \boldsymbol{\mathcal{Y}}_{\mathcal{B}_2\mathcal{A}_4} & \boldsymbol{\mathcal{Y}}_{\mathcal{B}_2\mathcal{B}_2} \\
\boldsymbol{\mathcal{Y}}_{\mathcal{C}_1\mathcal{A}_3} & \boldsymbol{\mathcal{Y}}_{\mathcal{C}_1\mathcal{A}_4} & \boldsymbol{\mathcal{Y}}_{\mathcal{C}_1\mathcal{B}_2} \\
\boldsymbol{\mathcal{Y}}_{\mathcal{C}_2\mathcal{A}_3} & \boldsymbol{\mathcal{Y}}_{\mathcal{C}_2\mathcal{A}_4} & \boldsymbol{\mathcal{Y}}_{\mathcal{C}_2\mathcal{B}_2}
\end{array}\right] * \left[\begin{array}{c} \boldsymbol{\psi}_{\mathcal{A}_3} \\ \boldsymbol{\psi}_{\mathcal{A}_4} \\ \boldsymbol{\psi}_{\mathcal{B}_2} \end{array}\right]\right)(t) \\
&= \left[\begin{array}{c} \mathbf{0} \\ \mathbf{0} \\ \mathbf{0} \\ \mathbf{0} \\ \boldsymbol{\theta}_{\mathcal{B}_1}(t) \\ \boldsymbol{\theta}_{\mathcal{B}_2}(t) \\ \mathbf{0} \\ \mathbf{0} \end{array}\right] + \left[\begin{array}{c} \boldsymbol{\theta}_{\mathcal{A}_1}(t) \\ \mathbf{0} \\ \boldsymbol{\theta}_{\mathcal{A}_3}(t) \\ \mathbf{0} \\ \mathbf{0} \\ \mathbf{0} \\ \boldsymbol{\theta}_{\mathcal{C}_1}(t) \\ \mathbf{0} \end{array}\right] + \left[\begin{array}{c} \mathbf{0} \\ \boldsymbol{\theta}_{\mathcal{A}_2}(t) \\ \mathbf{0} \\ \boldsymbol{\theta}_{\mathcal{A}_4}(t) \\ \mathbf{0} \\ \mathbf{0} \\ \mathbf{0} \\ \boldsymbol{\theta}_{\mathcal{C}_2}(t) \end{array}\right]
\end{aligned}
\tag{6.13}
$$

compactly expressed as

$$\left(\begin{bmatrix}\boldsymbol{\mathcal{Y}}_{k1}\\ \hdashline \boldsymbol{\mathcal{Y}}_{k2}\\ \hdashline \boldsymbol{\mathcal{Y}}_{k3}\end{bmatrix} * \boldsymbol{\psi}_k\right)(t) + \left(\begin{bmatrix}\boldsymbol{\mathcal{Y}}_{m1}\\ \hdashline \boldsymbol{\mathcal{Y}}_{m2}\\ \hdashline \boldsymbol{\mathcal{Y}}_{m3}\end{bmatrix} * \boldsymbol{\psi}_m\right)(t) + \left(\begin{bmatrix}\boldsymbol{\mathcal{Y}}_{u1}\\ \hdashline \boldsymbol{\mathcal{Y}}_{u2}\\ \hdashline \boldsymbol{\mathcal{Y}}_{u3}\end{bmatrix} * \boldsymbol{\psi}_u\right)(t)$$
$$= \begin{bmatrix}\mathbf{0}\\ \hdashline \boldsymbol{\theta}_k(t)\\ \hdashline \mathbf{0}\end{bmatrix} + \begin{bmatrix}\boldsymbol{\theta}_m(t)\\ \hdashline \mathbf{0}\\ \hdashline \mathbf{0}\end{bmatrix} + \begin{bmatrix}\mathbf{0}\\ \hdashline \mathbf{0}\\ \hdashline \boldsymbol{\theta}_u(t)\end{bmatrix}$$

where the new matrices are interpreted as follows: $\boldsymbol{\mathcal{Y}}_{xy}$ describes the admittance map from the nodal pressures in nodal set $x = k, m, u$ to the nodal flows in the node sets $y = 1, 2, 3$, and are given by

$$\boldsymbol{\mathcal{Y}}_{k1}(t) = \begin{bmatrix}\boldsymbol{\mathcal{Y}}_{\mathcal{A}_1\mathcal{C}_1}(t) & \boldsymbol{\mathcal{Y}}_{\mathcal{A}_1\mathcal{C}_2}(t)\\ \hdashline \boldsymbol{\mathcal{Y}}_{\mathcal{A}_3\mathcal{C}_1}(t) & \boldsymbol{\mathcal{Y}}_{\mathcal{A}_3\mathcal{C}_2}(t)\\ \hdashline \boldsymbol{\mathcal{Y}}_{\mathcal{C}_1\mathcal{C}_1}(t) & \boldsymbol{\mathcal{Y}}_{\mathcal{C}_1\mathcal{C}_2}(t)(t)\end{bmatrix}, \tag{6.14}$$

$$\boldsymbol{\mathcal{Y}}_{k2}(t) = \begin{bmatrix}\boldsymbol{\mathcal{Y}}_{\mathcal{B}_1\mathcal{C}_1}(t) & \boldsymbol{\mathcal{Y}}_{\mathcal{B}_1\mathcal{C}_2}(t)\\ \hdashline \boldsymbol{\mathcal{Y}}_{\mathcal{B}_2\mathcal{C}_1}(t) & \boldsymbol{\mathcal{Y}}_{\mathcal{B}_2\mathcal{C}_2}(t)\end{bmatrix}, \tag{6.15}$$

$$\boldsymbol{\mathcal{Y}}_{k3}(t) = \begin{bmatrix}\boldsymbol{\mathcal{Y}}_{\mathcal{A}_2\mathcal{C}_1}(t) & \boldsymbol{\mathcal{Y}}_{\mathcal{A}_2\mathcal{C}_2}(t)\\ \hdashline \boldsymbol{\mathcal{Y}}_{\mathcal{A}_4\mathcal{C}_1}(t) & \boldsymbol{\mathcal{Y}}_{\mathcal{A}_4\mathcal{C}_2}(t)\\ \hdashline \boldsymbol{\mathcal{Y}}_{\mathcal{C}_2\mathcal{C}_1}(t) & \boldsymbol{\mathcal{Y}}_{\mathcal{C}_2\mathcal{C}_2}(t)\end{bmatrix}, \tag{6.16}$$

for the admittance matrices acting on the known nodal states,

$$\boldsymbol{\mathcal{Y}}_{m1}(t) = \begin{bmatrix}\boldsymbol{\mathcal{Y}}_{\mathcal{A}_1\mathcal{A}_1}(t) & \boldsymbol{\mathcal{Y}}_{\mathcal{A}_1\mathcal{A}_2}(t) & \boldsymbol{\mathcal{Y}}_{\mathcal{A}_1\mathcal{B}_1}(t)\\ \hdashline \boldsymbol{\mathcal{Y}}_{\mathcal{A}_3\mathcal{A}_1}(t) & \boldsymbol{\mathcal{Y}}_{\mathcal{A}_3\mathcal{A}_2}(t) & \boldsymbol{\mathcal{Y}}_{\mathcal{A}_3\mathcal{B}_1}(t)\\ \hdashline \boldsymbol{\mathcal{Y}}_{\mathcal{C}_1\mathcal{A}_1}(t) & \boldsymbol{\mathcal{Y}}_{\mathcal{C}_1\mathcal{A}_2}(t) & \boldsymbol{\mathcal{Y}}_{\mathcal{C}_1\mathcal{B}_1}(t)\end{bmatrix}, \tag{6.17}$$

$$\boldsymbol{\mathcal{Y}}_{m2}(t) = \begin{bmatrix}\boldsymbol{\mathcal{Y}}_{\mathcal{B}_1\mathcal{A}_1}(t) & \boldsymbol{\mathcal{Y}}_{\mathcal{B}_1\mathcal{A}_2}(t) & \boldsymbol{\mathcal{Y}}_{\mathcal{B}_1\mathcal{B}_1}(t)\\ \hdashline \boldsymbol{\mathcal{Y}}_{\mathcal{B}_2\mathcal{A}_1}(t) & \boldsymbol{\mathcal{Y}}_{\mathcal{B}_2\mathcal{A}_2}(t) & \boldsymbol{\mathcal{Y}}_{\mathcal{B}_2\mathcal{B}_1}(t)\end{bmatrix}, \tag{6.18}$$

$$\boldsymbol{\mathcal{Y}}_{m3}(t) = \begin{bmatrix}\boldsymbol{\mathcal{Y}}_{\mathcal{A}_2\mathcal{A}_1}(t) & \boldsymbol{\mathcal{Y}}_{\mathcal{A}_2\mathcal{A}_2}(t) & \boldsymbol{\mathcal{Y}}_{\mathcal{A}_2\mathcal{B}_1}(t)\\ \hdashline \boldsymbol{\mathcal{Y}}_{\mathcal{A}_4\mathcal{A}_1}(t) & \boldsymbol{\mathcal{Y}}_{\mathcal{A}_4\mathcal{A}_2}(t) & \boldsymbol{\mathcal{Y}}_{\mathcal{A}_4\mathcal{B}_1}(t)\\ \hdashline \boldsymbol{\mathcal{Y}}_{\mathcal{C}_2\mathcal{A}_1}(t) & \boldsymbol{\mathcal{Y}}_{\mathcal{C}_2\mathcal{A}_2}(t) & \boldsymbol{\mathcal{Y}}_{\mathcal{C}_2\mathcal{B}_1}(t)\end{bmatrix}, \tag{6.19}$$

for the admittance matrices acting on the measured nodal states, and

$$\boldsymbol{\mathcal{Y}}_{u1}(t) = \left[\begin{array}{c:c:c} \boldsymbol{\mathcal{Y}}_{\mathcal{A}_1\mathcal{A}_3}(t) & \boldsymbol{\mathcal{Y}}_{\mathcal{A}_1\mathcal{A}_4}(t) & \boldsymbol{\mathcal{Y}}_{\mathcal{A}_1\mathcal{B}_2}(t) \\ \hdashline \boldsymbol{\mathcal{Y}}_{\mathcal{A}_3\mathcal{A}_3}(t) & \boldsymbol{\mathcal{Y}}_{\mathcal{A}_3\mathcal{A}_4}(t) & \boldsymbol{\mathcal{Y}}_{\mathcal{A}_3\mathcal{B}_2}(t) \\ \hdashline \boldsymbol{\mathcal{Y}}_{\mathcal{C}_1\mathcal{A}_3}(t) & \boldsymbol{\mathcal{Y}}_{\mathcal{C}_1\mathcal{A}_4}(t) & \boldsymbol{\mathcal{Y}}_{\mathcal{C}_1\mathcal{B}_2}(t) \end{array}\right], \tag{6.20}$$

$$\boldsymbol{\mathcal{Y}}_{u2}(t) = \left[\begin{array}{c:c:c} \boldsymbol{\mathcal{Y}}_{\mathcal{B}_1\mathcal{A}_3}(t) & \boldsymbol{\mathcal{Y}}_{\mathcal{B}_1\mathcal{A}_4}(t) & \boldsymbol{\mathcal{Y}}_{\mathcal{B}_1\mathcal{B}_2}(t) \\ \hdashline \boldsymbol{\mathcal{Y}}_{\mathcal{B}_2\mathcal{A}_3}(t) & \boldsymbol{\mathcal{Y}}_{\mathcal{B}_2\mathcal{A}_4}(t) & \boldsymbol{\mathcal{Y}}_{\mathcal{B}_2\mathcal{B}_2}(t) \end{array}\right], \tag{6.21}$$

$$\boldsymbol{\mathcal{Y}}_{u3}(t) = \left[\begin{array}{c:c:c} \boldsymbol{\mathcal{Y}}_{\mathcal{A}_2\mathcal{A}_3}(t) & \boldsymbol{\mathcal{Y}}_{\mathcal{A}_2\mathcal{A}_4}(t) & \boldsymbol{\mathcal{Y}}_{\mathcal{A}_2\mathcal{B}_2}(t) \\ \hdashline \boldsymbol{\mathcal{Y}}_{\mathcal{A}_4\mathcal{A}_3}(t) & \boldsymbol{\mathcal{Y}}_{\mathcal{A}_4\mathcal{A}_4}(t) & \boldsymbol{\mathcal{Y}}_{\mathcal{A}_4\mathcal{B}_2}(t) \\ \hdashline \boldsymbol{\mathcal{Y}}_{\mathcal{C}_2\mathcal{A}_3}(t) & \boldsymbol{\mathcal{Y}}_{\mathcal{C}_1\mathcal{A}_4}(t) & \boldsymbol{\mathcal{Y}}_{\mathcal{C}_1\mathcal{B}_2}(t) \end{array}\right]. \tag{6.22}$$

for the admittance matrices acting on the unknown and unmeasured nodal states. Without loss of generality it can be assumed that the known variables are zero. This is a reasonable assumption as either the pressure is held constant (in the case of a reservoir) or the flow injection is zero (in the case of a junction) which means that the transient fluctuations in both these cases are zero. All other nodal controls (*e.g.* flow injections or nodal demands) require measurement and are not known exactly. This means that the important terms within the system equation are only the measured and unmeasured variables, that is

$$\left(\left[\begin{array}{c} \boldsymbol{\mathcal{Y}}_{m1} \\ \hdashline \boldsymbol{\mathcal{Y}}_{m2} \\ \hdashline \boldsymbol{\mathcal{Y}}_{m3} \end{array}\right] * \boldsymbol{\psi}_m\right)(t) + \left(\left[\begin{array}{c} \boldsymbol{\mathcal{Y}}_{u1} \\ \hdashline \boldsymbol{\mathcal{Y}}_{u2} \\ \hdashline \boldsymbol{\mathcal{Y}}_{u3} \end{array}\right] * \boldsymbol{\psi}_u\right)(t) = \left[\begin{array}{c} \boldsymbol{\theta}_m(t) \\ \hdashline \mathbf{0} \\ \hdashline \mathbf{0} \end{array}\right] + \left[\begin{array}{c} \mathbf{0} \\ \hdashline \mathbf{0} \\ \hdashline \boldsymbol{\theta}_u(t) \end{array}\right]. \tag{6.23}$$

As discussed above, (6.23) cannot be used directly as it contains the unmeasured variables $\boldsymbol{\psi}_u$ and $\boldsymbol{\theta}_u$. Two different approaches are adopted to tackle this, the first method derives a full rank dynamic system relating the measured variables $\boldsymbol{\psi}_m$ and $\boldsymbol{\theta}_m$ uncoupled from the unmeasured variables. This first case, termed the decoupled MLE method, applies to the case where $\mathcal{A}_4 = \emptyset$ (that is, there are no nodes for which the pressure and flow are unknown[9], see Table 6.1). The second approach is based on the EM algorithm [*Watanabe and Yamaguchi*, 2004], where the unmeasured states are statistically integrated out. This approach is more general in that it can deal

[9]At first this restriction may seem limiting but in most instances either pressure of flow are known. For example, at an an unmeasured junction point, the nodal flow (the flow injected into the network from an external source) is known to be zero. Similarly, at a point of on open pipe outfall, the nodal pressure is known to be the atmospheric pressure. In fact the only common case of an $i \in \mathcal{A}_4$ node is when the network of interest is a subnetwork of a larger network, and i is an unmeasured connection point between the two.

with the case of nonempty $\mathcal{A}_4$.

6.3.4 Frequency-domain identification

The focus of this chapter in on the development of a new frequency-domain parameter identification methodology. The motivation in this application is due to the flexibility and numerical efficiency of the Laplace-domain model as opposed to the time-domain model, but additional known benefits are [*Pintelon et al.*, 1994] (i) easy noise reduction by removing non-excited frequencies, (ii) data reduction from long time series to a small number of frequencies, (iii) convenient statistical properties of the transform's data, and (iv) it is easy to combine data from different experiments. An additional benefit for pipeline identification is that the use of frequency-domain data in combination with persistent inputs provides data that is not effected by the uncontrolled underlying transients that can affect time-domain methods [*Stephens*, 2008][10].

As explained in Chapter 3, the Laplace-transform of dynamic systems serves as the basis for frequency-domain models. The Laplace-transform of (6.23) can be arranged to yield

$$\begin{bmatrix} \boldsymbol{Y}_{m1}(s) \\ \hdashline \boldsymbol{Y}_{m2}(s) \\ \hdashline \boldsymbol{Y}_{m3}(s) \end{bmatrix} \boldsymbol{\Psi}_m(s) + \begin{bmatrix} \boldsymbol{Y}_{u1}(s) \\ \hdashline \boldsymbol{Y}_{u2}(s) \\ \hdashline \boldsymbol{Y}_{u3}(s) \end{bmatrix} \boldsymbol{\Psi}_u(s) = \begin{bmatrix} \boldsymbol{I} \\ \hdashline \boldsymbol{0} \\ \hdashline \boldsymbol{0} \end{bmatrix} \boldsymbol{\Theta}_m(s) + \begin{bmatrix} \boldsymbol{0} \\ \hdashline \boldsymbol{0} \\ \hdashline \boldsymbol{I} \end{bmatrix} \boldsymbol{\Theta}_u(s) \quad (6.24)$$

where the frequency-domain model is obtained by restricting $s = \mathrm{i}\omega, \omega \in \mathbb{R}_+$. Noting the connection with (6.5) that the actual measured states are

$$\begin{bmatrix} \boldsymbol{\Psi}_m(s) \\ \hdashline \boldsymbol{\Theta}_m(s) \end{bmatrix} = \left[\begin{array}{c:c} \boldsymbol{A}_\psi & \boldsymbol{0} \\ \hdashline \boldsymbol{0} & \boldsymbol{A}_\theta \end{array}\right] \begin{bmatrix} \boldsymbol{\Psi}(s) \\ \hdashline \boldsymbol{\Theta}(s) \end{bmatrix}$$

the frequency-domain corrupted measurements are

$$\begin{bmatrix} \widetilde{\boldsymbol{\Psi}}_m(\mathrm{i}\omega) \\ \hdashline \widetilde{\boldsymbol{\Theta}}_m(\mathrm{i}\omega) \end{bmatrix} = \begin{bmatrix} \boldsymbol{\Psi}_m(\mathrm{i}\omega) \\ \hdashline \boldsymbol{\Theta}_m(\mathrm{i}\omega) \end{bmatrix} + \begin{bmatrix} \boldsymbol{e}_\Psi(\mathrm{i}\omega) \\ \hdashline \boldsymbol{e}_\Theta(\mathrm{i}\omega) \end{bmatrix}.$$

In practice, temporal digital acquisition systems are used for transient pipeline measurements, and hence the measurements (6.5) occur at discrete points $t = n\Delta t, n = 0, 1, \ldots$, thus creating a sampled data system [*Franklin et al.*, 1998]. The

[10] Persistent inputs induce a response within a system of effectively constant oscillatory (or statistical) properties [*Ljung*, 1999]. In this instance, if a sufficiently long time series is recorded, any transient excitations (*i.e.* those that are not a part of the persistent input) have a negligible affect on the computed frequency response.

frequencies of interest within hydraulic systems are typically orders of magnitude below the sampling frequency (*e.g.* tens or hundreds of Hertz compared to thousands of Hertz), and so aliasing effects from constructing the frequency-domain data from the time-domain data are negligible [*Franklin et al.*, 1998]. For sampled data systems, the discrete Fourier transform (DFT) of the the time-domain signal is used to estimate the frequency distribution of a measured signal. The following theorem, adapted from *Brillinger* [1974] outlines the connection between temporal stochastic processes and their DFTs.

Theorem 6.1. ***[Brillinger, 1974]:*** *Let $\boldsymbol{x}(t), t = n\Delta t, n \in \mathbb{N}$, be a strictly stationary vector valued series with covariance function $\boldsymbol{\Sigma}(t), t = n\Delta t, n \in \mathbb{N}$. Consider the normalised DFT*

$$\boldsymbol{X}(\omega) = \frac{1}{N} \sum_{n=0}^{N-1} \boldsymbol{x}(n\Delta t) e^{-\mathrm{i}\omega n \Delta t}$$

As $N \to \infty$ it holds that for $j = 1, \ldots, N-1$ the variates $\boldsymbol{X}(\omega_j)$ are asymptotically independent and distributed as

$$\boldsymbol{X}(\omega_j) \sim \mathcal{N}_c \left(\boldsymbol{0}, \frac{1}{N} \boldsymbol{S}(\omega_j) \right)$$

*where $\mathcal{N}_c$ is the complex normal distribution, ω_j are the Fourier frequencies $\omega_j = 2\pi j / N\Delta t$ and $\boldsymbol{S}(\omega_j)$ is the the power spectrum of $\boldsymbol{x}(t), t = n\Delta t, n \in \mathbb{N}$ (*i.e. *DFT of the covariance function $\boldsymbol{\Sigma}(t), t = n\Delta t, n \in \mathbb{N}$).*

Remarks:

1. The advantage of dealing with the frequency-domain data can be seen to be threefold. Firstly, the data at each frequency point $\omega_j, j = 1, \ldots, N-1$ are all independent, thus greatly simplifying the joint distribution of the data. Therefore, the only correlation that exists is between the variate element terms at the same frequencies. Secondly, regardless of the distribution of the time-domain data, the distribution of the frequency-domain data is the convenient zero mean complex normal. Lastly, an increasing number of terms included in the construction of $\boldsymbol{X}$ reduces the variance at a rate of $1/N$.

2. The zero frequency term $\omega_0 = 0$ gives the mean of the stochastic process.

Therefore, given a sufficiently long data sequence $\widetilde{\boldsymbol{\psi}}(t), \widetilde{\boldsymbol{\theta}}(t), t = 0, \Delta t, \ldots, (N-1)\Delta\, t$, and that the error terms $\boldsymbol{e}_\psi(t), \boldsymbol{e}_\theta(t), t = 0, \Delta t, \ldots, (N-1)\Delta t$ are stationary processes with power spectrums $\boldsymbol{S}_\psi(\mathrm{i}\omega)$ and $\boldsymbol{S}_\theta(\mathrm{i}\omega)$, the frequency-domain data at

the Fourier frequencies $\omega_j = 2\pi j/N\Delta t, j = 1, \ldots, (N-1)$ is distributed as

$$\left[\begin{array}{c} \widetilde{\boldsymbol{\Psi}}_m(\mathrm{i}\omega_j) \\ \hdashline \widetilde{\boldsymbol{\Theta}}_m(\mathrm{i}\omega_j) \end{array}\right] \sim \mathcal{N}_c\left(\left[\begin{array}{c} \boldsymbol{\Psi}_m(\mathrm{i}\omega_j) \\ \hdashline \boldsymbol{\Theta}_m(\mathrm{i}\omega_j) \end{array}\right], \frac{1}{N}\left[\begin{array}{c:c} \boldsymbol{S}_\psi(\mathrm{i}\omega_j) & \mathbf{0} \\ \hdashline \mathbf{0} & \boldsymbol{S}_\theta(\mathrm{i}\omega_j) \end{array}\right]\right), \quad j = 1, \ldots, N. \tag{6.25}$$

It is important to note that the distribution mean values in (6.25) (*i.e.* the actual measured state values $\boldsymbol{\Psi}_m$ and $\boldsymbol{\Theta}_m$) are unknown, and hence they serve as additional parameters that also require estimation [*Pintelon et al.*, 1994] in addition to the network parameters $\boldsymbol{\vartheta}$. The power spectra are also unknown, however, in the case that the error is a measurement error arising from imperfections in the data acquisition system, approximations for these can be assigned *a priori*.

6.4 Decoupled System and Maximum Likelihood Estimation

This section concerns the development of a maximum likelihood estimation (MLE) frequency-domain parameter identification methodology based on the construction of a measurement system decoupled from the unmeasured nodal variables. This involves two main steps. Firstly, Section 6.4.1 derives a new decoupled measurement model, where the nature and existence conditions for a system of the form

$$\boldsymbol{G}(\boldsymbol{\vartheta}, s)\left[\begin{array}{c} \boldsymbol{\Psi}_m(s) \\ \hdashline \boldsymbol{\Theta}_m(s) \end{array}\right] = \mathbf{0} \tag{6.26}$$

from (6.24) are determined. The second step in Section 6.4.2 involves the use of this form to determine the MLEs for the network parameters $\boldsymbol{\vartheta}$.

As explained, for practical identification within an $\mathscr{M}$-network, there is no meaningful differentiation between input and output variables and hence (6.26) is the most natural way to express the relationship between the measured state variables. Therefore, rather than the model describing the system in an input/output, the model (6.26) can be interpreted as describing the frequency-dependent vector space that the vector-valued state variable exists in. That is, (6.26) states that the state vector $\boldsymbol{u}(s)$ is orthogonal (in a complex vector inner product sense) to every column of the matrix $\boldsymbol{G}^H(\boldsymbol{\vartheta}, s)$ for every $s \in \mathbb{C}$. Or more compactly

$$\boldsymbol{u}(s) \perp \text{span}\left\{\boldsymbol{G}_1^H(\boldsymbol{\vartheta}, s), \ldots, \boldsymbol{G}_n^H(\boldsymbol{\vartheta}, s)\right\}, \quad s \in \mathbb{C} \tag{6.27}$$

where $\boldsymbol{G}_i$ are the rows of $\boldsymbol{G}$.

6.4.1 Decoupled network measurement model

Collecting the measured and unmeasured variables, (6.24) can be reorganised as

$$\boldsymbol{G}_m(s)\begin{bmatrix}\boldsymbol{\Psi}_m(s)\\ \hdashline \boldsymbol{\Theta}_m(s)\end{bmatrix}+\boldsymbol{G}_u(s)\begin{bmatrix}\boldsymbol{\Psi}_u(s)\\ \hdashline \boldsymbol{\Theta}_u(s)\end{bmatrix}=\mathbf{0} \tag{6.28}$$

where

$$\boldsymbol{G}_m(s)=\left[\begin{array}{c:c}\boldsymbol{Y}_{m1}(s) & -\boldsymbol{I}\\ \hdashline \boldsymbol{Y}_{m2}(s) & \mathbf{0}\\ \hdashline \boldsymbol{Y}_{m3}(s) & \mathbf{0}\end{array}\right] \tag{6.29}$$

and

$$\boldsymbol{G}_u(s)=\left[\begin{array}{c:c}\boldsymbol{Y}_{u1}(s) & \mathbf{0}\\ \hdashline \boldsymbol{Y}_{u2}(s) & \mathbf{0}\\ \hdashline \boldsymbol{Y}_{u3}(s) & -\boldsymbol{I}\end{array}\right]. \tag{6.30}$$

It is seen that a decoupled system for the measured states independent of the unmeasured states relies on the existence of a decoupling filter defined in the following and discussed in the ensuing remarks.

Definition 6.7. *The complex matrix function* $\boldsymbol{L}(s):\mathbb{C}\mapsto\mathbb{C}^{K\times n}$ *is described as a* decoupling filter *for the* $\mathscr{M}$*-network* $(\mathcal{G}(\mathcal{N},\Xi),\mathcal{M})$ *if the following conditions hold*

1. $\boldsymbol{L}(s)\boldsymbol{G}_u(s)=\mathbf{0}$*, for all* $s\in\mathbb{C}_+$
2. $\boldsymbol{L}(s)\boldsymbol{G}_m(s)\neq\mathbf{0}$*, for some* $s\in\mathbb{C}_+$
3. $\boldsymbol{L}(s)$ *is stable*
4. $\operatorname{rank}\boldsymbol{L}(s)\geq K$ *on* $s\in\mathbb{C}_+$

where the nodal partitioning and submatrix notation is as defined in Section 6.3.3.

Remarks:

1. The first property is, essentially, the definition of the filter $\boldsymbol{L}(s)$, which requires that the filter removes all the dynamics of the unmeasured variables (mathematically, the rows of $\boldsymbol{L}(s)$ must lie in the left nullspace of the matrix operator $\boldsymbol{G}_u$ that acts on the unmeasured variables for all $s\in\mathbb{C}_+$).
2. The second property ensures that after the dynamics of the unmeasured variables are removed, there are some residual dynamics (mathematically, the rows

of $\boldsymbol{L}(s)$ cannot lie in the left nullspace of the matrix operator that acts on the measured variables for all $s \in \mathbb{C}_+$). That is, with reference to (6.26)

$$\boldsymbol{G}(s) = \boldsymbol{L}(s)\boldsymbol{G}_m(s). \tag{6.31}$$

3. The requirement of stability is one of practical utility.

4. Finally, property 4 states that $\boldsymbol{L}(s)$ cannot have a diminishing rank on $s \in \mathbb{C}_+$. This ensures that each row of $\boldsymbol{L}(s)$ describes a unique property of the dynamics of the decoupled system, and satisfies a necessary requirement that $\boldsymbol{G}(s)$ is of full row rank on $s \in \mathbb{C}_+$.

This definition is now used to formulate the existence of a system for the measured states, decoupled from the unmeasured states.

Theorem 6.2. *Consider the $\mathscr{M}$-network $(\mathcal{G}(\mathcal{N}, \Xi), \mathcal{M})$ with the nodal partitioning as defined in Section 6.3.3 where $\mathcal{A}_4 = \emptyset$. Given that there exists some strictly passive $\xi \in \Xi_i$ for each $i \in \mathcal{A}_3 \cup \mathcal{B}_2$, then a decoupled system of the form (6.31) exists where $\boldsymbol{L}(s)$ is a decoupling filter (Definition 6.7) and is given by*

$$\boldsymbol{L}(s) = \boldsymbol{U}_O^T - \boldsymbol{U}_O^T \boldsymbol{Y}_u(s) \left[\boldsymbol{U}_I^T \boldsymbol{Y}_u(s)\right]^{-1} \boldsymbol{U}_I^T \tag{6.32}$$

where where $\boldsymbol{U}_O$ and $\boldsymbol{U}_I$ are block identity matrices that pick out the appropriate submatrices from the matrix $\boldsymbol{Y}_u(s)$ and are given by

$$\boldsymbol{U}_O = \left[\begin{array}{c:c:c} \boldsymbol{U}_{O1}^T & \boldsymbol{U}_{O2}^T & \boldsymbol{0} \end{array}\right]^T, \quad \boldsymbol{U}_I = \left[\begin{array}{c:c:c} \boldsymbol{U}_{I1}^T & \boldsymbol{U}_{I2}^T & \boldsymbol{0} \end{array}\right]^T$$

where the partitions are organised so as to act on submatrices $\boldsymbol{Y}_{u1}(s)$, $\boldsymbol{Y}_{u2}(s)$, and $\boldsymbol{Y}_{u3}(s)$ where

$$\begin{aligned} \boldsymbol{U}_{O1} &= \left[\begin{array}{c:c:c} \boldsymbol{I} & \boldsymbol{0} & \boldsymbol{0} \\ \hdashline \boldsymbol{0} & \boldsymbol{0} & \boldsymbol{0} \\ \hdashline \boldsymbol{0} & \boldsymbol{0} & \boldsymbol{I} \end{array}\right], \quad \boldsymbol{U}_{I1} = \left[\begin{array}{c:c} \boldsymbol{0} & \boldsymbol{0} \\ \hdashline \boldsymbol{I} & \boldsymbol{0} \\ \hdashline \boldsymbol{0} & \boldsymbol{0} \end{array}\right], \\ \boldsymbol{U}_{O2} &= \left[\begin{array}{c:c:c} \boldsymbol{0} & \boldsymbol{I} & \boldsymbol{0} \\ \hdashline \boldsymbol{0} & \boldsymbol{0} & \boldsymbol{0} \end{array}\right], \quad \boldsymbol{U}_{I2} = \left[\begin{array}{c:c} \boldsymbol{0} & \boldsymbol{0} \\ \hdashline \boldsymbol{0} & \boldsymbol{I} \end{array}\right] \end{aligned}$$

where the identities are sized according to the block matrix partitions in (6.29)-(6.30).

The proof to this theorem is constructive.

Proof. To facilitate the proof, the the matrix operator $\boldsymbol{G}_u(s)$ that acts on the unmeasured variables is expanded out into the block matrix forms of the primary sets

as

$$\boldsymbol{G}_u(s) = \left[\begin{array}{c:c:c:c:c:c} \boldsymbol{Y}_{\mathcal{A}_1\mathcal{A}_3}(s) & \boldsymbol{Y}_{\mathcal{A}_1\mathcal{A}_4}(s) & \boldsymbol{Y}_{\mathcal{A}_1\mathcal{B}_2}(s) & \boldsymbol{0} & \boldsymbol{0} & \boldsymbol{0} \\ \boldsymbol{Y}_{\mathcal{A}_3\mathcal{A}_3}(s) & \boldsymbol{Y}_{\mathcal{A}_3\mathcal{A}_4}(s) & \boldsymbol{Y}_{\mathcal{A}_3\mathcal{B}_2}(s) & \boldsymbol{0} & \boldsymbol{0} & \boldsymbol{0} \\ \boldsymbol{Y}_{\mathcal{C}_1\mathcal{A}_3}(s) & \boldsymbol{Y}_{\mathcal{C}_1\mathcal{A}_4}(s) & \boldsymbol{Y}_{\mathcal{C}_1\mathcal{B}_2}(s) & \boldsymbol{0} & \boldsymbol{0} & \boldsymbol{0} \\ \boldsymbol{Y}_{\mathcal{B}_1\mathcal{A}_3}(s) & \boldsymbol{Y}_{\mathcal{B}_1\mathcal{A}_4}(s) & \boldsymbol{Y}_{\mathcal{B}_1\mathcal{B}_2}(s) & \boldsymbol{0} & \boldsymbol{0} & \boldsymbol{0} \\ \boldsymbol{Y}_{\mathcal{B}_2\mathcal{A}_3}(s) & \boldsymbol{Y}_{\mathcal{B}_2\mathcal{A}_4}(s) & \boldsymbol{Y}_{\mathcal{B}_2\mathcal{B}_2}(s) & \boldsymbol{0} & \boldsymbol{0} & \boldsymbol{0} \\ \boldsymbol{Y}_{\mathcal{A}_2\mathcal{A}_3}(s) & \boldsymbol{Y}_{\mathcal{A}_2\mathcal{A}_4}(s) & \boldsymbol{Y}_{\mathcal{A}_2\mathcal{B}_2}(s) & -\boldsymbol{I} & \boldsymbol{0} & \boldsymbol{0} \\ \boldsymbol{Y}_{\mathcal{A}_4\mathcal{A}_3}(s) & \boldsymbol{Y}_{\mathcal{A}_4\mathcal{A}_4}(s) & \boldsymbol{Y}_{\mathcal{A}_4\mathcal{B}_2}(s) & \boldsymbol{0} & -\boldsymbol{I} & \boldsymbol{0} \\ \boldsymbol{Y}_{\mathcal{C}_2\mathcal{A}_3}(s) & \boldsymbol{Y}_{\mathcal{C}_1\mathcal{A}_4}(s) & \boldsymbol{Y}_{\mathcal{C}_1\mathcal{B}_2}(s) & \boldsymbol{0} & \boldsymbol{0} & -\boldsymbol{I} \end{array}\right] \tag{6.33}$$

which suggests the following partition for the decoupling filter

$$\left[\begin{array}{c:c:c:c:c:c:c} \boldsymbol{L}_{\mathcal{A}_1}(s) & \boldsymbol{L}_{\mathcal{A}_3}(s) & \boldsymbol{L}_{\mathcal{C}_1}(s) & \boldsymbol{L}_{\mathcal{B}_1}(s) & \boldsymbol{L}_{\mathcal{B}_2}(s) & \boldsymbol{L}_{\mathcal{A}_2}(s) & \boldsymbol{L}_{\mathcal{A}_4}(s) & \boldsymbol{L}_{\mathcal{C}_2}(s) \end{array}\right].$$

where the matrix functions $\boldsymbol{L}_X(s) : \mathbb{C} \mapsto \mathbb{C}^{K\times n_X}$, $X = \mathcal{A}_1, \mathcal{A}_3, \mathcal{C}_1, \mathcal{B}_1, \mathcal{B}_2, \mathcal{A}_2, \mathcal{A}_4$ and $\mathcal{C}_2$. This partitioning enables the construction of $\boldsymbol{L}(s)$ based on the properties the submatrices. Due to the identities in block rows $\mathcal{A}_2$, $\mathcal{A}_4$ and $\boldsymbol{L}_{\mathcal{C}_2}(s)$, it is clear that for Point 1 in Definition 6.7 to hold

$$\boldsymbol{L}_{\mathcal{A}_2}(s), \boldsymbol{L}_{\mathcal{A}_4}(s), \boldsymbol{L}_{\mathcal{C}_2}(s) = \boldsymbol{0} \tag{6.34}$$

implying the following relationship between the remaining free matrix functions

$$\begin{aligned} &\left[\begin{array}{c:c:c:c:c} \boldsymbol{L}_{\mathcal{A}_1}(s) & \boldsymbol{L}_{\mathcal{A}_3}(s) & \boldsymbol{L}_{\mathcal{C}_1}(s) & \boldsymbol{L}_{\mathcal{B}_1}(s) & \boldsymbol{L}_{\mathcal{B}_2}(s) \end{array}\right] \\ &\qquad \times \left[\begin{array}{c:c:c} \boldsymbol{Y}_{\mathcal{A}_1\mathcal{A}_3}(s) & \boldsymbol{Y}_{\mathcal{A}_1\mathcal{A}_4}(s) & \boldsymbol{Y}_{\mathcal{A}_1\mathcal{B}_2}(s) \\ \boldsymbol{Y}_{\mathcal{A}_3\mathcal{A}_3}(s) & \boldsymbol{Y}_{\mathcal{A}_3\mathcal{A}_4}(s) & \boldsymbol{Y}_{\mathcal{A}_2\mathcal{B}_2}(s) \\ \boldsymbol{Y}_{\mathcal{C}_1\mathcal{A}_3}(s) & \boldsymbol{Y}_{\mathcal{C}_1\mathcal{A}_4}(s) & \boldsymbol{Y}_{\mathcal{C}_1\mathcal{B}_2}(s) \\ \boldsymbol{Y}_{\mathcal{B}_1\mathcal{A}_3}(s) & \boldsymbol{Y}_{\mathcal{B}_1\mathcal{A}_4}(s) & \boldsymbol{Y}_{\mathcal{B}_1\mathcal{B}_2}(s) \\ \boldsymbol{Y}_{\mathcal{B}_2\mathcal{A}_3}(s) & \boldsymbol{Y}_{\mathcal{B}_2\mathcal{A}_4}(s) & \boldsymbol{Y}_{\mathcal{B}_2\mathcal{B}_2}(s) \end{array}\right] = \boldsymbol{0} \end{aligned}$$

for all s within the right hand plane. Under the restriction $\mathcal{A}_4 = \emptyset$, the central block row can be neglected from consideration and the requirement for the free matrices $\boldsymbol{L}_{\mathcal{A}_1}(s)$, $\boldsymbol{L}_{\mathcal{A}_3}(s)$, $\boldsymbol{L}_{\mathcal{B}_1}(s)$, and $\boldsymbol{L}_{\mathcal{C}_1}(s)$ is

$$\begin{aligned} &\left[\begin{array}{c:c:c:c:c} \boldsymbol{L}_{\mathcal{A}_1}(s) & \boldsymbol{L}_{\mathcal{A}_3}(s) & \boldsymbol{L}_{\mathcal{C}_1}(s) & \boldsymbol{L}_{\mathcal{B}_1}(s) & \boldsymbol{L}_{\mathcal{B}_2}(s) \end{array}\right] \\ &\qquad \times \left[\begin{array}{c:c} \boldsymbol{Y}_{\mathcal{A}_1\mathcal{A}_3}(s) & \boldsymbol{Y}_{\mathcal{A}_1\mathcal{B}_2}(s) \\ \boldsymbol{Y}_{\mathcal{A}_3\mathcal{A}_3}(s) & \boldsymbol{Y}_{\mathcal{A}_3\mathcal{B}_2}(s) \\ \boldsymbol{Y}_{\mathcal{C}_1\mathcal{A}_3}(s) & \boldsymbol{Y}_{\mathcal{C}_1\mathcal{B}_2}(s) \\ \boldsymbol{Y}_{\mathcal{B}_1\mathcal{A}_3}(s) & \boldsymbol{Y}_{\mathcal{B}_1\mathcal{B}_2}(s) \\ \boldsymbol{Y}_{\mathcal{B}_2\mathcal{A}_3}(s) & \boldsymbol{Y}_{\mathcal{B}_2\mathcal{B}_2}(s) \end{array}\right] = \boldsymbol{0} \end{aligned} \tag{6.35}$$

for all s within the right hand plane. The matrix on the right in (6.35) contains the following principal minor of the network admittance matrix $\boldsymbol{Y}(s)$

$$\left[\begin{array}{c:c} \boldsymbol{Y}_{\mathcal{A}_3\mathcal{A}_3}(s) & \boldsymbol{Y}_{\mathcal{A}_3\mathcal{B}_2}(s) \\ \hdashline \boldsymbol{Y}_{\mathcal{B}_2\mathcal{A}_3}(s) & \boldsymbol{Y}_{\mathcal{B}_2\mathcal{B}_2}(s) \end{array}\right] \tag{6.36}$$

which, given Lemma B.1, is full rank on $s \in \mathbb{C}_+$. Therefore the matrix on the right in (6.35) has the form

$$\left[\begin{array}{c} \boldsymbol{B}(s) \\ \hdashline \boldsymbol{A}(s) \end{array}\right] \tag{6.37}$$

where $\boldsymbol{A}(s)$ is a square full rank matrix on $s \in \mathbb{C}_+$. Given that both $\boldsymbol{A}(s)$ and $\boldsymbol{B}(s)$ are analytic in $s \in \mathbb{C}_+$, the left nullspace of a matrix of the form (6.37) on $s \in \mathbb{C}_+$ is of the dimension of the number of rows in $\boldsymbol{B}$. This implies that

$$= \text{nullity}\left\{\left[\begin{array}{c:c} \boldsymbol{Y}_{\mathcal{A}_1\mathcal{A}_3}(s) & \boldsymbol{Y}_{\mathcal{A}_1\mathcal{B}_2}(s) \\ \hdashline \boldsymbol{Y}_{\mathcal{A}_3\mathcal{A}_3}(s) & \boldsymbol{Y}_{\mathcal{A}_3\mathcal{B}_2}(s) \\ \hdashline \boldsymbol{Y}_{\mathcal{C}_1\mathcal{A}_3}(s) & \boldsymbol{Y}_{\mathcal{C}_1\mathcal{B}_2}(s) \\ \hdashline \boldsymbol{Y}_{\mathcal{B}_1\mathcal{A}_3}(s) & \boldsymbol{Y}_{\mathcal{B}_1\mathcal{B}_2}(s) \\ \hdashline \boldsymbol{Y}_{\mathcal{B}_2\mathcal{A}_3}(s) & \boldsymbol{Y}_{\mathcal{B}_2\mathcal{B}_2}(s) \end{array}\right]^T\right\} = n_{\mathcal{A}_1} + n_{\mathcal{B}_1} + n_{\mathcal{C}_1},$$

for $\mathbb{R}\mathrm{e}\{s\} \geq 0$. As the partitions of $\boldsymbol{L}(s)$ in (6.35) span the left nullspace of the matrix on the right in (6.35), it is observed that the full row rank matrix $\boldsymbol{L}(s)$ has rank

$$\text{rank}\,\{\boldsymbol{L}(s)\} = n_{\mathcal{A}_1} + n_{\mathcal{B}_1} + n_{\mathcal{C}_1}, \quad s \in \mathbb{C}_+.$$

Simple algebraic manipulations show that a left nullifier for (6.37) can be constructed from the partitions in (6.37) as

$$\left[\begin{array}{c:c} \boldsymbol{I} & -\boldsymbol{B}(s)\boldsymbol{A}^{-1}(s) \end{array}\right]$$

where $\boldsymbol{A}^{-1}(s)$ exists on $s \in \mathbb{C}_+$ by assumption of the full rank of $\boldsymbol{A}(s)$ on $s \in \mathbb{C}_+$. By analogy, suitable candidates for the partitions of $\boldsymbol{L}(s)$ can be constructed as the constant matrices

$$\boldsymbol{L}_{\mathcal{A}_1} = \left[\begin{array}{c} \boldsymbol{I} \\ \hdashline \boldsymbol{0} \\ \hdashline \boldsymbol{0} \end{array}\right], \boldsymbol{L}_{\mathcal{B}_1} = \left[\begin{array}{c} \boldsymbol{0} \\ \hdashline \boldsymbol{I} \\ \hdashline \boldsymbol{0} \end{array}\right], \boldsymbol{L}_{\mathcal{C}_1} = \left[\begin{array}{c} \boldsymbol{0} \\ \hdashline \boldsymbol{0} \\ \hdashline \boldsymbol{I} \end{array}\right],$$

and the s dependent matrix functions

$$\boldsymbol{L}_{\mathcal{A}_3}(s) = -\left[\begin{array}{c:c} \boldsymbol{Y}_{\mathcal{A}_1\mathcal{A}_3}(s) & \boldsymbol{Y}_{\mathcal{A}_1\mathcal{B}_2}(s) \\ \hdashline \boldsymbol{Y}_{\mathcal{C}_1\mathcal{A}_3}(s) & \boldsymbol{Y}_{\mathcal{C}_1\mathcal{B}_2}(s) \\ \hdashline \boldsymbol{Y}_{\mathcal{B}_1\mathcal{A}_3}(s) & \boldsymbol{Y}_{\mathcal{B}_1\mathcal{B}_2}(s) \end{array}\right]\left[\begin{array}{c} \boldsymbol{Z}_{\mathcal{A}_3\mathcal{A}_3}(s) \\ \hdashline \boldsymbol{Z}_{\mathcal{B}_2\mathcal{A}_3}(s) \end{array}\right],$$

$$\boldsymbol{L}_{\mathcal{B}_2}(s) = -\left[\begin{array}{c:c} \boldsymbol{Y}_{\mathcal{A}_1\mathcal{A}_3}(s) & \boldsymbol{Y}_{\mathcal{A}_1\mathcal{B}_2}(s) \\ \hdashline \boldsymbol{Y}_{\mathcal{C}_1\mathcal{A}_3}(s) & \boldsymbol{Y}_{\mathcal{C}_1\mathcal{B}_2}(s) \\ \hdashline \boldsymbol{Y}_{\mathcal{B}_1\mathcal{A}_3}(s) & \boldsymbol{Y}_{\mathcal{B}_1\mathcal{B}_2}(s) \end{array}\right]\left[\begin{array}{c} \boldsymbol{Z}_{\mathcal{B}_2\mathcal{A}_3}(s) \\ \hdashline \boldsymbol{Z}_{\mathcal{B}_2\mathcal{B}_2}(s) \end{array}\right]$$

where the impedance matrices are submatrices of the inverse of the principal minor (6.36)

$$\left[\begin{array}{c:c} \boldsymbol{Z}_{\mathcal{A}_3\mathcal{A}_3}(s) & \boldsymbol{Z}_{\mathcal{A}_3\mathcal{B}_2}(s) \\ \hdashline \boldsymbol{Z}_{\mathcal{B}_2\mathcal{A}_3}(s) & \boldsymbol{Z}_{\mathcal{B}_2\mathcal{B}_2}(s) \end{array}\right] = \left[\begin{array}{c:c} \boldsymbol{Y}_{\mathcal{A}_3\mathcal{A}_3}(s) & \boldsymbol{Y}_{\mathcal{A}_3\mathcal{B}_2}(s) \\ \hdashline \boldsymbol{Y}_{\mathcal{B}_2\mathcal{A}_3}(s) & \boldsymbol{Y}_{\mathcal{B}_2\mathcal{B}_2}(s) \end{array}\right]^{-1}$$

which, from Theorem B.3 exists for all $s \in \mathbb{C}_+$. Given the form of $\boldsymbol{L}_{\mathcal{A}_1}$, $\boldsymbol{L}_{\mathcal{C}_1}$, and $\boldsymbol{L}_{\mathcal{B}_1}$, $\boldsymbol{L}(s)$ is clearly full row rank. This representation is observed as being equivalent to (6.32) by recognition of the relations

$$\begin{aligned} \boldsymbol{U}_O &= \left[\begin{array}{c:c:c:c:c:c:c} \boldsymbol{L}_{\mathcal{A}_1} & \boldsymbol{0} & \boldsymbol{L}_{\mathcal{C}_1} & \boldsymbol{L}_{\mathcal{B}_1} & \boldsymbol{0} & \boldsymbol{L}_{\mathcal{A}_2} & \boldsymbol{L}_{\mathcal{C}_2} \end{array}\right]^T \\ \boldsymbol{U}_I^T\boldsymbol{Y}_u(s) &= \left[\begin{array}{c:c} \boldsymbol{Y}_{\mathcal{A}_3\mathcal{A}_3}(s) & \boldsymbol{Y}_{\mathcal{A}_3\mathcal{B}_2}(s) \\ \hdashline \boldsymbol{Y}_{\mathcal{B}_2\mathcal{A}_3}(s) & \boldsymbol{Y}_{\mathcal{B}_2\mathcal{B}_2}(s) \end{array}\right]. \end{aligned} \tag{6.38}$$

□

Remarks:

1. The system above is of the dimensions

   $$(n_{\mathcal{A}_1} + n_{\mathcal{B}_1} + n_{\mathcal{C}_1}) \times (2n_{\mathcal{A}_1} + n_{\mathcal{A}_2} + n_{\mathcal{A}_3} + n_{\mathcal{B}_1} + n_{\mathcal{C}_1}),$$

   and is hence always under determined by the degree $n_{\mathcal{A}_1} + n_{\mathcal{A}_2} + n_{\mathcal{A}_3}$. The number $n_{\mathcal{A}_1} + n_{\mathcal{B}_1} + n_{\mathcal{C}_1}$ is the number of nodes for which both the nodal pressure and flow is known or measured. The number $n_{\mathcal{A}_1} + n_{\mathcal{A}_2} + n_{\mathcal{A}_3}$ is the number of nodes for which there are measurements but no known values.

2. Within this theorem, the set $\mathcal{A}_4$ is omitted from consideration. This nodal set corresponds to nodes for which there are no known or measured variables. Obtaining a reduced state model in the presence of such node types is significantly more complex than that outlined here, and is treated later in the context of the EM algorithm.

3. An interesting interpretation for $\boldsymbol{L}(s)$ exists by considering it as a projection.

The expression

$$\overline{\boldsymbol{P}}(s) = \boldsymbol{Y}_u(s)\left[\boldsymbol{U}_I^T\boldsymbol{Y}_u(s)\right]^{-1}\boldsymbol{U}_I^T \tag{6.39}$$

is interpreted as an oblique projection matrix [*Hansen*, 2004] onto the vector space defined by the two requirements

$$\begin{cases} \overline{\boldsymbol{P}}(s)\boldsymbol{x} \in \text{range}\,\{\boldsymbol{Y}_u(s)\}, \text{ for each } s \in \mathbb{C}_+, \text{ and } \boldsymbol{x} \in \mathbb{C}^n \\ \overline{\boldsymbol{P}}(s)\boldsymbol{x} = 0 \text{ if } \boldsymbol{x} \in \text{range}\,\{\boldsymbol{U}_I\}^\perp \text{ for each } s \in \mathbb{C}_+ \end{cases} \tag{6.40}$$

where the range refers only to vector operations and for a matrix function $\boldsymbol{A}(s) : \mathbb{C} \mapsto \mathbb{C}^{m\times n}$ analytic on $s \in \mathbb{C}_+$, the range is defined at each $s \in \mathbb{C}_+$ simply as

$$\text{range}\,\{\boldsymbol{A}(s)\} = \text{span}\,\{\boldsymbol{A}_{\bullet 1}(s), \ldots, \boldsymbol{A}_{\bullet n}(s)\}$$

where $\boldsymbol{A}_{\bullet i}$ is the i-th column of $\boldsymbol{A}$. Stated simply, $\overline{\boldsymbol{P}}$ is an oblique projector that at each $s \in \mathbb{C}_+$ projects onto the vector space that is spanned by the columns of $\boldsymbol{Y}_u$, and possesses the nullspace defined by range $\{\boldsymbol{U}_I\}^\perp$. As $\overline{\boldsymbol{P}}$ is a projection matrix, the matrix

$$\boldsymbol{P}(s) = \boldsymbol{I} - \overline{\boldsymbol{P}}(s) = \boldsymbol{I} - \boldsymbol{Y}_u(s)\left[\boldsymbol{U}_I^T\boldsymbol{Y}_u(s)\right]^{-1}\boldsymbol{U}_I^T \tag{6.41}$$

is also a projection matrix, this time defined by the properties

$$\begin{cases} \boldsymbol{P}(s)\boldsymbol{x} \in \text{range}\,\{\boldsymbol{Y}_u(s)\}^\perp \cap \text{range}\,\{\boldsymbol{U}_I\}^\perp, \text{ for each } s \in \mathbb{C}_+, \text{ and } \boldsymbol{x} \in \mathbb{C}^n \\ \boldsymbol{P}(s)\boldsymbol{x} = 0 \text{ if } \boldsymbol{x} \in \text{range}\,\{\boldsymbol{Y}_u(s)\} \text{ for each } s \in \mathbb{C}_+ \end{cases} \tag{6.42}$$

which can be demonstrated from (6.40) and (6.41). Straight forward algebraic operations demonstrate that

$$\text{range}\,\{\boldsymbol{U}_I\} \perp \text{range}\,\{\boldsymbol{U}_U\} \cup \text{range}\,\{\boldsymbol{U}_O\}$$

where

$$\boldsymbol{U}_U = \begin{bmatrix} \boldsymbol{0} \\ \cdots \\ \boldsymbol{I} \end{bmatrix}$$

where the $\boldsymbol{I}$ is an $(n_{\mathcal{A}_2} + n_{\mathcal{C}_2}) \times (n_{\mathcal{A}_2} + n_{\mathcal{C}_2})$ identity matrix. This means that $\boldsymbol{P}$ projects onto part of the space given by range $\{\boldsymbol{U}_U\} \cup$ range $\{\boldsymbol{U}_O\}$. Noting that also

$$\text{range}\,\{\boldsymbol{U}_O\} \perp \text{range}\,\{\boldsymbol{U}_U\}$$

it is observed that the matrix operator $\boldsymbol{U}_O^T\boldsymbol{P}(s)$ possesses a nullspace defined by

$$\text{range}\,\{\boldsymbol{Y}_u(s)\} \cup \text{range}\,\{\boldsymbol{U}_U\}$$

and is full row rank with

$$\text{rank}\left\{\boldsymbol{U}_O^T\boldsymbol{P}(s)\right\} = n_{\mathcal{A}_1} + n_{\mathcal{B}_1} + n_{\mathcal{C}_1}$$

at each $s \in \mathbb{C}_+$, where the full row rank is ensured as $\boldsymbol{P}$ projects onto the range of $\boldsymbol{U}_O$. This is related to the decoupling filter $\boldsymbol{L}$ by realising that

$$\boldsymbol{L}(s) = \boldsymbol{U}_O^T\boldsymbol{P}(s).$$

As in Definition 6.7, it is required that the columns of $\boldsymbol{G}_u$ are within the nullspace of $\boldsymbol{L}$ for $s \in \mathbb{C}_+$, where given (6.33), it holds that

$$\text{range}\left\{\boldsymbol{G}_u(s)\right\} = \text{range}\left\{\boldsymbol{Y}_u(s)\right\} \cup \text{range}\left\{\boldsymbol{U}_U\right\}$$

which is exactly the nullspace of $\boldsymbol{U}_O^T\boldsymbol{P}$.

With reference to the primary node sets, a computationally useful expression of the decoupled measured system is

$$\boldsymbol{G}(s) = \left[\begin{array}{c:c:c:c:c:c} \boldsymbol{G}_{\mathcal{A}_1\mathcal{A}_1}(s) & \boldsymbol{G}_{\mathcal{A}_1\mathcal{A}_2}(s) & \boldsymbol{G}_{\mathcal{A}_1\mathcal{B}_1}(s) & -\boldsymbol{I} & \boldsymbol{G}_{\mathcal{A}_1\mathcal{A}_3}(s) & \boldsymbol{0} \\ \hdashline \boldsymbol{G}_{\mathcal{B}_1\mathcal{A}_1}(s) & \boldsymbol{G}_{\mathcal{B}_1\mathcal{A}_2}(s) & \boldsymbol{G}_{\mathcal{B}_1\mathcal{B}_1}(s) & \boldsymbol{0} & \boldsymbol{G}_{\mathcal{B}_1\mathcal{A}_3}(s) & \boldsymbol{0} \\ \hdashline \boldsymbol{G}_{\mathcal{C}_1\mathcal{A}_1}(s) & \boldsymbol{G}_{\mathcal{C}_1\mathcal{A}_2}(s) & \boldsymbol{G}_{\mathcal{C}_1\mathcal{B}_1}(s) & \boldsymbol{0} & \boldsymbol{G}_{\mathcal{C}_1\mathcal{A}_3}(s) & -\boldsymbol{I} \end{array}\right] \tag{6.43}$$

where the first three block columns are associated with the measured nodal pressure variables $\boldsymbol{\Psi}_{\mathcal{A}_1}(s)$, $\boldsymbol{\Psi}_{\mathcal{A}_2}(s)$, and $\boldsymbol{\Psi}_{\mathcal{B}_1}(s)$, and the last three are associated with the measured nodal flow variables $\boldsymbol{\Theta}_{\mathcal{A}_1}(s)$, $\boldsymbol{\Theta}_{\mathcal{A}_3}(s)$, and $\boldsymbol{\Theta}_{\mathcal{C}_1}(s)$, and the block expressions are given by the submatrices

$$\boldsymbol{G}_{XY}(s) = \begin{cases} \boldsymbol{Y}_{XY}(s) - \widetilde{\boldsymbol{G}}_{XY}(s) & \text{for } X = \mathcal{A}_1, \mathcal{B}_1, \mathcal{C}_1, \\ & \text{and } Y = \mathcal{A}_1, \mathcal{A}_2, \mathcal{B}_1 \\ -\left[\begin{array}{c:c} \boldsymbol{Y}_{X\mathcal{A}_3}(s) & \boldsymbol{Y}_{X\mathcal{B}_2}(s) \end{array}\right] \left[\begin{array}{c} \boldsymbol{Z}_{\mathcal{A}_3\mathcal{A}_3}(s) \\ \hdashline \boldsymbol{Z}_{\mathcal{B}_2\mathcal{A}_3}(s) \end{array}\right] & \text{for } X = \mathcal{A}_1, \mathcal{B}_1, \mathcal{C}_1, \\ & \text{and } Y = \mathcal{A}_3 \end{cases}$$

where

$$\widetilde{\boldsymbol{G}}_{XY}(s) = \left[\begin{array}{c:c} \boldsymbol{Y}_{X\mathcal{A}_3}(s) & \boldsymbol{Y}_{X\mathcal{B}_2}(s) \end{array}\right] \left[\begin{array}{c:c} \boldsymbol{Z}_{\mathcal{A}_3\mathcal{A}_3}(s) & \boldsymbol{Z}_{\mathcal{A}_3\mathcal{B}_2}(s) \\ \hdashline \boldsymbol{Z}_{\mathcal{B}_2\mathcal{A}_3}(s) & \boldsymbol{Z}_{\mathcal{B}_2\mathcal{B}_2}(s) \end{array}\right] \left[\begin{array}{c} \boldsymbol{Y}_{\mathcal{A}_3Y}(s) \\ \hdashline \boldsymbol{Y}_{\mathcal{B}_2Y}(s) \end{array}\right]$$

for $X = \mathcal{A}_1, \mathcal{B}_1, \mathcal{C}_1$, and $Y = \mathcal{A}_1, \mathcal{A}_2, \mathcal{B}_1$. Equation (6.43) represents a computationally preferable expression to (6.31) and (6.32) as the overall matrix computations are resolved down to operations involving the smaller submatrices.

Remark: In terms of parametric dependency, it can be demonstrated that

$$\boldsymbol{G}_{XY}|_s = fn\left(\Xi_X, \Xi_Y, \Xi_{\mathcal{A}_3}, \Xi_{\mathcal{B}_2}\right) \tag{6.44}$$

which means that for a given $s \in \mathbb{C}$, $\boldsymbol{G}_{XY}$ is a function of the parameters of the elements in the sets Ξ_X, Ξ_Y, $\Xi_{\mathcal{A}_3}$, and $\Xi_{\mathcal{B}_2}$. Clearly the system is more sensitive to variations in $\Xi_{\mathcal{A}_3}$, and $\Xi_{\mathcal{B}_2}$ as these feature in all functions. It is seen that the system is totally insensitive to any elements exclusively in $\Xi_{\mathcal{C}_2}$. But this is not a problem, as links within this set correspond to links connected only to reservoirs, where the flows are not measured.

The representation (6.43) also facilitates the following corollary concerning the rank of $\boldsymbol{G}(s)$.

Corollary 6.1. *The decoupled system matrix $\boldsymbol{G}(s)$ constructed as in (6.43) under the assumptions of Theorem 6.2, is full row rank, and has a nondiminishing rank on $s \in \mathbb{C}_+$ provided that there exist some strictly passive $j \in \Xi_i$ for each $i \in \mathcal{A}_3 \cup \mathcal{B}_1 \cup \mathcal{B}_2$.*

Proof. Given the presence of the identities in the first and third block rows of (6.43), it remains to show that the second block row is of full row rank on $s \in \mathbb{C}_+$. This is done by showing that the second block row possesses a submatrix of size $n_{\mathcal{B}_1} \times n_{\mathcal{B}_1}$ that is strictly positive definite on $s \in \mathbb{C}_+$. Consider the $n_{\mathcal{B}_1} \times n_{\mathcal{B}_1}$ submatrix

$$\boldsymbol{G}_{\mathcal{B}_1\mathcal{B}_1}(s) = \boldsymbol{Y}_{\mathcal{B}_1\mathcal{B}_1}(s) - \widetilde{\boldsymbol{G}}_{\mathcal{B}_1\mathcal{B}_1}(s),$$

this is recognised as being the Schur complement of

$$\left[\begin{array}{c:c} \boldsymbol{Y}_{\mathcal{B}_1\mathcal{B}_1}(s) & \begin{bmatrix} \boldsymbol{Y}_{\mathcal{B}_1\mathcal{A}_3}(s) & \boldsymbol{Y}_{\mathcal{B}_1\mathcal{B}_2}(s) \end{bmatrix} \\ \hdashline \begin{bmatrix} \boldsymbol{Y}_{\mathcal{A}_3 Y}(s) \\ \hdashline \boldsymbol{Y}_{\mathcal{B}_2 Y}(s) \end{bmatrix} & \left[\begin{array}{c:c} \boldsymbol{Y}_{\mathcal{A}_3\mathcal{A}_3}(s) & \boldsymbol{Y}_{\mathcal{A}_3\mathcal{B}_2}(s) \\ \hdashline \boldsymbol{Y}_{\mathcal{B}_2\mathcal{A}_3}(s) & \boldsymbol{Y}_{\mathcal{B}_2\mathcal{B}_2}(s) \end{array}\right] \end{array}\right]. \tag{6.45}$$

which is a principal minor of the network admittance matrix. Being a principal minor of a matrix that is positive definite on $s \in \mathbb{C}_+$, (6.45) is itself positive definite on $s \in \mathbb{C}_+$, and further, this positive definiteness is strict due to the strict passivity of all of its principal minors (resulting from a strictly passive element being incident to each node in $\mathcal{A}_3$, $\mathcal{B}_1$, and $\mathcal{B}_2$). The Schur complement of a strictly positive definite matrix is itself strictly positive definite [*Rao*, 2006], therefore, $\boldsymbol{G}_{\mathcal{B}_1\mathcal{B}_1}(s)$ is strictly positive definite on $s \in \mathbb{C}_+$. □

Remark: The development of the MLE process in the next section requires that the rank of the resulting system matrix to be full row rank. The intuitive interpretation

of this requirement is that each row of the decoupled system matrix describes a unique relationship between the measured states.

6.4.2 Maximum likelihood estimation for decoupled system

The expression for the MLE of the decoupled system is presented in two steps. Firstly the statistical problem is framed and solved in a general context as a complex Gaussian MLE process given linear constraints on the unknown means. Secondly, the specific problem instance for the decoupled system (6.43) is given.

Theorem 6.3. *Consider the data set of complex vectors* $\widetilde{\mathcal{U}} = \{\tilde{\boldsymbol{u}}_i : i = 1, \ldots, M\}$ *distributed as*

$$\tilde{\boldsymbol{u}}_i \sim \mathcal{N}_c\left(\boldsymbol{u}_i, \boldsymbol{\Sigma}_i\right), \quad i = 1, \ldots, M \tag{6.46}$$

where the $\boldsymbol{\Sigma}_i$ *are positive definite real matrices and the* $\boldsymbol{u}_i$ *are unknown means subjected to*

$$\boldsymbol{G}_i(\boldsymbol{\vartheta})\boldsymbol{u}_i = \boldsymbol{0}, \quad i = 1, \ldots, M \tag{6.47}$$

where the $\boldsymbol{G}_i$ *are complex valued matrices and of full row rank on the entire parameter space* $\boldsymbol{\vartheta} \in \boldsymbol{\Upsilon} \subset \mathbb{R}^n$ *where* n *is the dimension of the parameter space* $\boldsymbol{\Upsilon}$*. Given these conditions, the MLE for the parameter* $\boldsymbol{\vartheta}$ *is given by the minimiser*

$$\widehat{\boldsymbol{\vartheta}} = \arg\min_{\boldsymbol{\vartheta}\in\boldsymbol{\Upsilon}} \sum_{i=1}^{M} \tilde{\boldsymbol{u}}_i^H \boldsymbol{G}_i^H(\boldsymbol{\vartheta}) \left[\boldsymbol{G}_i(\boldsymbol{\vartheta})\boldsymbol{\Sigma}_i\boldsymbol{G}_i^H(\boldsymbol{\vartheta})\right]^{-1} \boldsymbol{G}_i(\boldsymbol{\vartheta})\tilde{\boldsymbol{u}}_i. \tag{6.48}$$

Proof. The probability density function of the entire data set $\widetilde{\mathcal{U}} = \{\tilde{\boldsymbol{u}}_i : i = 1, \ldots, M\}$ can be expressed as

$$f\left(\widetilde{\mathcal{U}}\middle|\mathcal{U}, \mathcal{S}\right) = \prod_{i=1}^{M} \pi^{-n} \left|\boldsymbol{\Sigma}_i\right|^{-1} \exp\left\{-\left(\tilde{\boldsymbol{u}}_i - \boldsymbol{u}_i\right)^H \boldsymbol{\Sigma}_i^{-1} \left(\tilde{\boldsymbol{u}}_i - \boldsymbol{u}_i\right)\right\} \tag{6.49}$$

where $\mathcal{U}$ and $\mathcal{S}$ are the sets mean values

$$\mathcal{U} = \{\boldsymbol{u}_i : i = 1, \ldots, M\}$$

and the error variance matrices

$$\mathcal{S} = \{\boldsymbol{\Sigma}_i : i = 1, \ldots, M\}.$$

The parameters requiring estimation are elements of the mean set $\mathcal{U}$ and the system parameter set $\boldsymbol{\vartheta}$. Therefore, the MLEs $\widehat{\mathcal{U}}$ and $\hat{\boldsymbol{\vartheta}}$ can be expressed as the solution to

the following constrained optimisation problem

$$\arg\max_{\mathcal{U},\boldsymbol{\vartheta}} f\left(\widetilde{\mathcal{U}}\middle|\mathcal{U},\mathcal{S}\right), \quad \text{subject to:} \quad \boldsymbol{G}_i(\boldsymbol{\vartheta})\boldsymbol{u}_i = \boldsymbol{0}, \quad i = 1,\ldots,M. \tag{6.50}$$

The solution to (6.50) involves two steps. Firstly the MLEs $\widehat{\mathcal{U}}$ are determined analytically using a Lagrange multiplier method based on a multidimensional extension of the method implemented in *Schoukens and Pintelon* [1991]. Secondly, the analytic expression for the $\widehat{\mathcal{U}}$ are used to express $\hat{\boldsymbol{\vartheta}}$ as the minimiser (6.48).

To use the Lagrange multiplier technique to determine an expression for $\widehat{\mathcal{U}}$, the differentiability of $f\left(\widetilde{\mathcal{U}}\middle|\mathcal{U},\mathcal{S}\right)$ with respect to the elements of $\mathcal{U}$ is required. Therefore, to avoid issues with the Hermitian operator, the real and imaginary components of $\mathcal{U}$ are dealt with separately. To do this, the operator $\breve{}$ is defined as performing the following concatenations of the real and imaginary parts of complex matrices and vectors

$$\breve{\boldsymbol{A}} = \left[\begin{array}{c|c} \mathbb{R}\mathrm{e}\left\{\boldsymbol{A}\right\} & -\mathbb{I}\mathrm{m}\left\{\boldsymbol{A}\right\} \\ \hline \mathbb{I}\mathrm{m}\left\{\boldsymbol{A}\right\} & \mathbb{R}\mathrm{e}\left\{\boldsymbol{A}\right\} \end{array}\right], \quad \breve{\boldsymbol{a}} = \left[\begin{array}{c} \mathbb{R}\mathrm{e}\left\{\boldsymbol{a}\right\} \\ \hline \mathbb{I}\mathrm{m}\left\{\boldsymbol{a}\right\} \end{array}\right].$$

where $\boldsymbol{A}$ is a complex matrix, and $\boldsymbol{a}$ is a complex vector. Given this definition of the operator $\breve{}$, the cost function resulting from the logarithm of the likelihood function $f\left(\widetilde{\mathcal{U}}\middle|\mathcal{U},\mathcal{S}\right)$ can be written as

$$\sum_{i=1}^{M}\left[\breve{\widetilde{\boldsymbol{u}}}_i - \breve{\boldsymbol{u}}_i\right]^T \breve{\boldsymbol{\Sigma}}_i^{-1}\left[\breve{\widetilde{\boldsymbol{u}}}_i - \breve{\boldsymbol{u}}_i\right]. \tag{6.51}$$

where the constant terms are neglected. Considering the constraints in (6.50), the Lagrange multiplier cost function can be expressed as

$$K\left(\mathcal{U},\mathcal{S},\boldsymbol{\vartheta},\mathcal{L}\right) = \sum_{i=1}^{M}\left[\breve{\widetilde{\boldsymbol{u}}}_i - \breve{\boldsymbol{u}}_i\right]^T \breve{\boldsymbol{\Sigma}}_i^{-1}\left[\breve{\widetilde{\boldsymbol{u}}}_i - \breve{\boldsymbol{u}}_i\right] + \boldsymbol{\lambda}_i^T \breve{\boldsymbol{G}}_i\left(\boldsymbol{\vartheta}\right)\breve{\boldsymbol{u}}_i \tag{6.52}$$

where $\boldsymbol{\lambda}_i \in \mathbb{R}^{2N}$ are the Lagrange multiplier vectors and $\mathcal{L} = \{\boldsymbol{\lambda}_1,\ldots,\boldsymbol{\lambda}_M\}$. As (6.52) is clearly a continuous function of $\breve{\boldsymbol{u}}$ and $\boldsymbol{\lambda}$, the extrema of K with respect to these variables satisfies the stationarity conditions

$$\frac{\partial K}{\partial \breve{\boldsymbol{u}}_i} = \boldsymbol{0}, \quad \frac{\partial K}{\partial \boldsymbol{\lambda}_i} = \boldsymbol{0}, \quad i = 1,\ldots,M, \tag{6.53}$$

where the derivatives with respect to the vectors are the usual matrix calculus operations [*Magnus and Neudecker*, 1999]. From the first derivative in (6.53), it

holds that

$$\breve{\boldsymbol{u}}_i = \breve{\tilde{\boldsymbol{u}}}_i - \frac{1}{2}\breve{\boldsymbol{\Sigma}}_i \breve{\boldsymbol{G}}_i^T(\boldsymbol{\vartheta})\,\boldsymbol{\lambda}_i. \tag{6.54}$$

The second derivative in (6.53) resolves down to the condition that $\breve{\boldsymbol{G}}_i \breve{\boldsymbol{u}}_i = \boldsymbol{0}$, therefore, premultiplying (6.54) by $\breve{\boldsymbol{G}}_i$ yields the following expression for the i-th Lagrange multiplier

$$\boldsymbol{\lambda}_i = 2\left[\breve{\boldsymbol{G}}_i(\boldsymbol{\vartheta})\,\breve{\boldsymbol{\Sigma}}_i \breve{\boldsymbol{G}}_i^T(\boldsymbol{\vartheta})\right]^{-1} \breve{\boldsymbol{G}}_i(\boldsymbol{\vartheta})\,\breve{\tilde{\boldsymbol{u}}}_i. \tag{6.55}$$

Combining (6.55) and (6.54), the MLE $\breve{\hat{\boldsymbol{u}}}$ for $\breve{\boldsymbol{u}}$ can then be expressed as

$$\breve{\hat{\boldsymbol{u}}}_i = \left[\boldsymbol{I} - \breve{\boldsymbol{\Sigma}}_i \breve{\boldsymbol{G}}_i^T(\boldsymbol{\vartheta})\left[\breve{\boldsymbol{G}}_i(\boldsymbol{\vartheta})\,\breve{\boldsymbol{\Sigma}}_i \breve{\boldsymbol{G}}_i^T(\boldsymbol{\vartheta})\right]^{-1} \breve{\boldsymbol{G}}_i(\boldsymbol{\vartheta})\right] \breve{\tilde{\boldsymbol{u}}}_i. \tag{6.56}$$

As defined by the $\breve{}$ operator, the first n rows of (6.56) correspond to $\mathbb{R}\mathrm{e}\{\hat{\boldsymbol{u}}\}$ and the last n rows correspond to $\mathbb{I}\mathrm{m}\{\hat{\boldsymbol{u}}\}$. Therefore, carefully dividing (6.56) into these two sets of rows and recombining the expressions in terms of complex variables, the complex MLE $\hat{\boldsymbol{u}}$ is given as

$$\hat{\boldsymbol{u}}_i = \hat{\boldsymbol{u}}_i(\boldsymbol{\vartheta}) = \left[\boldsymbol{I} - \boldsymbol{\Sigma}_i \boldsymbol{G}_i^H(\boldsymbol{\vartheta})\left[\boldsymbol{G}_i(\boldsymbol{\vartheta})\boldsymbol{\Sigma}_i \boldsymbol{G}_i^H(\boldsymbol{\vartheta})\right]^{-1} \boldsymbol{G}_i(\boldsymbol{\vartheta})\right] \tilde{\boldsymbol{u}}_i. \tag{6.57}$$

for $i = 1, \ldots, M$. The expression (6.57) holds the interesting interpretation that it is the $\boldsymbol{\Sigma}_i$ weighted projection of the measured data $\tilde{\boldsymbol{u}}_i$ onto the null space of $\boldsymbol{G}_i(\boldsymbol{\vartheta})$.

To undertake the second step and determine the MLE for $\boldsymbol{\vartheta}$, it is recognised that as $\widehat{\mathcal{U}} = \widehat{\mathcal{U}}(\boldsymbol{\vartheta})$, then $\hat{\boldsymbol{\vartheta}}$ is then given as

$$\hat{\boldsymbol{\vartheta}} = \arg\max_{\boldsymbol{\vartheta}\in\boldsymbol{\Upsilon}} f\left(\widetilde{\mathcal{U}}\middle|\,\widehat{\mathcal{U}}(\boldsymbol{\vartheta}), \mathcal{S}\right)$$

which, under the usual approach of taking the negative of the log-likelihood function f and ignoring the constant terms, is equivalent to

$$\hat{\boldsymbol{\vartheta}} = \arg\min_{\boldsymbol{\vartheta}} \sum_{i=1}^{M} \left[\tilde{\boldsymbol{u}}_i - \hat{\boldsymbol{u}}_i(\boldsymbol{\vartheta})\right]^H \boldsymbol{\Sigma}_i^{-1} \left[\tilde{\boldsymbol{u}}_i - \hat{\boldsymbol{u}}_i(\boldsymbol{\vartheta})\right].$$

Substituting in (6.57) yields the minimiser expression (6.48). □

Remark: Under the interpretation that $\boldsymbol{G}_i(\boldsymbol{\vartheta})\tilde{\boldsymbol{u}}_i$ is the residuals of the system measurements that do not lie in the space defined in (6.27), Equation (6.48) can be interpreted as a weighted sum of the squared residuals, with the weighting function $\left[\boldsymbol{G}_i(\boldsymbol{\vartheta})\boldsymbol{\Sigma}_i \boldsymbol{G}_i^H(\boldsymbol{\vartheta})\right]^{-1}$.

This leads us to the expression for the MLE for the parameters of a $\mathscr{M}$-network.

The following corollary is the main result for this section.

Corollary 6.2. *Consider the $\mathscr{M}$-network $(\mathcal{G}(\mathcal{N},\Xi),\mathcal{M})$ with the nodal partitioning as defined in Section 6.3.3 where $\mathcal{A}_4=\emptyset$, for which there exists the measurement set $\left\{\widetilde{\boldsymbol{\psi}}_m(t),\widetilde{\boldsymbol{\theta}}_m(t):t=0,\Delta t,\dots,M\Delta t\right\}$ where*

$$\begin{bmatrix}\tilde{\boldsymbol{\psi}}_m(t)\\ \hdashline \tilde{\boldsymbol{\theta}}_m(t)\end{bmatrix}=\begin{bmatrix}\boldsymbol{\psi}_m(t)\\ \hdashline \boldsymbol{\theta}_m(t)\end{bmatrix}+\begin{bmatrix}\boldsymbol{e}_\psi(t)\\ \hdashline \boldsymbol{e}_\theta(t)\end{bmatrix} \tag{6.58}$$

where $\boldsymbol{\psi}_m$ and $\boldsymbol{\theta}_m$ are as defined in Section 6.3.3 and are periodic with fixed frequency distribution (with negligible spectral energy above $(2\Delta t)^{-1}$ Hz), and $\boldsymbol{e}_\psi(t),\boldsymbol{e}_\theta(t),t=0,\Delta t,\dots$ are stationary processes with power spectrum's $\boldsymbol{S}_\psi(\mathrm{i}\omega)$ and $\boldsymbol{S}_\theta(\mathrm{i}\omega)$. Given that there exists some strictly passive $\xi\in\Xi_i$ for each $i\in\mathcal{A}_3\cup\mathcal{B}_2$, then the MLE solution to the network parameter estimation problem in Definition 6.4 is given by (6.48) in Theorem 6.3 with the following substitutions

$$\widetilde{\boldsymbol{u}}_i=\begin{bmatrix}\widetilde{\boldsymbol{\Psi}}_m(\mathrm{i}\omega_i)\\ \hdashline \widetilde{\boldsymbol{\Theta}}_m(\mathrm{i}\omega_i)\end{bmatrix} \tag{6.59}$$

$$\boldsymbol{G}_i(\boldsymbol{\vartheta})=\boldsymbol{G}(\boldsymbol{\vartheta},\mathrm{i}\omega_i) \tag{6.60}$$

$$\boldsymbol{\Sigma}_i=\frac{1}{M}\left[\begin{array}{c:c}\boldsymbol{S}_\psi(\mathrm{i}\omega_j) & \boldsymbol{0}\\ \hdashline \boldsymbol{0} & \boldsymbol{S}_\theta(\mathrm{i}\omega_j)\end{array}\right] \tag{6.61}$$

where $\boldsymbol{G}$ is the decoupled measurement system from Theorem 6.2, and the ω_i are the Fourier frequencies from the DFT of the time-domain data.

Proof. The parameter estimation problem outlined in the corollary can be cast as the complex Gaussian, constrained MLE problem from Theorem 6.3 by recognising (i) the frequency-domain data (6.59) from the DFT of (6.58) is complex Gaussian (Theorem 6.1) with mean $\boldsymbol{u}_i=[\boldsymbol{\Psi}_m^T(\mathrm{i}\omega_i)\,\boldsymbol{\Theta}_m^T(\mathrm{i}\omega_i)]^T$ and covariance matrix (6.61), and (ii) the constraints on the mean are given by the decoupled measurement system from Theorem 6.2, which leads to (6.60) where the full row rank of $\boldsymbol{G}$ is ensured by Corollary 6.1 under the condition that there exists some strictly passive $\xi\in\Xi_i$ for each $i\in\mathcal{A}_3\cup\mathcal{B}_2$. □

Remarks:

1. An implicit assumption is that the passivity of each component $\xi\in\Xi$ remains unaffected by parameter variations throughout the parameter space Υ_ξ. That is to say that Υ appropriately restricts the parameter space to those values for which the dynamics of each component $\xi\in\Xi$ remain passive or strictly passive.

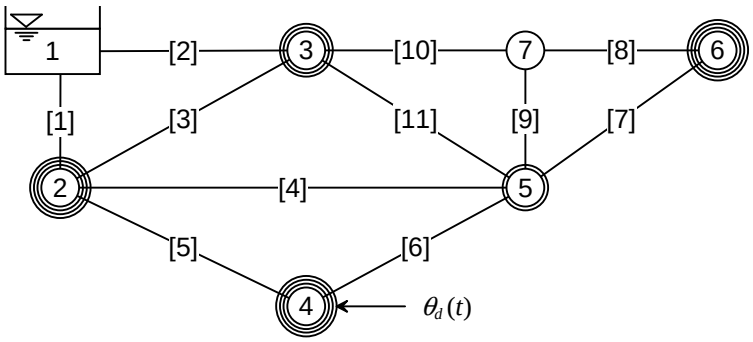

Figure 6.1: The 11-pipe network from Examples 6.5 and 6.6. The rings around the nodes indicate the locations of pressure measurements for the different cases described in Table 6.2: case 1 and 2 nodes have three rings (nodes 2, 4, and 6); case 3 nodes have two or three rings (nodes 2, 4, 6, and 3); case 4 nodes have one, two or three rings (nodes 2, 4, 6, 3 and 5); case 5 includes all the nodes. Note that for case 1, the demand at node 4 $\theta_d(t)$ is not measured. Also note that $\theta_d(t)$ is taken as directed into node 4.

2. The proposed method above assumes that the error variance matrices in $\mathcal{S}$ can be adequately estimated from the measurement system specifications.

6.4.3 Numerical examples

The following numerical examples demonstrate the ability of the proposed decoupling MLE method as outlined in Corollary 6.2 to accurately estimate a hydraulic network's parameters. All computational procedures were undertaken as outlined in Appendix E.

Example 6.5. *Consider the 11-pipe network in Figure 6.1 comprised of TSF pipes (network details are in Appendix D), for which there are five different nodal partitioning cases as depicted in Figure 6.1: case 1 consists of only pressure measurements at nodes* $\{2, 4, 6\}$*; case 2 consists of a flow measurement at node 4 and pressure measurements at nodes* $\{2, 4, 6\}$*; case 3 consists of a flow measurement at node 4 and pressure measurements at nodes* $\{2, 3, 4, 6\}$*; case 4 consists of a flow measurement at node 4 and pressure measurements at nodes* $\{2, 3, 4, 5, 6\}$*; case 5 consists of a flow measurement at node 4 and pressure measurements at nodes* $\{2, 3, 4, 5, 6, 7\}$*. The nodal set partitions from Definition 6.6 corresponding to these cases is given in Table 6.2.*

The raw time-domain data is obtained from a MOC simulation with added Gaussian noise. The frequency-domain data is obtained from the DFT of the time-domain data. For the MOC simulation, the system is excited into a steady-oscillatory transient state by a multi-sine flow perturbation at node 4 consisting of 983 equi-spaced

Table 6.2: The $\mathscr{M}$-network nodal partitioning for Examples 6.5 and 6.6 from Definition 6.6.

Nodal set	Node sets for each case				
	case 1	case 2	case 3	case 4	case 5
$\mathcal{A}_1$	$\emptyset$	$\{4\}$	$\{4\}$	$\{4\}$	$\{4\}$
$\mathcal{A}_2$	$\{4\}$	$\emptyset$	$\emptyset$	$\emptyset$	$\emptyset$
$\mathcal{A}_3$	$\emptyset$	$\emptyset$	$\emptyset$	$\emptyset$	$\emptyset$
$\mathcal{A}_4$	$\emptyset$	$\emptyset$	$\emptyset$	$\emptyset$	$\emptyset$
$\mathcal{B}_1$	$\{2,6\}$	$\{2,6\}$	$\{2,3,6\}$	$\{2,3,5,6\}$	$\{2,3,5,6,7\}$
$\mathcal{B}_2$	$\{3,5,7\}$	$\{3,5,7\}$	$\{5,7\}$	$\{7\}$	$\emptyset$
$\mathcal{C}_1$	$\emptyset$	$\emptyset$	$\emptyset$	$\emptyset$	$\emptyset$
$\mathcal{C}_2$	$\{1\}$	$\{1\}$	$\{1\}$	$\{1\}$	$\{1\}$

frequencies from 0 to 15 Hz with amplitudes ranging from 0.01 to 0.1 L/s. The time-domain measurement errors are taken as independent zero mean Gaussian variates with standard deviations of 1 kPa for the pressure measurements and 0.32 L/s for the flow measurement. It is assumed that none of the pipeline parameter values are known, but that: the wavespeed is on the interval [900,1200] m/s; the friction factor is on the interval [0.015,0.04]; the diameters are known to within ±10 mm of their actual value; and the pipe lengths are known to within ±20 m of their actual value. Given the parameterisation of the TSF pipes from Example 6.1, the parameter space is 33-dimensional and is given by

$$\boldsymbol{\vartheta} = \{r_{o1}, \Gamma_{o1}, Z_{co1}\} \cup \cdots \cup \{r_{o11}, \Gamma_{o11}, Z_{co11}\}\,.$$

Corollary 6.2 was used as the framework to determine the MLE, where the minimiser $\widehat{\boldsymbol{\vartheta}}$ was computed using particle swarm optimisation (PSO). The results of 10 independent trials for each case are summarised in the box plots in Figure 6.2 and the statistics in Table 6.3

Considering Figure 6.2 and Table 6.3, a first observation is that as the number of measured states increases, so does the quality of the parameter estimates as quantified by the, on average, reduced bias (lower value of the error medians) and lower variability variable (lower value of the error IQRs). This improvement is increasingly significant when the flow measurement is utilised in the estimation process (cases 2, 3, 4, and 5). For the cases that incorporate the flow measurement, the variability in the estimates is significantly reduced.

Interesting observations can be made by comparing the estimates for the differ-

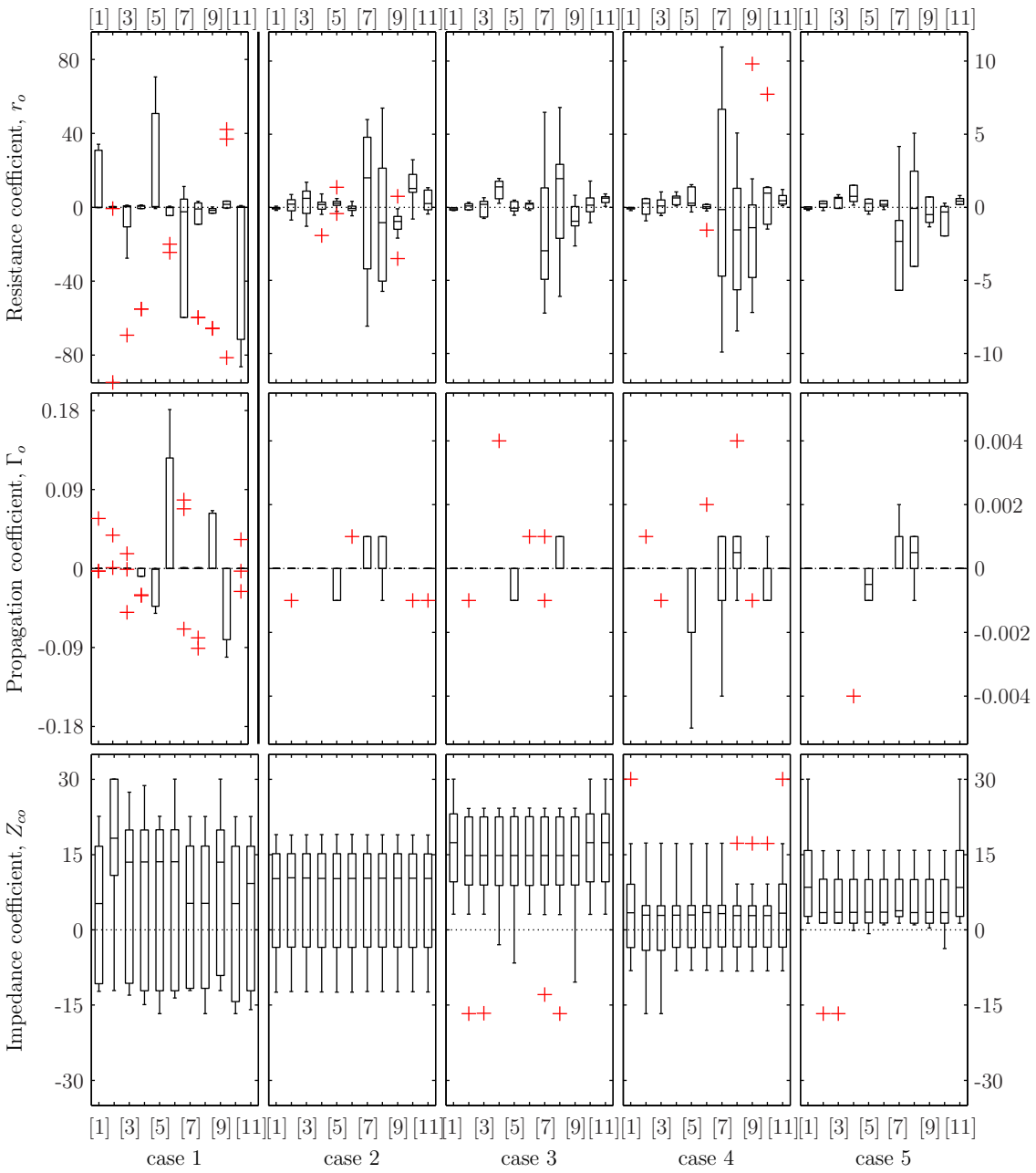

Figure 6.2: Box plots of the relative errors (%) (given on the vertical scale) of the parameter estimates from Example 6.5. The figure rows are associated with particular parameters, and the figure columns with particular cases. Each box and whisker set is associated with a pipe. For each case, 10 independent trials were performed. The + indicate outliers. Note that the top two figures in the first column have independent vertical axes.

ent parameters. For all pipes the resistance coefficient r_o was accurately estimated by the median of the 10 trials for all cases, even for case 1 despite the high IQR. The propagation coefficient Γ_o was the most accurately estimated parameter with a consistently low interquartile range IQR for all cases. The accuracy of the estimates is quite surprising (the estimate medians are all within 0.001% of the true values for

Table 6.3: Summary statistics of relative errors of pipe parameter estimates for Example 6.5. The parameter statistics for each pipe (median and the interquartile range, IQR) are based on 10 trials. The summary statistics (minimum, mean and maximum) are based on the parameter statistics from the 11 pipes (the mean of the medians was taken as the average of the absolute values of the medians).

Parameter	Statistic type		Relative error statistics (%)				
			case 1	case 2	case 3	case 4	case 5
r_o	median	*min*	*-2.462*	*-1.057*	*-2.979*	*-1.545*	*-2.326*
		mean	0.762	0.636	0.796	0.534	0.522
		max	*1.597*	*2.019*	*1.958*	*0.971*	*0.755*
	IQR	*min*	*0.391*	*0.091*	*0.168*	*0.096*	*0.174*
		mean	23.043	2.148	1.624	2.779	1.743
		max	*71.953*	*9.004*	*6.264*	*11.412*	*6.516*
Γ_o	median	*min*	*-0.0010*	*0.0000*	*0.0000*	*0.0000*	*-0.0005*
		mean	0.0001	0.0000	0.0000	0.0000	0.0001
		max	*0.0000*	*0.0000*	*0.0000*	*0.0005*	*0.0005*
	IQR	*min*	*0.0000*	*0.0000*	*0.0000*	*0.0000*	*0.0000*
		mean	0.0295	0.0003	0.0002	0.0005	0.0003
		max	*0.1260*	*0.0010*	*0.0010*	*0.0020*	*0.0010*
Z_{co}	median	*min*	*5.25*	*10.22*	*14.82*	*2.83*	*3.45*
		mean	10.58	10.28	15.53	3.06	4.41
		max	*18.27*	*10.36*	*17.40*	*3.46*	*8.48*
	IQR	*min*	*19.19*	*18.61*	*13.53*	*8.18*	*7.38*
		mean	29.00	18.65	13.59	9.18	9.39
		max	*32.10*	*18.70*	*13.70*	*12.63*	*13.17*

all pipes in all cases), but can be understood as follows. The parameter $\Gamma_o = l/c_o$ is essentially the inverse of the pipes period, and as such it is involved in determining the actual location of the network's harmonics in the frequency response. If the model harmonics are even slightly mismatched to the measured harmonics, the error between the model and the measured data will be large. Hence the estimation process is highly sensitive to the harmonic locations and, by implication, the parameter Γ_o.

The impedance coefficient was estimated with the lowest accuracy and highest variability of all the parameters. As illustrated in Figure 6.2, the positive bias in the errors implies that the estimates for Z_{co} were typically high. In comparison to Γ_o, both the parameters r_o and Z_{co} affect the damping nature of the networks dynamic behaviour, and hence are involved in determining the magnitude of the network's harmonics in the frequency response. The error between the model and

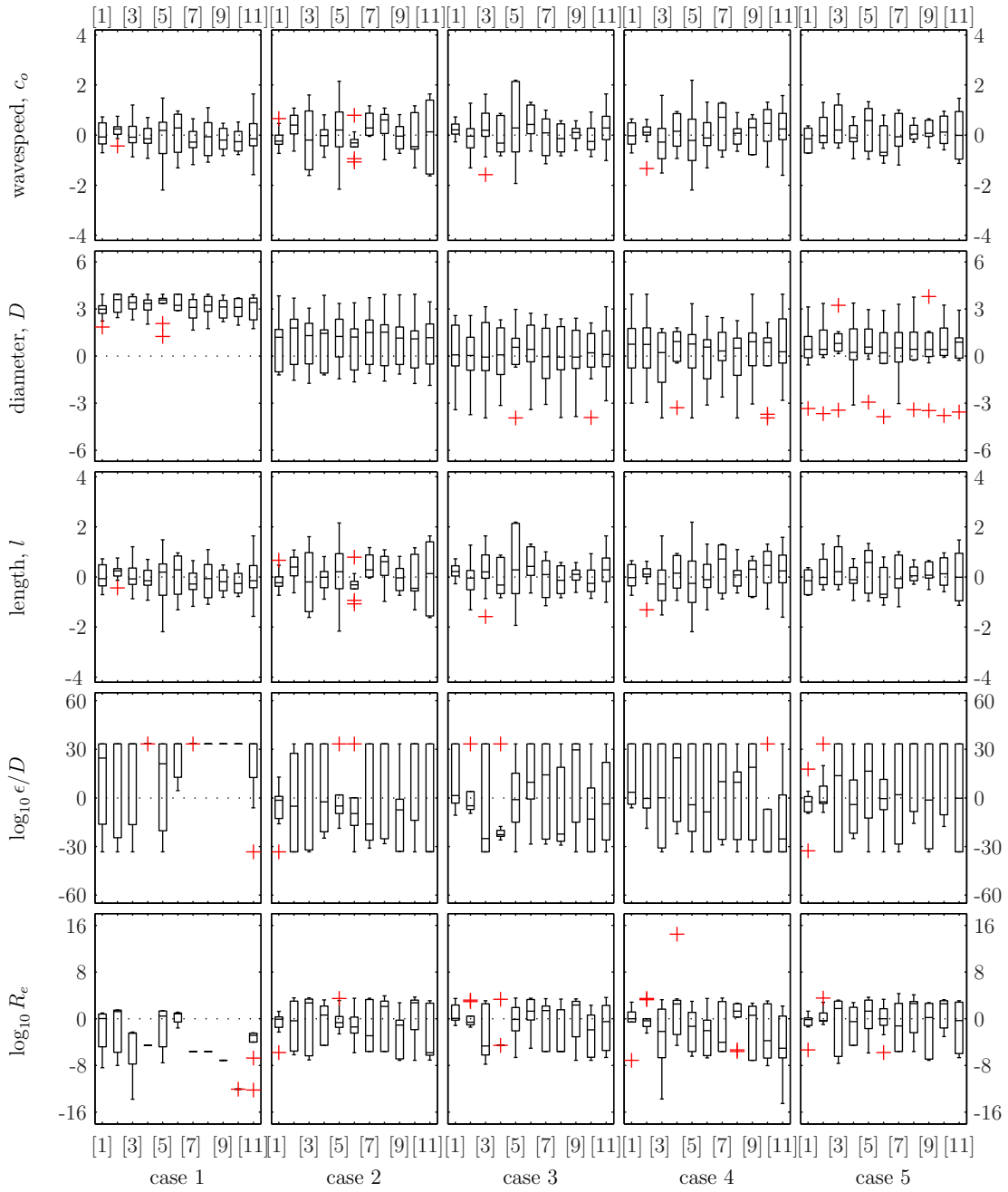

Figure 6.3: Box plots of the relative errors (%) of the parameter estimates from Example 6.6. The figure rows are associated with particular parameters, and the figure columns with particular cases. Each box and whisker set is associated with a pipe. For each case, 10 independent trials were performed. The + indicate outliers.

the measured data is still sensitive to the harmonic magnitudes, but not as sensitive as it is to the harmonic locations. Hence the estimation process is less sensitive to r_o and Z_{co}.

The parameters for all pipes seemed to be similarly identifiable, with the box plots for r_o and Γ_o showing slightly higher IQRs for pipes [7] to [9].

Table 6.4: Summary statistics of relative errors of pipe parameter estimates for Example 6.6. The parameter statistics for each pipe (median and the interquartile range, IQR) are based on 10 trials. The summary statistics (minimum, mean and maximum) are based on the parameter statistics from the 11 pipes (the mean of the medians was taken as the average of the absolute values of the medians).

Parameter	Statistic type		Relative error statistics (%)				
			case 1	case 2	case 3	case 4	case 5
wavespeed, c_o	median	*min*	*-0.282*	*-0.456*	*-0.320*	*-0.280*	*-0.690*
		mean	0.179	0.262	0.215	0.246	0.189
		max	*0.286*	*0.608*	*0.422*	*0.716*	*0.581*
	IQR	*min*	*0.299*	*0.304*	*0.401*	*0.324*	*0.546*
		mean	0.875	1.160	1.117	1.137	1.141
		max	*1.524*	*2.957*	*2.807*	*1.883*	*1.895*
diameter, D	median	*min*	*2.984*	*1.096*	*-0.072*	*0.226*	*0.207*
		mean	3.288	1.331	0.158	0.628	0.486
		max	*3.604*	*1.785*	*0.564*	*0.929*	*0.892*
	IQR	*min*	*0.334*	*2.367*	*1.664*	*1.771*	*1.105*
		mean	0.926	2.606	2.502	2.330	1.611
		max	*1.378*	*2.884*	*3.192*	*3.161*	*1.968*
length, l	median	*min*	*-0.280*	*-0.457*	*-0.320*	*-0.280*	*-0.689*
		mean	0.179	0.262	0.215	0.250	0.189
		max	*0.284*	*0.608*	*0.422*	*0.716*	*0.580*
	IQR	*min*	*0.299*	*0.304*	*0.401*	*0.324*	*0.545*
		mean	0.875	1.160	1.117	1.146	1.141
		max	*1.525*	*2.957*	*2.806*	*1.930*	*1.895*
$C_\epsilon = \log_{10}\left(\frac{\epsilon}{D}\right)$	median	*min*	*21.10*	*-33.23*	*-25.12*	*-33.33*	*-4.06*
		mean	31.42	16.41	13.43	12.61	9.98
		max	*33.33*	*33.33*	*29.60*	*24.73*	*33.33*
	IQR	*min*	*0.00*	*11.48*	*3.78*	*26.27*	*9.46*
		mean	22.94	44.26	38.42	48.27	42.09
		max	*57.90*	*66.67*	*66.66*	*66.67*	*66.67*
$C_{\mathbb{R}_e} = \log_{10} \mathbb{R}_e$	median	*min*	*-12.045*	*-5.833*	*-5.616*	*-5.031*	*-1.232*
		mean	3.898	1.867	2.092	2.100	0.991
		max	*1.221*	*2.747*	*2.332*	*2.511*	*2.603*
	IQR	*min*	*0.000*	*1.820*	*0.000*	*1.350*	*1.300*
		mean	2.487	6.319	5.118	6.046	5.731
		max	*7.224*	*9.697*	*8.759*	*9.300*	*9.551*

Example 6.6. *Consider the 11-pipe network in Figure 6.1 comprised of TUF pipes (network details are in Appendix D), for which there are four different nodal parti-*

tioning cases as depicted in Figure 6.1 and described in Example 6.5 (the nodal set partitions from Definition 6.6 corresponding to these cases is given in Table 6.2).

All details pertaining to system excitation, measurement error and parameter uncertainty for this example are taken from Example 6.5 with the addition that the relative roughnesses are known to be on the interval [0.0001, 0.01] and the steady-state velocities are known to be on the interval [0.1, 10] m/s. Given the parameterisation of the TUF pipes from Example 6.2, the parameter space is 55 dimensional and is given by $\boldsymbol{\vartheta} = \boldsymbol{\vartheta}_1 \cup \cdots \cup \boldsymbol{\vartheta}_{11}$ *where*

$$\boldsymbol{\vartheta}_i = \{c_i, D_i, l_i, C_\epsilon, C_{\mathbb{R}_e}\}\,.$$

where

$$C_\epsilon = \log_{10}\left(\frac{\epsilon_i}{D_i}\right), \quad C_{\mathbb{R}_e} = \log_{10}\mathbb{R}_{ei}.$$

Corollary 6.2 was used as the framework to determine the MLE, where the minimiser $\widehat{\boldsymbol{\Upsilon}}$ *was computed using PSO. The results of 10 independent trials for each case are summarised in the box plots in Figure 6.3 and the statistics in Table 6.4*

As observed with Example 6.5, Figure 6.3 and Table 6.4 show that the inclusion of the flow measurement in cases 2 to 5 yields particularly better parameter estimates than for case 1 where the flow measurement was not included. This is particularly true for the estimates of the parameters D, C_ϵ and $C_{\mathbb{R}_e}$ where significant biases are clearly observed for case 1 in Figure 6.3.

Consistent with Example 6.5, the parameters that influence the harmonic locations (wavespeed c_o and pipe length l) are estimated with a higher accuracy than the other parameters. Interestingly, it is observed that the distributions of the errors for the estimates of c_o and l are nearly the same. This can be explained in that it is the ratio l/c_o that determines the harmonic locations. Therefore, if the estimate for l is high, then the estimate for c_o will also tend to be high to ensure a better match of the harmonic locations of the model with the measured data.

The parameters D and $C_{\mathbb{R}_e}$ were accurately estimated, particularly for cases 2 to 5. However, the other parameter associated with energy loss and dissipation, C_ϵ, was not as accurately identified consistently for all pipes in any case. This apparent lack of sensitivity of the likelihood function to the C_ϵ parameters may be understood by the fact that ϵ/D only appears in the expression for the pipeline functions Γ and Z_c through the *Vardy and Brown* [2007] functions A^* and B^* (see Example 2.7) which are also dependent on $\mathbb{R}_e$.

In summary, Examples 6.5 and 6.6 have demonstrated the ability of the decoupled MLE method to successfully estimate most hydraulic network parameters for

networks comprised of the TSF and TUF pipe types. Difficulty with some of the parameters associated with energy dissipation was observed. However, these difficulties are not surprising given that both the examples represent complex high dimensional optimisation problems, being 33 and 55 dimensions respectively.

6.5 An Expectation-Maximisation Method

The existence of the decoupling filter developed in the Section 6.4 relied on the nodal partitioning from Definition 6.6 to be configured such that $\mathcal{A}_4 = \emptyset$, which means that there existed no node within the network for which both the pressure and flow were unknown and unmeasured[11]. This scenario is common, and in practical field tests it has generally been achieved [*Stephens*, 2008]. However, it is important to consider techniques that are able to deal with scenarios for which it may not be possible to know or measure the state variables at each node.

This section presents a new methodology that deals the identification of $\mathscr{M}$-networks under the case that there are nodes for which no information exists (*i.e.* nodes for which neither the pressure or nodal flow are known or measures, meaning that $\mathcal{A}_4 \neq \emptyset$). This treatment adopts the framework of the expectation-maximisation (EM) algorithm [*Dempster et al.*, 1977], which is a statistical method of parameter identification used in situations where the data is incomplete, or there exist hidden state variables upon which the system depends [*Watanabe and Yamaguchi*, 2004]. This section is structured as follows. Section 6.5.1 summarises the EM algorithm and gives a theorem presenting the form of the EM algorithm for the general statistical model that encompasses the network identification problem considered here. Section 6.5.2 shows how the measured and unmeasured state model (6.23) fits into this framework, finally, Section 6.5.3 gives some numerical examples.

6.5.1 General statistical model

The fundamental theorem underlying the EM algorithm is presented below.

Theorem 6.4. ***The EM algorithm [Dempster et al., 1977]:*** *Given the complete data* $\left\{\widetilde{\mathcal{U}}, \widetilde{\mathcal{V}}\right\}$ *drawn from the joint distribution* $f\left(\widetilde{\mathcal{U}}, \widetilde{\mathcal{V}}|\boldsymbol{\vartheta}\right)$ *parameterised by* $\boldsymbol{\vartheta}$*, for a given* $\boldsymbol{\vartheta}_0$ *the following sequence of iterates*

$$\boldsymbol{\vartheta}_k = \arg\max_{\boldsymbol{\vartheta}} \mathrm{E}\left[\ln\left(f\left(\widetilde{\mathcal{U}}, \widetilde{\mathcal{V}}|\boldsymbol{\vartheta}\right)\right)\Big|\widetilde{\mathcal{U}}, \boldsymbol{\vartheta}_{k-1}\right], \quad k = 1, \ldots \tag{6.62}$$

[11] This requirement is essentially equivalent to that of the network problems in Definitions 3.5, and 4.4, where the all boundary conditions must be specified for the problems to be well posed.

converges to a local maximiser of the marginal likelihood function $f\left(\widetilde{\mathcal{U}}|\boldsymbol{\vartheta}\right)$ *of the incomplete data* $\widetilde{\mathcal{U}}$*, provided* $f\left(\mathcal{U}|\boldsymbol{\vartheta}\right)$ *is bounded on* $\mathcal{U}$*.*

Remarks:

1. The process (6.62) has many different interpretations [*Watanabe and Yamaguchi*, 2004], but the most simple explanation is as follows. The k-th iterate $\boldsymbol{\vartheta}_k$ is given as the value that maximises the expected log-likelihood of the joint distribution of the measured and unmeasured states $f\left(\widetilde{\mathcal{U}}, \widetilde{\mathcal{V}}|\boldsymbol{\vartheta}\right)$ over the conditional probability space $\widetilde{\mathcal{V}}|\widetilde{\mathcal{U}}, \boldsymbol{\vartheta}_{k-1}$ of the unmeasured states given the measured states and the $(k-1)$-th parameter estimate.

2. The useful aspect of this approach is that the expectation integrates over the unmeasured variables explicitly removing them from the maximisation function. Each iterate updates the conditional distribution of the unmeasured states.

3. The process (6.62) has the following properties that the sequence of iterates is nondecreasing, and will converge to a local maxima [*Watanabe and Yamaguchi*, 2004]. It is, however, not guaranteed that (6.62) will converge to the MLE.

For the application considered here, the general statistical model has $\widetilde{\mathcal{U}}$ and $\widetilde{\mathcal{V}}$ as collections of vector valued complex Gaussian variates, with unknown means, that are known to be related by the equality constraint (6.80) which is parameterised by $\boldsymbol{\vartheta}$. Given this, the problem is to derive an EM based process for the estimation of the parameter $\boldsymbol{\vartheta}$. The form of this process is outlined in the following theorem, and constructed in the ensuing proof.

Theorem 6.5. *Consider the data sets of complex vectors* $\widetilde{\mathcal{U}} = \{\widetilde{\boldsymbol{u}}_1, \ldots, \widetilde{\boldsymbol{u}}_M\}$*, and* $\widetilde{\mathcal{V}} = \{\widetilde{\boldsymbol{v}}_1, \ldots, \widetilde{\boldsymbol{v}}_M\}$ *distributed as the complex Gaussian variates*

$$\left[\begin{array}{c} \widetilde{\boldsymbol{u}}_i \\ \hdashline \widetilde{\boldsymbol{v}}_i \end{array}\right] \sim \mathcal{N}_c\left(\left[\begin{array}{c} \boldsymbol{u}_i \\ \hdashline \boldsymbol{v}_i \end{array}\right], \left[\begin{array}{c:c} \boldsymbol{\Sigma}_{mi} & \mathbf{0} \\ \hdashline \mathbf{0} & \boldsymbol{\Sigma}_{ui} \end{array}\right]\right), \quad i = 1, \ldots, M$$

where the $\boldsymbol{\Sigma}_{mi}$ *and* $\boldsymbol{\Sigma}_{ui}$ *are real positive definite matrices and*

$$\mathrm{COV}\left[\widetilde{\boldsymbol{u}}_i, \widetilde{\boldsymbol{u}}_j\right], \mathrm{COV}\left[\widetilde{\boldsymbol{u}}_i, \widetilde{\boldsymbol{v}}_j\right], \mathrm{COV}\left[\widetilde{\boldsymbol{v}}_i, \widetilde{\boldsymbol{v}}_j\right] = \mathbf{0}, \quad j \neq i.$$

The unknown means $\boldsymbol{u}_i$ *and* $\boldsymbol{v}_i$ *are related by the equality constraints*

$$\left[\begin{array}{c:c} \boldsymbol{G}_{mi}(\boldsymbol{\vartheta}) & \boldsymbol{G}_{ui}(\boldsymbol{\vartheta}) \end{array}\right] \left[\begin{array}{c} \boldsymbol{u}_i \\ \hdashline \boldsymbol{v}_i \end{array}\right] = \mathbf{0}, \quad i = 1, \ldots, M \tag{6.63}$$

where the complex matrices $\boldsymbol{G}_{mi} \in \mathbb{C}^{N\times n_m}$, *and* $\boldsymbol{G}_{ui} \in \mathbb{C}^{N\times n_u}$ *are parameterised by* $\boldsymbol{\vartheta}$ *and* $n_u \leq N \leq n_m$ *where*

$$\operatorname{rank} \boldsymbol{G}_{ui}(\boldsymbol{\vartheta}) = n_u \tag{6.64}$$

$$\operatorname{rank} \left[\begin{array}{c:c} \boldsymbol{G}_{mi}(\boldsymbol{\vartheta}) & \boldsymbol{G}_{ui}(\boldsymbol{\vartheta}) \end{array} \right] = N \tag{6.65}$$

for all $i = 1, \ldots, M$ *and* $\boldsymbol{\vartheta} \in \boldsymbol{\Upsilon}$. *The EM algorithm (Theorem 6.5) for estimating* $\boldsymbol{\vartheta}$ *based on the incomplete data* $\mathcal{U}$ *is given by the sequence*

$$\boldsymbol{\vartheta}_{k+1} = \arg\max_{\boldsymbol{\vartheta}\in\boldsymbol{\Upsilon}} \sum_{i=1}^{M} Q_i\left(\widetilde{\boldsymbol{u}}_i, \boldsymbol{\vartheta}_k, \boldsymbol{\vartheta}\right) \tag{6.66}$$

where $Q_i\left(\widetilde{\boldsymbol{u}}_i, \boldsymbol{\vartheta}_k, \boldsymbol{\vartheta}\right)$ *is the negative of the expectation of the log likelihood of the joint distribution of* $\widetilde{\boldsymbol{u}}_i$ *and* $\widetilde{\boldsymbol{v}}_i$ *conditional on* $\widetilde{\boldsymbol{u}}_i$ *and* $\boldsymbol{\vartheta}_k$ *(constant terms neglected), and is given by*

$$\begin{aligned} Q_i\left(\widetilde{\boldsymbol{u}}, \boldsymbol{\vartheta}_k, \boldsymbol{\vartheta}\right) = \; & \widetilde{\boldsymbol{u}}^H \boldsymbol{C}_{mmi}\left(\boldsymbol{\vartheta}\right) \widetilde{\boldsymbol{u}} \\ & -2\mathbb{R}\mathrm{e}\left\{\widetilde{\boldsymbol{u}}^H \boldsymbol{C}_{mui}\left(\boldsymbol{\vartheta}\right) \boldsymbol{C}_{uui}^{-1}\left(\boldsymbol{\vartheta}_k\right) \boldsymbol{C}_{umi}\left(\boldsymbol{\vartheta}_k\right) \widetilde{\boldsymbol{u}}\right\} \\ & +\operatorname{tr}\left\{\boldsymbol{C}_{uui}\left(\boldsymbol{\vartheta}\right) \boldsymbol{\Sigma}_{ui}\right\} \\ & +\widetilde{\boldsymbol{u}}^H \boldsymbol{C}_{mui}\left(\boldsymbol{\vartheta}_k\right) \boldsymbol{C}_{uui}^{-1}\left(\boldsymbol{\vartheta}_k\right) \boldsymbol{C}_{uui}\left(\boldsymbol{\vartheta}\right) \boldsymbol{C}_{uui}^{-1}\left(\boldsymbol{\vartheta}_k\right) \boldsymbol{C}_{umi}\left(\boldsymbol{\vartheta}_k\right) \widetilde{\boldsymbol{u}} \end{aligned} . \tag{6.67}$$

where the complex matrix terms are

$$\left.\begin{aligned} \boldsymbol{C}_{mmi}(\boldsymbol{\vartheta}) &= \boldsymbol{G}_{mi}^H(\boldsymbol{\vartheta})\boldsymbol{\Lambda}_i^{-1}(\boldsymbol{\vartheta})\boldsymbol{G}_{mi}(\boldsymbol{\vartheta}) \\ \boldsymbol{C}_{mui}(\boldsymbol{\vartheta}) &= \boldsymbol{G}_{mi}^H(\boldsymbol{\vartheta})\boldsymbol{\Lambda}_i^{-1}(\boldsymbol{\vartheta})\boldsymbol{G}_{ui}(\boldsymbol{\vartheta}) \\ \boldsymbol{C}_{umi}(\boldsymbol{\vartheta}) &= \boldsymbol{G}_{ui}^H(\boldsymbol{\vartheta})\boldsymbol{\Lambda}_i^{-1}(\boldsymbol{\vartheta})\boldsymbol{G}_{mi}(\boldsymbol{\vartheta}) \\ \boldsymbol{C}_{uui}(\boldsymbol{\vartheta}) &= \boldsymbol{G}_{ui}^H(\boldsymbol{\vartheta})\boldsymbol{\Lambda}_i^{-1}(\boldsymbol{\vartheta})\boldsymbol{G}_{ui}(\boldsymbol{\vartheta}) \end{aligned}\right\} \tag{6.68}$$

and

$$\boldsymbol{\Lambda}_i(\boldsymbol{\vartheta}) = \boldsymbol{G}_{mi}(\boldsymbol{\vartheta})\boldsymbol{\Sigma}_{mi}\boldsymbol{G}_{mi}^H(\boldsymbol{\vartheta}) + \boldsymbol{G}_{ui}(\boldsymbol{\vartheta})\boldsymbol{\Sigma}_{ui}\boldsymbol{G}_{ui}^H(\boldsymbol{\vartheta}). \tag{6.69}$$

Proof. The determination of an EM process for the parameter $\boldsymbol{\vartheta}$ requires three distinct steps. Firstly, the determination of the joint probability density function (PDF) for the $\widetilde{\boldsymbol{u}}_i$ and $\widetilde{\boldsymbol{v}}_i$ given analytic forms of the MLE for the unknown means $\widehat{\boldsymbol{u}}_i$ and $\widehat{\boldsymbol{v}}_i$. Secondly, the expectation of the log-likelihood of the joint density over the conditional density of the unmeasured data $\widetilde{\boldsymbol{v}}_i$ given our measured data $\widetilde{\boldsymbol{u}}_i$ and $\boldsymbol{\vartheta}$. Thirdly, the expression of this log-likelihood purely as a function of $\widetilde{\boldsymbol{u}}_i$ by determining an estimate for $\boldsymbol{v}_i$ given only $\widetilde{\boldsymbol{u}}_i$.

Concerning the first step, as all the variates are independent for each $i = 1, \ldots, M$, the Lagrange multiplier technique adopted in the proof of Theorem 6.3,

can be used to determine an analytic expression of the MLEs for the unknown means $\boldsymbol{u}_i$ and $\boldsymbol{v}_i$ as a function of $\widetilde{\boldsymbol{v}}_i$, $\widetilde{\boldsymbol{u}}_i$, and $\boldsymbol{\vartheta}$ as

$$\left[\begin{array}{c} \widehat{\boldsymbol{u}}_i(\boldsymbol{\vartheta}) \\ \hdashline \widehat{\boldsymbol{v}}_i(\boldsymbol{\vartheta}) \end{array}\right] = \left(\left[\begin{array}{c:c} \boldsymbol{I} & \boldsymbol{0} \\ \hdashline \boldsymbol{0} & \boldsymbol{I} \end{array}\right] - \left[\begin{array}{c:c} \boldsymbol{\Sigma}_{mi} & \boldsymbol{0} \\ \hdashline \boldsymbol{0} & \boldsymbol{\Sigma}_{ui} \end{array}\right] \left[\begin{array}{c} \boldsymbol{G}_{mi}^H(\boldsymbol{\vartheta}) \\ \hdashline \boldsymbol{G}_{ui}^H(\boldsymbol{\vartheta}) \end{array}\right] \boldsymbol{\Lambda}_i^{-1}(\boldsymbol{\vartheta}) \left[\begin{array}{c:c} \boldsymbol{G}_{mi}(\boldsymbol{\vartheta}) & \boldsymbol{G}_{ui}(\boldsymbol{\vartheta}) \end{array}\right]\right) \left[\begin{array}{c} \widetilde{\boldsymbol{u}}_i \\ \hdashline \widetilde{\boldsymbol{v}}_i \end{array}\right] \tag{6.70}$$

where

$$\boldsymbol{\Lambda}_i(\boldsymbol{\vartheta}) = \left[\begin{array}{c:c} \boldsymbol{G}_{mi}(\boldsymbol{\vartheta}) & \boldsymbol{G}_{ui}(\boldsymbol{\vartheta}) \end{array}\right] \left[\begin{array}{c:c} \boldsymbol{\Sigma}_{mi} & \boldsymbol{0} \\ \hdashline \boldsymbol{0} & \boldsymbol{\Sigma}_{ui} \end{array}\right] \left[\begin{array}{c:c} \boldsymbol{G}_{mi}(\boldsymbol{\vartheta}) & \boldsymbol{G}_{ui}(\boldsymbol{\vartheta}) \end{array}\right]^H \tag{6.71}$$

which is equivalent to (6.69). The existence of $\boldsymbol{\Lambda}_i^{-1}$ on $\boldsymbol{\vartheta} \in \boldsymbol{\Upsilon}$ can be demonstrated by the positive definiteness of $\boldsymbol{\Lambda}_i$ (as diag $\{\boldsymbol{\Sigma}_{mi}, \boldsymbol{\Sigma}_{mi}\}$ is positive definite, then so is $\boldsymbol{\Lambda}_i$ as $\left[\begin{array}{c:c} \boldsymbol{G}_{mi} & \boldsymbol{G}_{ui} \end{array}\right]$ is full row rank). Given these MLEs, the joint distribution for the measured and unmeasured i-th vector variates is

$$f_i\left(\widetilde{\boldsymbol{u}}_i, \widetilde{\boldsymbol{v}}_i | \widehat{\boldsymbol{u}}_i, \widehat{\boldsymbol{v}}_i, \boldsymbol{\vartheta}\right) = \frac{1}{\pi^n |\boldsymbol{\Sigma}_{mi}||\boldsymbol{\Sigma}_{ui}|} \exp\left\{ - \left[\begin{array}{c} \widetilde{\boldsymbol{u}}_i \\ \hdashline \widetilde{\boldsymbol{v}}_i \end{array}\right]^H \left[\begin{array}{c:c} \boldsymbol{C}_{mmi}(\boldsymbol{\vartheta}) & \boldsymbol{C}_{mui}(\boldsymbol{\vartheta}) \\ \hdashline \boldsymbol{C}_{umi}(\boldsymbol{\vartheta}) & \boldsymbol{C}_{uui}(\boldsymbol{\vartheta}) \end{array}\right] \left[\begin{array}{c} \widetilde{\boldsymbol{u}}_i \\ \hdashline \widetilde{\boldsymbol{v}}_i \end{array}\right] \right\} \tag{6.72}$$

for $i = 1, \ldots, M$, where the complex matrix functions $\boldsymbol{C}_{mmi}$, $\boldsymbol{C}_{mui}$, $\boldsymbol{C}_{mmi}$, and $\boldsymbol{C}_{uui}$ are given by (6.68). The negative of the log-likelihood of the joint distribution (6.72) can be expressed as

$$\begin{aligned} &-\ln\left(f_i\left(\widetilde{\boldsymbol{u}}_i, \widetilde{\boldsymbol{v}}_i | \widehat{\boldsymbol{u}}_i, \widehat{\boldsymbol{v}}_i, \boldsymbol{\vartheta}\right)\right) = \\ &\quad \pi^n + |\Sigma_{mi}| + |\Sigma_{ui}| + \underbrace{\widetilde{\boldsymbol{u}}_i^H \boldsymbol{C}_{mmi} \widetilde{\boldsymbol{u}}_i}_{\text{term I}} + \underbrace{\widetilde{\boldsymbol{u}}_i^H \boldsymbol{C}_{mui} \widetilde{\boldsymbol{v}}_i + \widetilde{\boldsymbol{v}}_i^H \boldsymbol{C}_{umi} \widetilde{\boldsymbol{u}}_i}_{\text{term II}} + \underbrace{\widetilde{\boldsymbol{v}}_i^H \boldsymbol{C}_{uui} \widetilde{\boldsymbol{v}}_i}_{\text{term III}} \cdot \end{aligned} \tag{6.73}$$

Concerning the second step, as $\widetilde{\boldsymbol{u}}_i$ and $\widetilde{\boldsymbol{v}}_i$ are independent, the conditional density of $\widetilde{\boldsymbol{v}}_i$ is in fact the marginal [*Rice*, 1995] which is given by

$$\widetilde{\boldsymbol{v}}_i \sim \mathcal{N}_c\left(\boldsymbol{v}_i, \boldsymbol{\Sigma}_{ui}\right), \quad i = 1, \ldots, M,$$

however, as $\boldsymbol{v}_i$ is unknown and, in the conditional context, requires estimation conditional on knowing $\widetilde{\boldsymbol{u}}_i$ and $\boldsymbol{\vartheta}_k$, the conditional density of $\widetilde{\boldsymbol{v}}_i$ is expressed as

$$\widetilde{\boldsymbol{v}}_i \sim \mathcal{N}_c\left(\overline{\boldsymbol{v}}_i, \boldsymbol{\Sigma}_{ui}\right), \quad i = 1, \ldots, M, \tag{6.74}$$

where $\overline{\boldsymbol{v}}_i = \mathrm{E}\left[\boldsymbol{v}_i | \widetilde{\boldsymbol{u}}_i, \boldsymbol{\vartheta}_k\right]$. Given the conditional distribution (6.74), the expectation

of the log-likelihood of the joint distribution (6.72) with respect to this probability measure can be determined. The EM algorithm requires the expectation of (6.73) over the probability space defined by the conditional PDF (6.74). Performing this integration term by term, neglecting the terms that are constant with respect to $\boldsymbol{\vartheta}$, yields

$$\begin{aligned}
\mathrm{E}\left[\text{term I}|\,\widetilde{\boldsymbol{u}}_i, \boldsymbol{\vartheta}_k\right] &= \widetilde{\boldsymbol{u}}_i^H \boldsymbol{C}_{mmi}\left(\boldsymbol{\vartheta}\right)\widetilde{\boldsymbol{u}}_i \\
\mathrm{E}\left[\text{term II}|\,\widetilde{\boldsymbol{u}}_i, \boldsymbol{\vartheta}_k\right] &= \widetilde{\boldsymbol{u}}_i^H \boldsymbol{C}_{mui}\left(\boldsymbol{\vartheta}\right)\overline{\boldsymbol{v}}_i + \overline{\boldsymbol{v}}_i^H \boldsymbol{C}_{mui}\left(\boldsymbol{\vartheta}\right)\widetilde{\boldsymbol{u}}_i \\
&= 2\mathbb{R}\mathrm{e}\left\{\widetilde{\boldsymbol{u}}_i^H \boldsymbol{C}_{mui}\left(\boldsymbol{\vartheta}\right)\overline{\boldsymbol{v}}_i\right\} \\
\mathrm{E}\left[\text{term III}|\,\widetilde{\boldsymbol{u}}_i, \boldsymbol{\vartheta}_k\right] &= \mathrm{tr}\left\{\boldsymbol{C}_{uui}\left(\boldsymbol{\vartheta}\right)\boldsymbol{\Sigma}_{ui}\right\} + \overline{\boldsymbol{v}}_i^H \boldsymbol{C}_{uui}\left(\boldsymbol{\vartheta}\right)\overline{\boldsymbol{v}}_i
\end{aligned}$$

The integrations for the expectations of terms I and II are straightforward, but the expectation for term III is somewhat more complex, but it arises from a standard result in quadratic form theory for random variables [*Mathai and Provost*, 1992].

Concerning the third step, it is required to determine an expression for $\overline{\boldsymbol{v}}_i$ dependent only on $\widetilde{\boldsymbol{u}}_i$ and $\boldsymbol{\vartheta}_k$. To do this, note that (6.63) and (6.65) imply that

$$\boldsymbol{v}_i = -\boldsymbol{G}_{ui}^{+}(\boldsymbol{\vartheta})\boldsymbol{G}_{mi}(\boldsymbol{\vartheta})\boldsymbol{u}_i \tag{6.75}$$

where $\boldsymbol{G}_{ui}^{+}$ is a Moore-Penrose pseudoinverse to $\boldsymbol{G}_{ui}$. The equation (6.75) suggests the estimator

$$\overline{\boldsymbol{v}}_i = -\boldsymbol{G}_{ui}^{+}(\boldsymbol{\vartheta}_k)\boldsymbol{G}_{mi}(\boldsymbol{\vartheta}_k)\widetilde{\boldsymbol{u}}_i, \tag{6.76}$$

for which the expectation satisfies (6.75), meaning that (6.76) is an unbiased estimator. An appropriate expression for the Moore-Penrose inverse is

$$\boldsymbol{G}_{ui}^{+}(\boldsymbol{\vartheta}) = \boldsymbol{C}_{uui}^{-1}(\boldsymbol{\vartheta})\boldsymbol{G}_{ui}^{H}(\boldsymbol{\vartheta})\boldsymbol{\Lambda}_i^{-1}(\boldsymbol{\vartheta}) \tag{6.77}$$

where $\boldsymbol{\Lambda}_i$ could be replaced by any nonsingular matrix of the correct size, but $\boldsymbol{\Lambda}_i$ was selected as it relates to the form of the MLEs (6.70). Defining

$$Q_i\left(\widetilde{\boldsymbol{u}}_i, \boldsymbol{\vartheta}_k, \boldsymbol{\vartheta}\right) = -\mathrm{E}\left[\ln\left(f_i\left(\widetilde{\boldsymbol{u}}_i, \widetilde{\boldsymbol{v}}_i|\widehat{\boldsymbol{u}}_i, \widehat{\boldsymbol{v}}_i, \boldsymbol{\vartheta}\right)\right)|\widetilde{\boldsymbol{u}}_i, \boldsymbol{\vartheta}_k\right],$$

with the substitution for $\overline{\boldsymbol{v}}_i$ as outlined above and combining all the terms $i = 1, \ldots, M$, and using (6.62) leads to the expression (6.66). □

Remark: As outlined in Theorem 6.4, the objective of the EM algorithm is to facilitate an approach for computing the MLE of the marginal distribution of the known data. However, as will be shown, the marginal distribution of the known data itself can be derived from (6.72), hence casting doubt on whether the use of

the EM algorithm is necessary. It turns out that the use of the EM algorithm is actually not necessary, but it is computationally advantageous as discussed in the following.

To determine the marginal PDF for $\widetilde{\boldsymbol{u}}_i$, the terms in (6.72) are separated into those dependent on, and independent of, $\widetilde{\boldsymbol{v}}_i$. Therefore the joint probability distribution can be expressed as

$$f_i\left(\widetilde{\boldsymbol{u}}_i, \widetilde{\boldsymbol{v}}_i | \widehat{\boldsymbol{u}}_i, \widehat{\boldsymbol{v}}_i, \boldsymbol{\vartheta}\right) = g_{1i}\left(\widetilde{\boldsymbol{u}}_i\right) g_{2i}\left(\widetilde{\boldsymbol{u}}_i, \widetilde{\boldsymbol{v}}_i\right)$$

where

$$g_{1i}\left(\widetilde{\boldsymbol{u}}\right) = \frac{1}{\pi^{n_m} |\boldsymbol{\Sigma}_{mi}||\boldsymbol{\Sigma}_{ui}||\boldsymbol{C}_{uui}|} \exp\left\{-\widetilde{\boldsymbol{u}}_i^H \left[\boldsymbol{C}_{mmi} - \boldsymbol{C}_{mui}\boldsymbol{C}_{uui}^{-1}\boldsymbol{C}_{umi}\right] \widetilde{\boldsymbol{u}}_i\right\}$$

and

$$g_{2i}\left(\widetilde{\boldsymbol{u}}_i, \widetilde{\boldsymbol{v}}\right) = \frac{|\boldsymbol{C}_{uui}|}{\pi^{n_u}} \exp\left\{-\left[\widetilde{\boldsymbol{v}}_i + \boldsymbol{C}_{uui}^{-1}\boldsymbol{C}_{umi}\widetilde{\boldsymbol{u}}_i\right]^H \boldsymbol{C}_{uui} \left[\widetilde{\boldsymbol{v}}_i + \boldsymbol{C}_{uui}^{-1}\boldsymbol{C}_{umi}\widetilde{\boldsymbol{u}}_i\right]\right\}.$$

Note that this factorisation is possible as $\boldsymbol{C}_{uui}$ is nonsingular due to the full column rank of $\boldsymbol{G}_{ui}$. The marginal probability for the measured data $\boldsymbol{u}$ is given by

$$f_i\left(\widetilde{\boldsymbol{u}}_i | \widehat{\boldsymbol{u}}_i, \widehat{\boldsymbol{v}}_i, \boldsymbol{\vartheta}\right) = \int_{\mathbb{C}^{n_u}} f_i\left(\widetilde{\boldsymbol{u}}_i, \widetilde{\boldsymbol{v}}_i | \widehat{\boldsymbol{u}}_i, \widehat{\boldsymbol{v}}_i, \boldsymbol{\vartheta}\right) \mathrm{d}\widetilde{\boldsymbol{v}}_i = g_{1i}\left(\widetilde{\boldsymbol{u}}_i\right) \int_{\mathbb{C}^{n_u}} g_{2i}\left(\widetilde{\boldsymbol{u}}_i, \widetilde{\boldsymbol{v}}_i\right) \mathrm{d}\widetilde{\boldsymbol{v}}_i.$$

Note that, for a given $\widetilde{\boldsymbol{u}}_i$, g_{2i} has the form of a complex normal PDF with mean $-\boldsymbol{C}_{uui}^{-1}\boldsymbol{C}_{umi}\widetilde{\boldsymbol{u}}_i$ and covariance $\boldsymbol{C}_{uui}^{-1}$. Therefore, it holds that

$$\int_{\mathbb{C}^{n_u}} g_{2i}\left(\widetilde{\boldsymbol{u}}_i, \widetilde{\boldsymbol{v}}_i\right) \mathrm{d}\widetilde{\boldsymbol{v}}_i = 1$$

and so, in fact the marginal $f_i\left(\widetilde{\boldsymbol{u}}_i | \widehat{\boldsymbol{u}}_i, \widehat{\boldsymbol{v}}_i, \boldsymbol{\vartheta}\right) = g_{1i}\left(\widetilde{\boldsymbol{u}}_i\right)$. The marginal distribution of the full known data set $\widetilde{\mathcal{U}}$ is given by

$$f\left(\widetilde{\mathcal{U}} | \widehat{\mathcal{U}}, \widehat{\mathcal{V}}, \boldsymbol{\vartheta}\right) = \prod_{i=1}^{M} f_i\left(\widetilde{\boldsymbol{u}}_i | \widehat{\boldsymbol{u}}_i, \widehat{\boldsymbol{v}}_i, \boldsymbol{\vartheta}\right) \tag{6.78}$$

where the MLE for $\widehat{\boldsymbol{\vartheta}}$ is given as the minimiser of the negative of the log-likelihood of (6.78) which, is given by the expression

$$\begin{aligned} &-\log f\left(\widetilde{\mathcal{U}} | \widehat{\mathcal{U}}, \widehat{\mathcal{V}}, \boldsymbol{\vartheta}\right) = \text{constant terms} + \\ &\sum_{i=1}^{M} \widetilde{\boldsymbol{u}}_i^H \left[\boldsymbol{C}_{mmi}\left(\boldsymbol{\vartheta}\right) - \boldsymbol{C}_{mui}\left(\boldsymbol{\vartheta}\right) \boldsymbol{C}_{uui}^{-1}\left(\boldsymbol{\vartheta}\right) \boldsymbol{C}_{umi}\left(\boldsymbol{\vartheta}\right)\right] \widetilde{\boldsymbol{u}}_i + \det \boldsymbol{C}_{uui}\left(\boldsymbol{\vartheta}\right) \end{aligned}. \tag{6.79}$$

Therefore, the computation of $-\log f\left(\widetilde{\mathcal{U}}|\widehat{\mathcal{U}},\widehat{\mathcal{V}},\boldsymbol{\vartheta}\right)$ is seen to involve the computation of the inverse of a complex matrix $\boldsymbol{C}_{uui}$ and the computation of its determinant in addition to matrix multplications. In comparison, within the $(k+1)$-th iteration, the Q_i terms in (6.66) involve the following computation

$$\widetilde{\boldsymbol{u}}_i^H \boldsymbol{C}_{mmi}\left(\boldsymbol{\vartheta}\right)\widetilde{\boldsymbol{u}}_i - 2\mathbb{R}\mathrm{e}\left\{\widetilde{\boldsymbol{u}}_i^H \boldsymbol{C}_{mui}\left(\boldsymbol{\vartheta}\right)\boldsymbol{x}_{ui}\right\} + \mathrm{tr}\left\{\boldsymbol{C}_{uui}\left(\boldsymbol{\vartheta}\right)\boldsymbol{\Sigma}_{ui}\right\} + \boldsymbol{x}_{ui}^H \boldsymbol{C}_{uui}\left(\boldsymbol{\vartheta}\right)\boldsymbol{x}_{ui}$$

where the term

$$\boldsymbol{x}_{ui} = \boldsymbol{C}_{uui}^{-1}\left(\boldsymbol{\vartheta}_k\right)\boldsymbol{C}_{umi}\left(\boldsymbol{\vartheta}_k\right)\widetilde{\boldsymbol{u}}_i$$

is treated as constants as it is only calculated once at the beginning of the $(k+1)$-th iteration, and it is not a variable term that requires repeated computation. Both the MLE approach based on the marginal PDF (6.79) and the EM algorithm require iterative optimisation algorithms to determine the estimate $\widehat{\boldsymbol{\vartheta}}$. As such, the numerical efficiency of each approach is extremely important.

The MLE approach involves one direct optimisation problem dealing with the fixed form of the marginal PDF as the objective function. In contrast, the EM algorithm presents a staged sequence of optimisation problems where each k-th stage deals with a slightly altered objective function (*i.e.* a different value of $\boldsymbol{x}_{ui}$). However, within the EM algorithm, the optimiser at each k-th stage does not require exact determination, but in fact only an improvement in the objective function is required at each stage to update the $\boldsymbol{x}_{ui}$ and to continue onto the next stage. Therefore, given the use of global iterative optimisation algorithms, the difference between the number of iterations required for the marginal PDF approach in comparison to the EM algorithm is not necessarily significant.

A breakdown of the computations required for each term in the marginal PDF from (6.79) and the EM algorithms Q_i terms in (6.80) and their associated operation counts is given in Table 6.5. From this table, it is clear that the matrix inversion and the determinant computation heavily penalise the marginal PDF approach as both of these involve $O\left\{n_u^3\right\}$ operations in comparison to highest operation count of $O\left\{n_u^2\right\}$ involved in the EM algorithm. Therefore, the action of the EM algorithm to defer the expensive operations (such as the matrix inversion) to occur only once for each of the k optimisation stages is observed to be a computationally advantageous strategy. Therefore, as long as the number of iterations required by the EM algorithm is not a factor near n_u greater than the number required by the MLE of the marginal PDF approach, then the EM algorithm will be more computationally efficient.

Additionally, the fact that the EM algorithm avoids the computation of $\det \boldsymbol{C}_{uu}$ is an additional advantage from the perspective of numerical stability as determinant calculations can often cause floating point overflows or underflows.

Table 6.5: Order of operation count for the EM algorithm terms in (6.66) and the marginal PDF terms in (6.79). In the expressions below, the symbols $\boldsymbol{X}_{uu} \in \mathbb{C}^{n_u \times n_u}$, $\boldsymbol{x}_m \in \mathbb{C}^{n_m}$, and $\boldsymbol{x}_u \in \mathbb{C}^{n_u}$ are used to make the important operations clear.

Approach	Operation	Expression	Operation count
EM algorithm	series multiplication	$\boldsymbol{x}_m^H \boldsymbol{C}_{mm} \boldsymbol{x}_m$	$O\{n_m^2\}$
	series multiplication	$\boldsymbol{x}_m^H \boldsymbol{C}_{mu} \boldsymbol{x}_u$	$O\{n_m n_u\}$
	trace of multiplication	$\mathrm{tr}\{\boldsymbol{C}_{uu} \boldsymbol{\Sigma}_u\}$	$O\{n_u^2\}$
	series multiplication	$\boldsymbol{x}_u^H \boldsymbol{C}_{uu} \boldsymbol{x}_u$	$O\{n_u^2\}$
		total	$O\{n_m^2, n_u^2, n_m n_u\}$
MLE of marginal PDF	series multiplication	$\boldsymbol{x}_m^H \boldsymbol{C}_{mm} \boldsymbol{x}_m$	$O\{n_m^2\}$
	inversion	$\boldsymbol{C}_{uu}^{-1}$	$O\{n_u^3\}$
	multiplication	$\boldsymbol{x}_m^H \boldsymbol{C}_{mu}$	$O\{n_m n_u\}$
	series multiplication	$\boldsymbol{x}_u^H \boldsymbol{X}_{uu} \boldsymbol{x}_u$	$O\{n_u^2\}$
	determinant	$\det \boldsymbol{C}_{uu}$	$O\{n_u^3\}$
		total	$O\{n_m^2, n_u^3, n_m n_u\}$

6.5.2 Expectation-maximisation $\mathscr{M}$-network model

The problem of parameter estimation within a $\mathscr{M}$-network for which there are unmeasured state variables is conveniently described by the parameter estimation problem outlined in Theorem 6.5. Firstly, clearly the known data $\widetilde{\mathcal{U}}$ corresponds to the transforms of the measured states $\widetilde{\boldsymbol{\Psi}}_m$ and $\widetilde{\boldsymbol{\Theta}}_m$, and the unknown data $\widetilde{\mathcal{V}}$ corresponds to the transforms of the unmeasured states $\widetilde{\boldsymbol{\Psi}}_u$ and $\widetilde{\boldsymbol{\Theta}}_u$. Secondly, the constraints on the data (6.63) in Theorem 6.5 corresponds to the network dynamics governing the interaction of the state variables as in (6.28), which can be reorganised similarly to (6.63) as

$$\left[\begin{array}{c:c} \boldsymbol{G}_m(\boldsymbol{\vartheta}, s) & \boldsymbol{G}_u(\boldsymbol{\vartheta}, s) \end{array}\right] \left[\begin{array}{c} \left[\begin{array}{c} \boldsymbol{\Psi}_m(s) \\ \hdashline \boldsymbol{\Theta}_m(s) \end{array}\right] \\ \hdashline \left[\begin{array}{c} \boldsymbol{\Psi}_u(s) \\ \hdashline \boldsymbol{\Theta}_u(s) \end{array}\right] \end{array}\right] = \boldsymbol{0}. \tag{6.80}$$

This relationship is formalised in the following corollary which outlines the EM parameter estimation model for an $\mathscr{M}$-network with a nodal partitioning for which $\mathcal{A}_4 \neq \emptyset$.

Corollary 6.3. *Consider the $\mathscr{M}$-network $(\mathcal{G}(\mathcal{N}, \Xi), \mathcal{M})$ with the nodal partitioning as defined in Section 6.3.3, for which there exists the measurement set*

$$\left\{\widetilde{\boldsymbol{\psi}}_m(t), \widetilde{\boldsymbol{\theta}}_m(t) : t = 0, \Delta t, \ldots, 2M\Delta t\right\}$$

where

$$\left[\begin{array}{c} \tilde{\boldsymbol{\psi}}_m(t) \\ \hdashline \tilde{\boldsymbol{\theta}}_m(t) \end{array}\right] = \left[\begin{array}{c} \boldsymbol{\psi}_m(t) \\ \hdashline \boldsymbol{\theta}_m(t) \end{array}\right] + \left[\begin{array}{c} \boldsymbol{e}_\psi(t) \\ \hdashline \boldsymbol{e}_\theta(t) \end{array}\right] \tag{6.81}$$

where $\boldsymbol{\psi}_m$ and $\boldsymbol{\theta}_m$ are as defined in Section 6.3.3 and are periodic with fixed frequency distribution (with negligible spectral energy above $(2\Delta t)^{-1}$ Hz), and $\boldsymbol{e}_\psi(t), \boldsymbol{e}_\theta(t), t = 0, \Delta, \ldots, 2M\Delta t$ are stationary processes with power spectrum's $\boldsymbol{S}_\psi(\mathrm{i}\omega)$ and $\boldsymbol{S}_\theta(\mathrm{i}\omega)$. Given that there exists some strictly passive $\xi \in \Xi_i$ for each $i \in \mathcal{A}_3 \cup \mathcal{A}_4 \cup \mathcal{B}_1 \cup \mathcal{B}_2$, then the EM algorithm solution to the network parameter estimation problem in Definition 6.4 is given by (6.66)-(6.69) in Theorem 6.5 with the following substitutions

$$\widetilde{\boldsymbol{u}}_i = \left[\begin{array}{c} \widetilde{\boldsymbol{\Psi}}_m(\mathrm{i}\omega_i), \\ \hdashline \widetilde{\boldsymbol{\Theta}}_m(\mathrm{i}\omega_i) \end{array}\right], \tag{6.82}$$

$$\boldsymbol{G}_{mi}(\boldsymbol{\vartheta}) = \boldsymbol{G}_m(\boldsymbol{\vartheta}, \mathrm{i}\omega_i), \tag{6.83}$$

$$\boldsymbol{G}_{ui}(\boldsymbol{\vartheta}) = \boldsymbol{G}_u(\boldsymbol{\vartheta}, \mathrm{i}\omega_i), \tag{6.84}$$

$$\boldsymbol{\Sigma}_{mi} = \frac{1}{2M}\left[\begin{array}{c:c} \boldsymbol{S}_\psi(\mathrm{i}\omega_i) & \boldsymbol{0} \\ \hdashline \boldsymbol{0} & \boldsymbol{S}_\theta(\mathrm{i}\omega_i) \end{array}\right], \tag{6.85}$$

$$\boldsymbol{\Sigma}_{ui} = \boldsymbol{A}_i \in \mathbb{R}^{n_u \times n_u} \quad \textit{where } \boldsymbol{A}_i \textit{ is positive definite}, \tag{6.86}$$

for $i = 1, \ldots, M$, where $\boldsymbol{G}_m$ and $\boldsymbol{G}_u$ are the network transfer matrices for the measured and unmeasured states from (6.29) and (6.30) respectively, and the ω_i are the Fourier frequencies from the DFT of the time-domain data.

Proof. As in the proof to Corollary 6.2, the parameter estimation problem outlined in Corollary 6.3 above can be cast as the constrained complex Gaussian problem from Theorem 6.5 for which there is incomplete data, which in the context of Corollary 6.3 are the unmeasured nodal states $\boldsymbol{\psi}_u$ and $\boldsymbol{\theta}_u$. The substitutions (6.82)-(6.86) are justified by a similar logic to that used in the proof to Corollary 6.2, with the addition that any positive definite matrix in $\mathbb{R}^{n_u \times n_u}$ is appropriate for the $\boldsymbol{\Sigma}_{ui}$ as the treatment of the unmeasured variables as complex Gaussian variates is superficial.

For the substitutions (6.83)-(6.84) to hold, it remains to show that they adhere to the rank conditions (6.64)-(6.65) in Theorem 6.5, namely that

$$\operatorname{rank} \boldsymbol{G}_u(s) = n_u \tag{6.87}$$

$$\operatorname{rank}\left[\begin{array}{c:c} \boldsymbol{G}_m(s) & \boldsymbol{G}_u(s) \end{array}\right] = N \tag{6.88}$$

for $s = \mathrm{i}\omega_i, i = 1, \ldots, M$. Given that $\boldsymbol{G}_u$ is $N \times n_u$ where $n_u < N$, (6.87) states that $\boldsymbol{G}_u$ be full column rank at $s = \mathrm{i}\omega_i, i = 1, \ldots, M$. Combining (6.30) with the

original partitions (6.20)-(6.22) reveals that

$$\boldsymbol{G}_u(s) = \left[\begin{array}{c|c|c|c|c|c} \boldsymbol{Y}_{\mathcal{A}_1\mathcal{A}_3}(s) & \boldsymbol{Y}_{\mathcal{A}_1\mathcal{A}_4}(s) & \boldsymbol{Y}_{\mathcal{A}_1\mathcal{B}_2}(s) & \boldsymbol{0} & \boldsymbol{0} & \boldsymbol{0} \\ \boldsymbol{Y}_{\mathcal{A}_3\mathcal{A}_3}(s) & \boldsymbol{Y}_{\mathcal{A}_3\mathcal{A}_4}(s) & \boldsymbol{Y}_{\mathcal{A}_3\mathcal{B}_2}(s) & \boldsymbol{0} & \boldsymbol{0} & \boldsymbol{0} \\ \boldsymbol{Y}_{\mathcal{C}_1\mathcal{A}_3}(s) & \boldsymbol{Y}_{\mathcal{C}_1\mathcal{A}_4}(s) & \boldsymbol{Y}_{\mathcal{C}_1\mathcal{B}_2}(s) & \boldsymbol{0} & \boldsymbol{0} & \boldsymbol{0} \\ \boldsymbol{Y}_{\mathcal{B}_1\mathcal{A}_3}(s) & \boldsymbol{Y}_{\mathcal{B}_1\mathcal{A}_4}(s) & \boldsymbol{Y}_{\mathcal{B}_1\mathcal{B}_2}(s) & \boldsymbol{0} & \boldsymbol{0} & \boldsymbol{0} \\ \boldsymbol{Y}_{\mathcal{B}_2\mathcal{A}_3}(s) & \boldsymbol{Y}_{\mathcal{B}_2\mathcal{A}_4}(s) & \boldsymbol{Y}_{\mathcal{B}_2\mathcal{B}_2}(s) & \boldsymbol{0} & \boldsymbol{0} & \boldsymbol{0} \\ \boldsymbol{Y}_{\mathcal{A}_2\mathcal{A}_3}(s) & \boldsymbol{Y}_{\mathcal{A}_2\mathcal{A}_4}(s) & \boldsymbol{Y}_{\mathcal{A}_2\mathcal{B}_2}(s) & -\boldsymbol{I} & \boldsymbol{0} & \boldsymbol{0} \\ \boldsymbol{Y}_{\mathcal{A}_4\mathcal{A}_3}(s) & \boldsymbol{Y}_{\mathcal{A}_4\mathcal{A}_4}(s) & \boldsymbol{Y}_{\mathcal{A}_4\mathcal{B}_2}(s) & \boldsymbol{0} & -\boldsymbol{I} & \boldsymbol{0} \\ \boldsymbol{Y}_{\mathcal{C}_2\mathcal{A}_3}(s) & \boldsymbol{Y}_{\mathcal{C}_1\mathcal{A}_4}(s) & \boldsymbol{Y}_{\mathcal{C}_1\mathcal{B}_2}(s) & \boldsymbol{0} & \boldsymbol{0} & -\boldsymbol{I} \end{array}\right]. \tag{6.89}$$

Given the identities in the last three block columns, $\boldsymbol{G}_u$ is full column rank only when the matrix composed of the first three block columns of (6.89) is full column rank. Swapping the block row ordering, it can be demonstrated that the first three block columns contain the submatrix

$$\left[\begin{array}{c|c|c} \boldsymbol{Y}_{\mathcal{A}_3\mathcal{A}_3}(s) & \boldsymbol{Y}_{\mathcal{A}_3\mathcal{A}_4}(s) & \boldsymbol{Y}_{\mathcal{A}_3\mathcal{B}_2}(s) \\ \boldsymbol{Y}_{\mathcal{A}_4\mathcal{A}_3}(s) & \boldsymbol{Y}_{\mathcal{A}_4\mathcal{A}_4}(s) & \boldsymbol{Y}_{\mathcal{A}_4\mathcal{B}_2}(s) \\ \boldsymbol{Y}_{\mathcal{B}_2\mathcal{A}_3}(s) & \boldsymbol{Y}_{\mathcal{B}_2\mathcal{A}_4}(s) & \boldsymbol{Y}_{\mathcal{B}_2\mathcal{B}_2}(s) \end{array}\right] \tag{6.90}$$

which is recognised as being a principal minor of the network admittance matrix $\boldsymbol{Y}$ for the $\mathscr{M}$-network $(\mathcal{G}(\mathcal{N}, \Xi), \mathcal{M})$. As a principal minor of the passive network admittance matrix $\boldsymbol{Y}$, the matrix (6.90) is nonnegative definite on $s \in \mathbb{C}_+$ (Lemma B.1) where positive definiteness is ensured by the existence of strictly passive links to each of the nodes $i \in \mathcal{A}_3 \cup \mathcal{A}_4 \cup \mathcal{B}_2$ associated with the submatrix (Theorem B.3). As (6.90) is positive definite on $s \in \mathbb{C}_+$, it is also full rank on $s \in \mathbb{C}_+$, meaning that the first three block rows in (6.89) represent a full column rank matrix and hence (6.87) holds on $s \in \mathbb{C}_+$.

The statement (6.88) is equivalent to saying that $\left[\begin{array}{c|c} \boldsymbol{G}_m & \boldsymbol{G}_u \end{array}\right]$ is full row rank. Combining (6.29) with the original partitions (6.17)-(6.19) reveals that

$$\boldsymbol{G}_m(s) = \left[\begin{array}{c|c|c|c|c|c} \boldsymbol{Y}_{\mathcal{A}_1\mathcal{A}_1}(s) & \boldsymbol{Y}_{\mathcal{A}_1\mathcal{A}_2}(s) & \boldsymbol{Y}_{\mathcal{A}_1\mathcal{B}_1}(s) & -\boldsymbol{I} & \boldsymbol{0} & \boldsymbol{0} \\ \boldsymbol{Y}_{\mathcal{A}_3\mathcal{A}_1}(s) & \boldsymbol{Y}_{\mathcal{A}_3\mathcal{A}_2}(s) & \boldsymbol{Y}_{\mathcal{A}_3\mathcal{B}_1}(s) & \boldsymbol{0} & -\boldsymbol{I} & \boldsymbol{0} \\ \boldsymbol{Y}_{\mathcal{C}_1\mathcal{A}_1}(s) & \boldsymbol{Y}_{\mathcal{C}_1\mathcal{A}_2}(s) & \boldsymbol{Y}_{\mathcal{C}_1\mathcal{B}_1}(s) & \boldsymbol{0} & \boldsymbol{0} & -\boldsymbol{I} \\ \boldsymbol{Y}_{\mathcal{B}_1\mathcal{A}_1}(s) & \boldsymbol{Y}_{\mathcal{B}_1\mathcal{A}_2}(s) & \boldsymbol{Y}_{\mathcal{B}_1\mathcal{B}_1}(s) & \boldsymbol{0} & \boldsymbol{0} & \boldsymbol{0} \\ \boldsymbol{Y}_{\mathcal{B}_2\mathcal{A}_1}(s) & \boldsymbol{Y}_{\mathcal{B}_2\mathcal{A}_2}(s) & \boldsymbol{Y}_{\mathcal{B}_2\mathcal{B}_1}(s) & \boldsymbol{0} & \boldsymbol{0} & \boldsymbol{0} \\ \boldsymbol{Y}_{\mathcal{A}_2\mathcal{A}_1}(s) & \boldsymbol{Y}_{\mathcal{A}_2\mathcal{A}_2}(s) & \boldsymbol{Y}_{\mathcal{A}_2\mathcal{B}_1}(s) & \boldsymbol{0} & \boldsymbol{0} & \boldsymbol{0} \\ \boldsymbol{Y}_{\mathcal{A}_4\mathcal{A}_1}(s) & \boldsymbol{Y}_{\mathcal{A}_4\mathcal{A}_2}(s) & \boldsymbol{Y}_{\mathcal{A}_4\mathcal{B}_1}(s) & \boldsymbol{0} & \boldsymbol{0} & \boldsymbol{0} \\ \boldsymbol{Y}_{\mathcal{C}_2\mathcal{A}_1}(s) & \boldsymbol{Y}_{\mathcal{C}_2\mathcal{A}_2}(s) & \boldsymbol{Y}_{\mathcal{C}_2\mathcal{B}_1}(s) & \boldsymbol{0} & \boldsymbol{0} & \boldsymbol{0} \end{array}\right]. \tag{6.91}$$

Given the structure of the identities in both $\boldsymbol{G}_m$ and $\boldsymbol{G}_u$, it is clear that both the top three and bottom three block rows of $\left[\begin{array}{c:c} \boldsymbol{G}_m & \boldsymbol{G}_u \end{array}\right]$ are linearly independent for all $s \in \mathbb{C}_+$. Therefore, to demonstrate the full row rank nature of this matrix, it is required to show that the centre two block rows create a full row rank matrix. Considering the centre two block rows in (6.89) and (6.91), by swapping the ordering of the columns it is seen that the two centre block rows contain the submatrix

$$\left[\begin{array}{c:c} \boldsymbol{Y}_{\mathcal{B}_1\mathcal{B}_1}(s) & \boldsymbol{Y}_{\mathcal{B}_1\mathcal{B}_2}(s) \\ \hdashline \boldsymbol{Y}_{\mathcal{B}_2\mathcal{B}_1}(s) & \boldsymbol{Y}_{\mathcal{B}_2\mathcal{B}_2}(s) \end{array}\right] \tag{6.92}$$

which is a principal minor of the network admittance matrix $\boldsymbol{Y}$. Therefore, using similar reasoning as in the case for (6.87) (this case relies on the strict passivity of at least one element incident to the nodes in $\mathcal{B}_1 \cup \mathcal{B}_2$), the centre two block rows are seen to be full row rank on $s \in \mathbb{C}_+$, and hence (6.88) holds for $s \in \mathbb{C}_+$. □

Remarks:

1. An artificial construction, implicit within Corollary 6.3, is that the unknown data $\widetilde{\boldsymbol{v}}$ corresponds to complex Gaussian variates centred on the unknown nodal states, that is

$$\widetilde{\boldsymbol{v}}_i = \left[\begin{array}{c} \widetilde{\boldsymbol{\Psi}}_u(\mathrm{i}\omega_i), \\ \hdashline \widetilde{\boldsymbol{\Theta}}_u(\mathrm{i}\omega_i) \end{array}\right] \sim \mathcal{N}_c\left(\left[\begin{array}{c} \boldsymbol{\Psi}_u(\mathrm{i}\omega_i), \\ \hdashline \boldsymbol{\Theta}_u(\mathrm{i}\omega_i) \end{array}\right], \boldsymbol{A}_i\right),$$

   for $i = 1, \ldots, M$, thus implying that the unmeasured data follows a complex Gaussian distribution. These variates clearly do not exist, but are used as a means of deriving the form of the EM algorithm. As such, the covariance matrices $\boldsymbol{A}_i$ have no quantifiable form, but can be arbitrarily selected positive definite matrices. These matrices appear in the estimation scheme (6.66) through the $\boldsymbol{\Lambda}_i$ terms. To reduce the importance of these terms in the estimation scheme, the $\boldsymbol{A}_i$ matrices were selected as diagonal matrices, where the diagonal terms were selected to be a couple of orders of magnitude smaller than the variance terms for the measured variables.

2. To improve the computational efficiency of the estimation process (6.66) for $\mathscr{M}$-networks, the analytic forms of $\boldsymbol{G}_m$ and $\boldsymbol{G}_u$ in (6.89) and (6.89) can be used to determine explicit expressions for the matrix functions $\boldsymbol{C}_{mm}$, $\boldsymbol{C}_{mu}$, $\boldsymbol{C}_{um}$, $\boldsymbol{C}_{uu}$ and $\boldsymbol{\Lambda}$. Expressing the covariance matrices in the general forms

$$\boldsymbol{\Sigma}_m(s) = \left[\begin{array}{c:c} \boldsymbol{\Sigma}_{m\psi}(s) & \boldsymbol{0} \\ \hdashline \boldsymbol{0} & \boldsymbol{\Sigma}_{m\theta}(s) \end{array}\right], \quad \boldsymbol{\Sigma}_u(s) = \left[\begin{array}{c:c} \boldsymbol{\Sigma}_{u\psi}(s) & \boldsymbol{0} \\ \hdashline \boldsymbol{0} & \boldsymbol{\Sigma}_{u\theta}(s) \end{array}\right]$$

(*i.e.* the nodal pressure and flow variables are independent), the following expression for $\boldsymbol{\Lambda}$ can be obtained, based on substituting (6.89) and (6.89) into (6.71),

$$\begin{aligned}\boldsymbol{\Lambda}(s) = &\left[\begin{array}{c|c|c} \boldsymbol{\Sigma}_{m\theta}(s) & \mathbf{0} & \mathbf{0} \\ \hline \mathbf{0} & \mathbf{0} & \mathbf{0} \\ \hline \mathbf{0} & \mathbf{0} & \boldsymbol{\Sigma}_{u\theta}(s) \end{array}\right] + \\ &\left[\begin{array}{c|c|c} \boldsymbol{Y}_{u1}(s)\boldsymbol{\Sigma}_{u\psi}(s)\boldsymbol{Y}_{u1}^H(s) & \boldsymbol{Y}_{u1}(s)\boldsymbol{\Sigma}_{u\psi}(s)\boldsymbol{Y}_{u2}^H(s) & \boldsymbol{Y}_{u1}(s)\boldsymbol{\Sigma}_{u\psi}(s)\boldsymbol{Y}_{u3}^H(s) \\ \hline \boldsymbol{Y}_{u2}(s)\boldsymbol{\Sigma}_{u\psi}(s)\boldsymbol{Y}_{u1}^H(s) & \boldsymbol{Y}_{u2}(s)\boldsymbol{\Sigma}_{u\psi}(s)\boldsymbol{Y}_{u2}^H(s) & \boldsymbol{Y}_{u2}(s)\boldsymbol{\Sigma}_{u\psi}(s)\boldsymbol{Y}_{u3}^H(s) \\ \hline \boldsymbol{Y}_{u3}(s)\boldsymbol{\Sigma}_{u\psi}(s)\boldsymbol{Y}_{u1}^H(s) & \boldsymbol{Y}_{u3}(s)\boldsymbol{\Sigma}_{u\psi}(s)\boldsymbol{Y}_{u2}^H(s) & \boldsymbol{Y}_{u3}(s)\boldsymbol{\Sigma}_{u\psi}(s)\boldsymbol{Y}_{u3}^H(s) \end{array}\right] + \\ &\left[\begin{array}{c|c|c} \boldsymbol{Y}_{m1}(s)\boldsymbol{\Sigma}_{m\psi}(s)\boldsymbol{Y}_{m1}^H(s) & \boldsymbol{Y}_{m1}(s)\boldsymbol{\Sigma}_{m\psi}(s)\boldsymbol{Y}_{m2}^H(s) & \boldsymbol{Y}_{m1}(s)\boldsymbol{\Sigma}_{m\psi}(s)\boldsymbol{Y}_{m3}^H(s) \\ \hline \boldsymbol{Y}_{m2}(s)\boldsymbol{\Sigma}_{m\psi}(s)\boldsymbol{Y}_{m1}^H(s) & \boldsymbol{Y}_{m2}(s)\boldsymbol{\Sigma}_{m\psi}(s)\boldsymbol{Y}_{m2}^H(s) & \boldsymbol{Y}_{m2}(s)\boldsymbol{\Sigma}_{m\psi}(s)\boldsymbol{Y}_{m3}^H(s) \\ \hline \boldsymbol{Y}_{m3}(s)\boldsymbol{\Sigma}_{m\psi}(s)\boldsymbol{Y}_{m1}^H(s) & \boldsymbol{Y}_{m3}(s)\boldsymbol{\Sigma}_{m\psi}(s)\boldsymbol{Y}_{m2}^H(s) & \boldsymbol{Y}_{m3}(s)\boldsymbol{\Sigma}_{m\psi}(s)\boldsymbol{Y}_{m3}^H(s) \end{array}\right]\end{aligned} \tag{6.93}$$

which can be more compactly expressed as

$$\boldsymbol{\Lambda}(s) = \left[\begin{array}{c|c|c} \boldsymbol{\Lambda}_{11}(s) & \boldsymbol{\Lambda}_{12}(s) & \boldsymbol{\Lambda}_{11}(s) \\ \hline \boldsymbol{\Lambda}_{21}(s) & \boldsymbol{\Lambda}_{22}(s) & \boldsymbol{\Lambda}_{23}(s) \\ \hline \boldsymbol{\Lambda}_{31}(s) & \boldsymbol{\Lambda}_{32}(s) & \boldsymbol{\Lambda}_{33}(s) \end{array}\right], \tag{6.94}$$

where the submatrices are given as

$$\boldsymbol{\Lambda}_{ij}(s) = \begin{cases} \boldsymbol{Y}_{m1}(s)\boldsymbol{\Sigma}_{m\psi}(s)\boldsymbol{Y}_{m1}^H(s) + \boldsymbol{Y}_{u1}(s)\boldsymbol{\Sigma}_{u\psi}(s)\boldsymbol{Y}_{u1}^H(s) + \boldsymbol{\Sigma}_{m\theta}(s) & \text{for } i,j = 1 \\ \boldsymbol{Y}_{m3}(s)\boldsymbol{\Sigma}_{m\psi}(s)\boldsymbol{Y}_{m3}^H(s) + \boldsymbol{Y}_{u3}(s)\boldsymbol{\Sigma}_{u\psi}(s)\boldsymbol{Y}_{u3}^H(s) + \boldsymbol{\Sigma}_{u\theta}(s) & \text{for } i,j = 3 \\ \boldsymbol{Y}_{mi}(s)\boldsymbol{\Sigma}_{m\psi}(s)\boldsymbol{Y}_{mj}^H(s) + \boldsymbol{Y}_{ui}(s)\boldsymbol{\Sigma}_{u\psi}(s)\boldsymbol{Y}_{uj}^H(s) & \text{otherwise} \end{cases}.$$

Using the forms of $\boldsymbol{G}_m$ and $\boldsymbol{G}_u$ from (6.29) and (6.94), and substituting (6.94) into (6.68) yields

$$\boldsymbol{C}_{mm}(s) = \left[\begin{array}{c|c} \boldsymbol{Y}_m^H(s)\boldsymbol{\Lambda}^{-1}(s)\boldsymbol{Y}_m(s) & -\boldsymbol{Y}_m^H(s)\left\{\boldsymbol{\Lambda}^{-1}(s)\right\}_{\bullet 1} \\ \hline -\left\{\boldsymbol{\Lambda}^{-1}(s)\right\}_{1\bullet}\boldsymbol{Y}_m(s) & \left\{\boldsymbol{\Lambda}^{-1}(s)\right\}_{11} \end{array}\right], \tag{6.95}$$

$$\boldsymbol{C}_{mu}(s) = \left[\begin{array}{c|c} \boldsymbol{Y}_m^H(s)\boldsymbol{\Lambda}^{-1}(s)\boldsymbol{Y}_u(s) & -\boldsymbol{Y}_m^H(s)\left\{\boldsymbol{\Lambda}^{-1}(s)\right\}_{\bullet 3} \\ \hline -\left\{\boldsymbol{\Lambda}^{-1}(s)\right\}_{1\bullet}\boldsymbol{Y}_u(s) & \left\{\boldsymbol{\Lambda}^{-1}(s)\right\}_{13} \end{array}\right], \tag{6.96}$$

$$\boldsymbol{C}_{um}(s) = \boldsymbol{C}_{mu}^H(s) \tag{6.97}$$

$$\boldsymbol{C}_{uu}(s) = \left[\begin{array}{c|c} \boldsymbol{Y}_u^H(s)\boldsymbol{\Lambda}^{-1}(s)\boldsymbol{Y}_u(s) & -\boldsymbol{Y}_u^H(s)\left\{\boldsymbol{\Lambda}^{-1}(s)\right\}_{\bullet 3} \\ \hline -\left\{\boldsymbol{\Lambda}^{-1}(s)\right\}_{3\bullet}\boldsymbol{Y}_u(s) & \left\{\boldsymbol{\Lambda}^{-1}(s)\right\}_{33} \end{array}\right], \tag{6.98}$$

where the $\bullet$ in the subscript indicates that a whole block row (or block column) is used, where the dimensions of the block rows and columns are taken from

Table 6.6: The $\mathscr{M}$-network nodal partitioning (from Definition 6.6) for cases 1 and 2 for the 13-pipe network from Example 6.7. The inclusion of $7 \in \mathcal{B}_2$ means that case 2 incorrectly assumes that $\theta_7(t) = 0$, where as $7 \in \mathcal{A}_4$ for case 1 correctly assumes that $\theta_7(t) \neq 0$.

Nodal set	Node sets for each case	
	case 1	case 2
$\mathcal{A}_1$	$\{4\}$	$\{4\}$
$\mathcal{A}_2$	$\emptyset$	$\emptyset$
$\mathcal{A}_3$	$\emptyset$	$\emptyset$
$\mathcal{A}_4$	$\{7\}$	$\emptyset$
$\mathcal{B}_1$	$\{2,6,3\}$	$\{2,6,3\}$
$\mathcal{B}_2$	$\{5\}$	$\{5,7\}$
$\mathcal{C}_1$	$\emptyset$	$\emptyset$
$\mathcal{C}_2$	$\{1\}$	$\{1\}$

(6.94), and

$$\boldsymbol{Y}_m(s) = \begin{bmatrix} \boldsymbol{Y}_{m1}(s) \\ \hdashline \boldsymbol{Y}_{m2}(s) \\ \hdashline \boldsymbol{Y}_{m3}(s) \end{bmatrix}, \quad \boldsymbol{Y}_u(s) = \begin{bmatrix} \boldsymbol{Y}_{u1}(s) \\ \hdashline \boldsymbol{Y}_{u2}(s) \\ \hdashline \boldsymbol{Y}_{u3}(s) \end{bmatrix}.$$

For the numerical examples in the next section, (6.94)-(6.98) formed the basis of the calculation of (6.66).

6.5.3 Numerical examples

The following examples explore the utility of the EM method to deal with cases where there are nodes for which both the nodal states of pressure and flow are unknown. This is undertaken through the use of an extended 11-pipe network (Figure 6.4), where the extensions (a two pipe branch) are considered to be unknown. The resulting scenario is one for which the network has a node where both the nodal flow and pressure are unknown. All computational procedures were undertaken as outlined in Appendix E.

Example 6.7. *Consider the 13-pipe TSF network in Figure 6.4(a) which is given by the 13-pipe network in Figure 6.1 with an additional branch from node 7 consisting of two pipes, a capacitance element and an emitter (network details are in Appendix D). The form of the branch from node 7 is considered an unknown, and thus the assumed form of the 13-pipe network is that of Figure 6.4 (b) where the nodal flow*

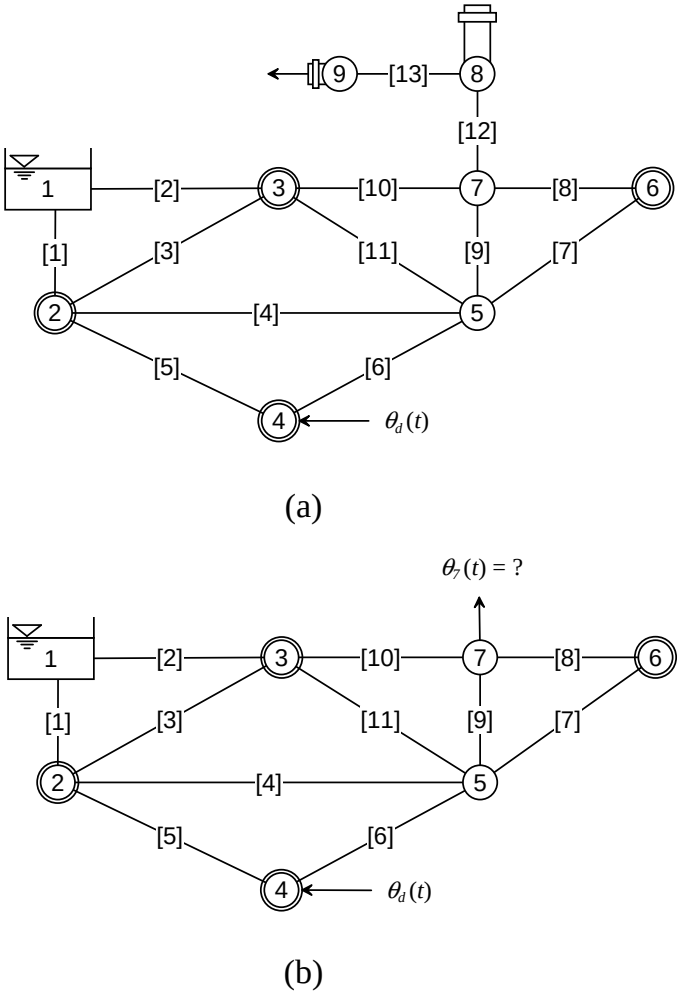

Figure 6.4: The extended 11-pipe network from Examples 6.7 and 6.8. The rings around the nodes indicate the locations of pressure measurements. Figure (a) represents the actual true network which is the 11-pipe network from Figure 6.1 with an additional branch from node 7 consisting of two pipes with a capacitor at node 8 and an emitter at node 9. Figure (b) represents the known configuration of the network involving an unknown nodal flow at node 7, as the existence of the branch is known but the form of the branch is unknown.

at node 7 is an unknown state variable. The parameter identification problem is to estimate the parameters of the 11 known pipes.

Two cases of nodal categorisations are considered. The first case assumes that the nodal flow for node 7 is an unknown (for this case is is assumed that node $7 \in \mathcal{A}_4$*), this represents a correct treatment of the unknown branch. The second case assumes that the nodal flow for node 7 is known to be zero (for this case it is assumed that node* $7 \in \mathcal{B}_2$*), that is the presence of the unknown branch is ignored. The nodal sets for these cases are given in Table 6.6. There is a flow measurement at node 4 and pressure measurements at nodes* $\{2, 3, 4, 6\}$.

As in Example 6.5, the raw time-domain data is obtained from a MOC simulation

with added Gaussian noise. The frequency-domain data is obtained from the DFT of the time-domain data. For the MOC simulation, the system is excited into a steady-oscillatory transient state by a multi-sine flow perturbation at node 4 consisting of 983 equi-spaced frequencies from 0 to 15 Hz with amplitudes ranging from 0.01 to 0.1 L/s. The time-domain measurement errors are taken as independent zero mean Gaussian variates with standard deviations of 1 kPa for the pressure measurements and 0.32 L/s for the flow measurement.

As in Example 6.5, it is assumed that none of the pipeline parameter values are known, but that: the wavespeed is on the interval [900,1200] m/s; the friction factor is on the interval [0.015,0.04]; the diameters are known to within ±10 mm of their actual value; and the pipe lengths are known to within ±20 m of their actual value. Given the parameterisation of the TSF pipes from Example 6.1, the parameter space is 33 dimensional and is given by

$$\boldsymbol{\vartheta} = \{r_{o1}, \Gamma_{o1}, Z_{co1}\} \cup \cdots \cup \{r_{o11}, \Gamma_{o11}, Z_{co11}\}\,.$$

Corollary 6.3 was used as the framework to determine the parameter estimates, where the minimiser $\widehat{\boldsymbol{\vartheta}}$ was computed using PSO. This was achieved by implementing a strategy of intermittently updating the estimate $\widehat{\boldsymbol{\vartheta}}_k$ to lead onto the $(k+1)$-th minimisation iteration for computing $\widehat{\boldsymbol{\vartheta}}_{k+1}$. The results of 10 independent trials for each case are summarised in the box plots in Figure 6.5 and the statistics in Table 6.7.

Comparing the performance of case 1 to case 2 as displayed in Figure 6.5 and Table 6.7, it is clear that the correct hypothesis concerning the node 7 flow in case 1 on average yielded more accurate parameter estimates than the incorrect hypothesis for case 2. In Table 6.7 it is seen that the median error estimates for case 1 are all lower than case 2, this is particularly so for the estimates for r_o and Z_{co}. Most notably is that the error for the parameter estimate of r_o for pipe [10] was less than 5% for case 1 but in the order of $O\{10^3\}$% for case 2.

A more thorough consideration of Figure 6.5 shows that some stronger patterns exist within the data. The parameter estimates for case 1 are significantly better than those for case 2 for all pipes that are incident to node 7 (*i.e.* pipes [8], [9], and [10]). This pattern indicates two observations. Firstly, incorrect nodal categorisations have a more significant impact on the parameter estimates for links that are incident to nodes that have been incorrectly characterised. Secondly, the proposed EM algorithm has successfully provided accurate parameter estimates for a system with a node for which no information exists. This has not been achieved before within the literature, the the authors knowledge.

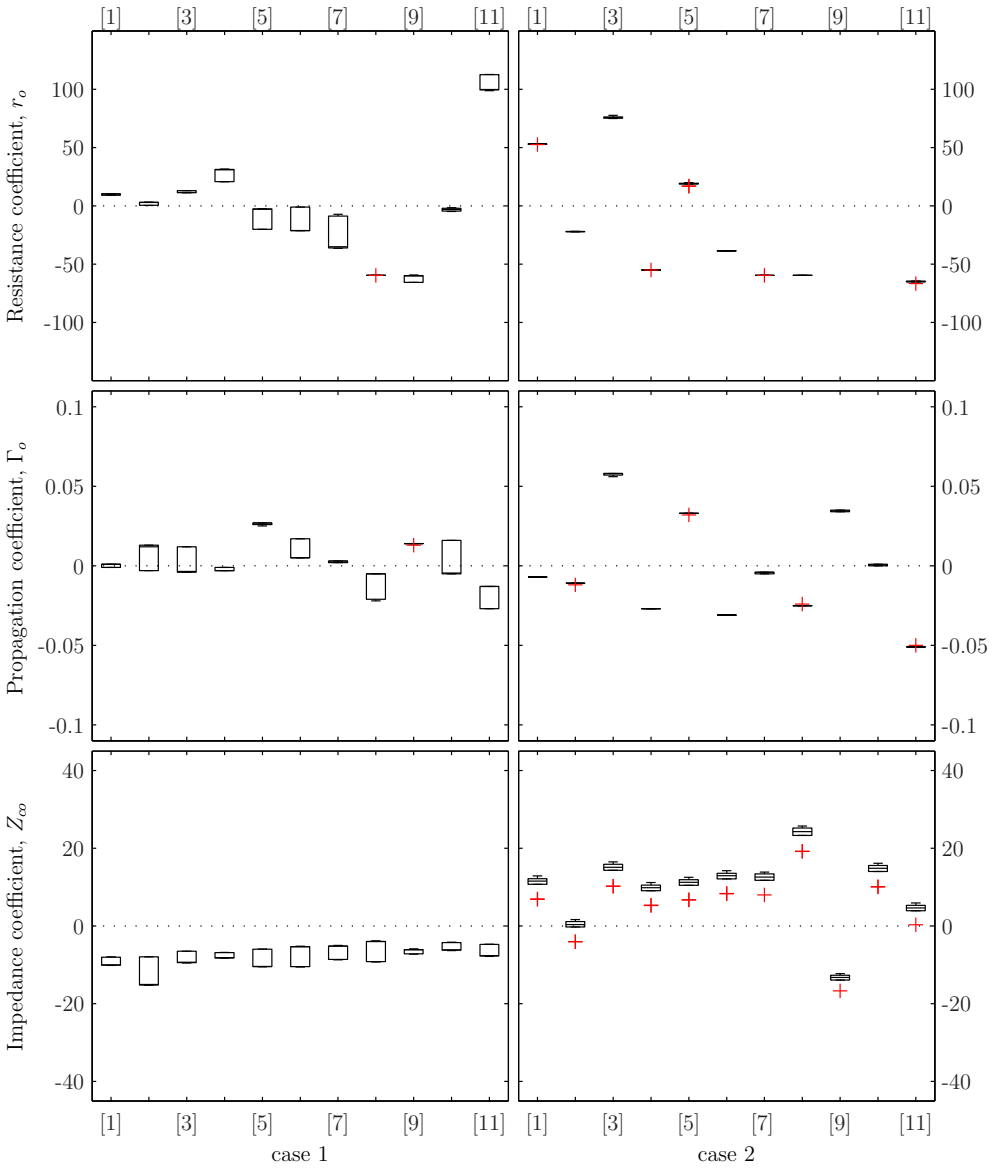

Figure 6.5: Box plots of the relative errors of the parameter estimates from Example 6.7. The figure rows are associated with particular parameters, and the figure columns with particular cases. Each box and whisker set is associated with a pipe. For each case, 10 independent trials were performed. The box plot of the error for the parameter estimate for r_o of pipes [9] and [10] in case 2 are not seen as they were $O\left\{10^3\right\}\%$. The + indicate outliers.

Considering the case 1 estimates for the different parameter types, a similar pattern is observed here as is observed for Example 6.5 in that the propagation coefficient Γ_o is estimated with a high accuracy, far higher than the resistance coefficient r_o and the impedance coefficient Z_{co}. As explained in Section 6.4.3, the hypothesised reason for this lies in the influence that the parameters have in the pattern of the system's frequency response. The parameter Γ_o is related to the period of a pipeline and hence the location of the harmonics in the frequency-domain, whereas r_o and

Table 6.7: Summary statistics of relative errors of pipe parameter estimates for Example 6.7. The parameter statistics for each pipe (median and the interquartile range , IQR) are based on 10 trials. The summary statistics (min, mean and max) are based on the parameter statistics from the 11 pipes.

Parameter	Statistic type		Relative error statistics (%)	
			case 1	case 2
r_o	median	*min*	*2.81*	*19.03*
		mean	30.68	$O\{10^2\}$
		max	*99.72*	$O\{10^3\}$
	IQR	*min*	*0.00*	*0.00*
		mean	9.30	0.96
		max	*27.30*	*5.33*
Γ_o	median	*min*	*0.0010*	*0.0005*
		mean	0.0050	0.0270
		max	*0.0270*	*0.0580*
	IQR	*min*	*0.0000*	*0.0000*
		mean	0.0120	0.0000
		max	*0.0210*	*0.0010*
Z_{co}	median	*min*	*4.04*	*0.36*
		mean	7.94	11.87
		max	*15.05*	*24.24*
	IQR	*min*	*1.10*	*1.25*
		mean	3.46	1.50
		max	*7.24*	*1.88*

Z_{co} are related to the energy dissipation within a pipeline and are hence related to the harmonic amplitudes in the frequency-domain. The error between the model predictions and the data is much more sensitive to mis-aligned harmonics than it is to well aligned harmonics with slightly different amplitudes. Therefore, by implication it is clear that the estimation process would be much more sensitive to Γ_o than r_o and Z_{co} resulting in much improved estimates for Γ_o in comparison to r_o and Z_{co}.

This reasoning also explains why the parameter estimates of Γ_o for case 2 were reasonably accurate despite the incorrect assumption about the flow at node 7. The presence of the branch from node 7 did not alter the locations of the networks harmonics that were associated with the periods of known 11 pipes. Hence the Γ_o parameters were still able to be estimated accurately. However, the presence of the branch did serve to dissipate energy within the system through the combined action of pipe friction and losses through the emitter. Therefore, as the branch changed the network's harmonic amplitudes, the estimates for r_o and Z_{co} were affected as

they are related to these amplitudes.

Example 6.8. *Consider the 13-pipe network, from Example 6.7 but this time modelled with TUF pipes. As in Example 6.7, the objective is to estimate the parameters of the known 11 pipes for the two cases of nodal categorisations are considered as outlined in Table 6.6.*

All details pertaining to system excitation, measurement error and parameter uncertainty for this example are taken from Example 6.8 with the addition that, as in Example 6.6, the relative roughnesses are known to be on the interval [0.0001, 0.01] and the steady-state velocities are known to be on the interval [0.1, 10] m/s. Given the parameterisation of the TUF pipes from Example 6.2, the parameter space is 55 dimensional and is given by $\boldsymbol{\vartheta} = \boldsymbol{\vartheta}_1 \cup \cdots \cup \boldsymbol{\vartheta}_{11}$ *where*

$$\boldsymbol{\vartheta}_i = \{c_i, D_i, l_i, C_{\epsilon,i}, C_{\mathbb{R}_e,i}\}\,.$$

where $C_{\epsilon,i} = \log_{10} \epsilon_i/D_i$ *and* $C_{\mathbb{R}_e,i} = \log_{10} \mathbb{R}_{ei}$.

Corollary 6.3 was used as the framework to determine the parameter estimates, where the minimiser $\widehat{\boldsymbol{\vartheta}}$ *was computed using PSO. This was achieved by implementing a strategy of intermittently updating the estimate* $\widehat{\boldsymbol{\vartheta}}_k$ *to lead onto the* $(k+1)$*-th minimisation iteration for computing* $\widehat{\boldsymbol{\vartheta}}_{k+1}$. *The results of 10 independent trials for each case are summarised in the box plots in Figure 6.6 and the statistics in Table 6.8.*

As demonstrated on Table 6.8, the case 1 EM algorithm with the correct assumption about node 7 on average yields more accurate parameter estimates for all parameters except the pipe diameters. Consistent with Example 6.7, is the pattern that the parameter estimates for case 1 are significantly better than those for case 2 for all pipes that are incident to node 7 (*i.e.* pipes [8], [9], and [10]). This reinforcing that (i) the correct categorisation of a node is particularly crucial for the accurate estimation of the parameters of all links incident to that node, and (ii) the proposed EM algorithm is effectively able to deal with nodes for which there is no information.

Drawing from both Examples 6.7 and 6.8, more detail can be given to these conclusions, in that it is mainly the parameters associated with energy dissipation that are effected by the incorrect categorisation of node 7. As case 2 does not allow for any flow to leave node 7, the energy that enters links [8] to [10] is considered as only being dissipated within the links. The implication of this is that the energy loss parameters (*e.g.* r_o for TSF pipes and $C_{\mathbb{R}_e}$ for TUF pipes), will be higher than the actual values. However, as case 1 correctly categorises node 7 and allows for energy loss through this node, the energy loss parameter estimates for the links connected to this node are more accurate.

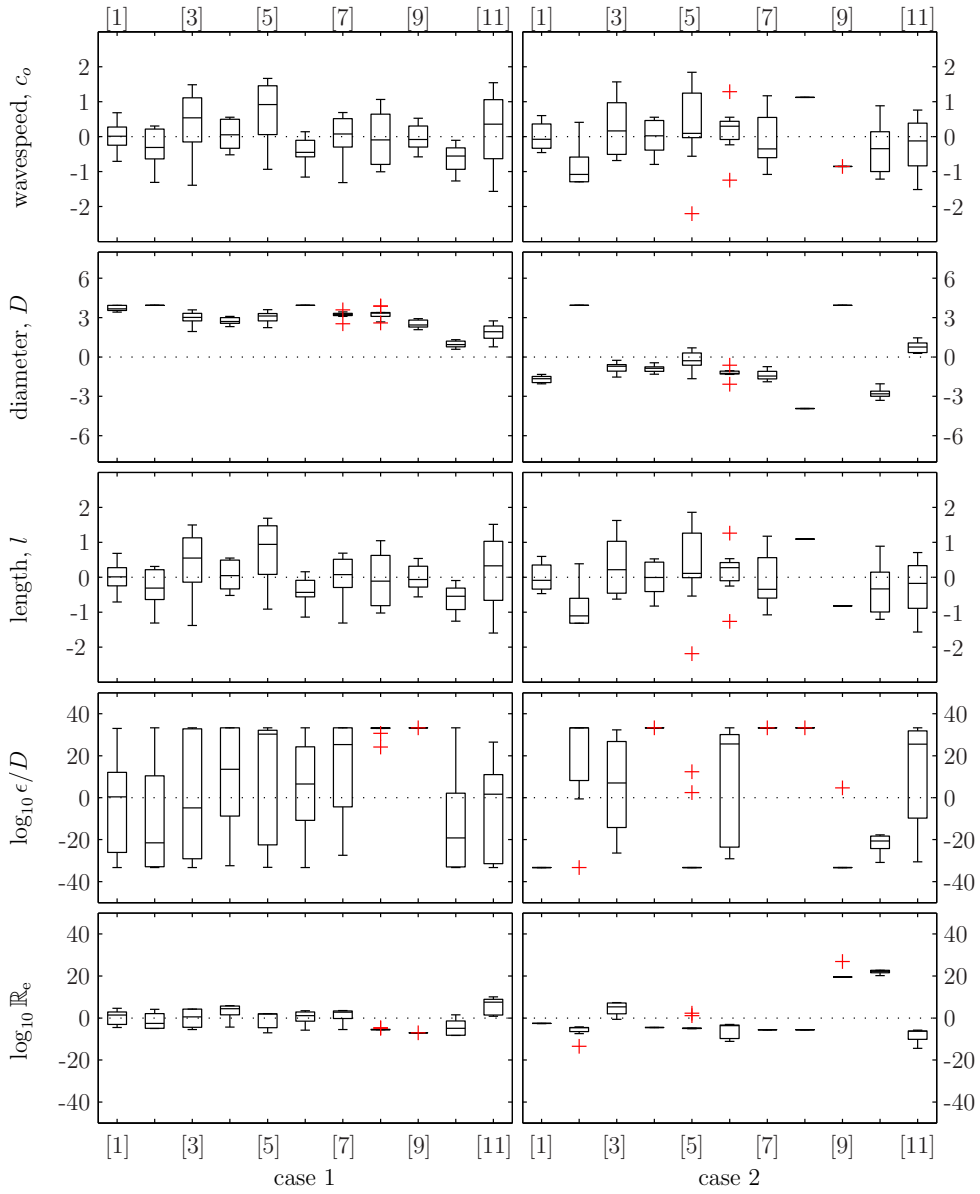

Figure 6.6: Box plots of the relative errors (%) of the parameter estimates from Example 6.8. The figure rows are associated with particular parameters, and the figure columns with particular cases. Each box and whisker set is associated with a pipe. For each case, 10 independent trials were performed. The + indicate outliers.

As with all the parameter estimation examples within this chapter, the variables related to the system harmonic locations (*i.e.* wavespeed and pipe length) were estimated with greater accuracy than the other parameters. This is particularly true for C_ϵ, where the apparent lack of sensitivity of the methodology to this parameter is attributed to the fact that ϵ/D only appears in the expression for the pipeline functions Γ and Z_c through the functions A^* and B^* *Vardy and Brown* [2007], thus potentially diminishing its influence.

In summary, despite the known difficulty in accurately estimating the parameters

Table 6.8: Summary statistics of relative errors of pipe parameter estimates for Example 6.8. The parameter statistics for each pipe (median and the interquartile range , IQR) are based on 10 trials. The summary statistics (min, mean and max) are based on the parameter statistics from the 11 pipes.

Parameter	Statistic type		Relative error statistics (%)	
			case 1	case 2
wavespeed, c_o	median	*min*	*0.012*	*0.021*
		mean	0.313	0.411
		max	*0.920*	*1.119*
	IQR	*min*	*0.473*	*0.000*
		mean	0.954	0.822
		max	*1.691*	*1.481*
diameter, D	median	*min*	*0.944*	*0.292*
		mean	2.933	1.963
		max	*3.937*	*3.937*
	IQR	*min*	*0.000*	*0.000*
		mean	0.392	0.377
		max	*0.933*	*0.922*
length, l	median	*min*	*0.011*	*0.007*
		mean	0.311	0.415
		max	*0.942*	*1.103*
	IQR	*min*	*0.474*	*0.000*
		mean	0.954	0.822
		max	*1.690*	*1.482*
$C_\epsilon = \log_{10}\left(\frac{\epsilon}{D}\right)$	median	*min*	*0.36*	*6.99*
		mean	17.26	28.37
		max	*33.33*	*33.33*
	IQR	*min*	*0.01*	*0.00*
		mean	35.51	15.21
		max	*61.89*	*53.61*
$C_{\mathbb{R}_e} = \log_{10} \mathbb{R}_e$	median	*min*	*0.499*	*2.586*
		mean	3.627	7.722
		max	*7.580*	*22.245*
	IQR	*min*	*0.000*	*0.000*
		mean	4.970	1.709
		max	*8.633*	*6.408*

associated with energy dissipation, Examples 6.7 and 6.7 demonstrate that the use of the EM methodology to correctly deal with unknown nodal variables leads to improved parameter estimates. The improvement of the estimates was observed to

generally hold for all pipes within the network. However, an important finding was that the improvement for the parameter estimates was significant for pipes within the vicinity of the nodal for which no information was known.

6.6 Conclusions

This chapter involved the study of the system identification of hydraulic networks based on transient fluid state measurements. From the extensive literature, it was seen that three classes of problems have been considered, namely (i) parameter estimation problems, including ITMs, (ii) detection problems, where the detection of system faults is the concern, and (iii) detection and estimation problems, which are a combination of the two problem types.

Based on a generalisation of the hydraulic network theory from Chapters 3 and 4, the problem types observed from the literature were given formal definitions (Section 6.3.2). These formal definitions led to the observation that the system dynamics, as defined by the admittance matrix expression from Chapters 3 and 4, defines the subspace within which the true system nodal state must lie, of which the measurements corrupted samples (due to noise) of the incomplete state (*i.e.* only selected nodal states are measured). This led to a necessary nodal partitioning categorising the networks nodes in terms of the information available from these nodes to inform the identification process. This nodal partitioning enabled a restructuring of the admittance matrix formulation of the system dynamics into subsystems involving the known, measured and unmeasured nodal state variables (Section 6.3.3). This restructuring, served as the basis of the development of two parameter estimation methodologies the MLE decoupled measurement system model, and the EM model.

The MLE decoupled measurement model (Section 6.4) involved the development of a dynamic system involving only the measured nodes decoupled from the influence of the unmeasured nodes. The development of this model first involved deriving the form of a decoupling filter. The filter was designed to essentially nullify the influence of the unmeasured nodes on the resulting system, thus creating a decoupled system. It was observed that the filter had the interpretation of being an oblique projection operator. The existence and stability of the filter where proved to be properties inherited from the passivity of the network elements. Posing the decoupled system in a constrained complex Gaussian framework, a MLE estimation process was derived for the network parameters using a combination of analytic and numeric techniques. A series of numerical experiments were performed using this method coupled with the evolutionary optimiser PSO. The experiments were performed on an 11-pipe network using TSF and TUF pipes, resulting in parameter estimation problems of 33

and 55 dimensions respectively. The results demonstrated the success of the method in yielding accurate parameter estimates, where the parameters associated with the pipeline delays (such as wavespeeds and lengths) were consistently estimated with a high accuracy and a greater variability was observed in the estimates for the parameters associated with inertial and resistive effects (such as impedance coefficients and pipeline roughnesses).

The EM methodology (Section 6.5) represents a philosophically different approach to dealing with the unmeasured nodal states. This method was formulated to deal with a broader class of measurement scenarios than the decoupled system method. Within this approach, the measured nodal states were treated as being only part of the complete data (the complete data consisting of both the measured and unmeasured nodal states). Based on posing the problem in a constrained complex Gaussian framework (different to the that used in the decoupled system above), the statistical EM algorithm was used to derive a scheme to estimate the network parameters based on only using the information from the measured nodal states. The computational benefits of using the EM approach over the MLE based on the marginal distribution of the known data were demonstrated. The feasibility of the method was demonstrated to be dependent on the passivity of the network. This proposed method is significant in that it is the only method within the literature that is able to deal with the case where there are nodes within the system for which no information exists. As with the decoupled system method, a series of numerical experiments were performed by coupling the EM method with a PSO algorithm. The experiments were designed to test the ability of the methodology to deal with unknown nodal states. This was undertaken by dealing with a 13-pipe network for which full topology of the network was considered unknown. That is, for the purposes of parameter identification the network was considered as an 11-pipe network with an unknown nodal flow. The results indicated that the use of the EM approach to correctly deal with the unknown nodal variables resulted in parameter estimates of a greater accuracy, particularly for the parameters of pipes incident to nodes for which no information exists.

Chapter 7

Conclusions

The majority of existing methods for modelling the Laplace-domain behaviour of a transient fluid line system have been limited to dealing only with certain classes of network types, namely, those that do not contain second-order loops. This thesis proposed a theoretical Laplace-domain framework that is able to deal with networks of an arbitrary structure and a broad class of hydraulic elements, termed the *network admittance matrix* method. Within this dissertation, this method was applied to two areas of fundamental interest within hydraulic network research, namely time-domain simulation, and system parameter identification.

7.1 Thesis Outcomes

A detailed breakdown of the main contributions of this dissertation are outlined in the introduction in Section 1.3. Below, the outcomes of each chapter are summarised.

Chapter 2 derived the basic equations of mass, momentum, and energy conservation governing the transient behaviour of one dimensional (1-D) fluid lines where a new and more comprehensive form of the 1-D energy equation including an energy term associated with the viscoelastic behaviour of the pipe wall was derived. A new framework for the for linear fluid lines was defined (termed the $\mathscr{L}$-class of fluid lines) and demonstrated to have a broad membership of most commonly accepted 1-D fluid line models. All pipeline models within this class were demonstrated as being passive systems. The Laplace-domain representation of the $\mathscr{L}$-class was derived, for which the causal organisations of the transfer matrix formulations (of which the admittance form is one instance) were demonstrated to also be passive.

Within Chapter 3, using graph theory concepts, a completely new formulation for arbitrarily configured networks comprised of pipes, junctions, demand nodes,

and reservoirs has been derived. The derived representation takes the form of an admittance matrix that maps from the nodal pressures to the nodal flow injections. The analytic nature of this representation was observed to enable significant qualitative insight into the structure of a network. The proposed admittance matrix served as the basis for an efficient model for computing the frequency response of a network of unknown nodal states subject to known nodal inputs. The passivity properties of the network's pipes was demonstrated to ensure the existence of this computable model. The theory was verified by a number of numerical examples.

The theory developed in Chapter 3 was extended in Chapter 4 to deal with networks comprised of a broader class of hydraulic elements, namely compound nodes whose dynamic structure yields an admittance type representation that can be expressed as a linear time-invariant system. An extensive framework for deriving the admittance matrix form for compound nodes, as well as conditions for the existence of this form, was presented. Based on this special admittance form, an analytic representation of the network admittance matrix was derived. A computable input/output (I/O) model mapping from the known nodal boundary conditions to the unknown nodal states was derived. The existence of this map was proven to exist and be dependent on the strict passivity of the networks link and compound node dynamics. The theory was verified by a number of numerical examples.

Chapter 5 presented a methodology for the development of a time-domain hydraulic network simulator based on coupling a numerical inverse Laplace transform (NILT) with the theory from Chapters 3 and 4. The approach is entirely novel in that it couples the Laplace-domain I/O model in a computationally efficient way with the Fourier-Crump NILT from *Abate and Whitt* [1995]. The parameters of the NILT were studied in detail for simple test functions and robust parameter heuristics were developed. Extensive numerical tests were performed comparing the NILT method to the method of characteristics (MOC) and it was observed that, despite the approximate linear nature of the Laplace-domain model, the NILT provided highly accurate approximations for all networks considered, with the time-scale of the accuracy of the approximation being dependent on the type of input signal used to excite the network. For large networks, NILT was found to be extremely computationally efficient with respect to the MOC. In addition to the computational efficiency, the NILT possesses the desirable property that it correctly captures wave propagation delays without the need for fine computational grids. As such, the NILT represents an ideal approach for modelling networks involving pipes with greatly varying wavespeeds.

Chapter 6 involved the study of the system identification of hydraulic networks based on transient fluid state measurements. Based on a generalisation of the general

hydraulic network theory from Chapters 3 and 4, a nodal partitioning framework was developed to deal with the different types of information available from the network nodes. This nodal partitioning enabled a restructuring of the admittance matrix formulation of the system dynamics into subsystems involving the known, measured and unmeasured nodal state variables. Based on this restructuring, two parameter estimation methodologies were developed. The first method, the decoupled measurement mode, involved the development of a dynamic system involving only the measured nodes decoupled from the influence of the unmeasured nodes. The development of this model first involved deriving the form of a decoupling filter. The existence and stability of the filter where proved to be properties inherited from the passivity of the network elements. Posing the decoupled system in a constrained complex Gaussian framework, a maximum likelihood estimation (MLE) estimation process was derived for the network parameters using partly analytic techniques.

The second methodology from Chapter 6, the expectation-maximisation (EM) method was formulated to deal with a broader class of measurement scenarios than the decoupled system method. Within this approach, the measured nodal states were treated as being only part of the complete data (the complete data consisting of both the measured and unmeasured nodal states). Based on posing the problem in a constrained complex Gaussian framework (different to that used in the decoupled system above), the statistical EM algorithm was used to derive a scheme to estimate the network parameters based on only using the information from the measured nodal states. The computational benefits of using the EM approach over the MLE based on the marginal of the known data were demonstrated. The feasibility of the method was demonstrated to be dependent on the passivity of the network. The utility of both methods from Chapter 6 was demonstrated using a number of numerical examples.

7.2 Scope for Future Work

A general network structure encompassing both network types from Chapters 3 and 4 is presented in Appendix B as a $\mathscr{M}$-network. Within this Appendix, the analogies between $\mathscr{M}$-networks and standard Kirchoff networks, such as those encountered in electrical circuits, are explored, the main difference being associated with the distributed parameter nature of the $\mathscr{M}$-networks elements. That is their transfer functions are not rational, like those encountered in Kirchoff networks, and the elements carry travelling wave forms. Continued research aimed at a deeper understanding of the analogies between these two network types could serve to deepen the theory for fluid networks given the vast theory for Kirchoff networks as driven

by the electrical circuits applications [*Desoer and Kuh*, 1969; *Wohlers*, 1969; *Chen*, 1983].

Despite the wide success of the proposed linear method in approximating nonlinear systems as demonstrated throughout this thesis, the Achilles heal of the proposed method is its inability to deal with nonlinearities. This limitation occurs at the basic level of the proposed method, as the Laplace transform is typically only applied to linear time-invariant systems. However, a potential avenue for dealing with nonlinearities within a Laplace-transform context is through the use of the Volterra series [*Rugh*, 1981]. The Volterra series is based on the theory that certain classes of nonlinearities can be described in the transformed domain by an infinite series of convolutions, thus transfer functions for nonlinear systems are actually convolution operators. Despite the complexity of the Volterra series representation, future research may demonstrate its utility for fluid line applications.

To increase the computational efficiency of the NILT process in other applications, many authors use sequence accelerators [*Crump*, 1976; *Abate and Whitt*, 1992]. Although, for reasons discussed in Section 5.4, the application here does not directly lend itself to standard sequence accelerators, there may be some scope for the use of more advanced accelerators.

Networks containing highly nonlinear elements (such as pressure relief valves) cannot be modelled accurately by the NILT. Future research could focus on developing a methodology generalising the approach outlined by *Washio et al.* [1979] in treating lumped nonlinear elements in series pipelines. This approach consists of a novel treatment of the lumped nonlinear element as an external boundary condition, and is well suited to be extended for incorporation with the proposed NILT method for generalised networks.

As demonstrated by the vast literature on the topic, there is a huge scope for further work within the field of identification of hydraulic systems, both theoretical and applied. This thesis deals exclusively with ideal numerical networks as it is mainly concerned with the theoretical questions of how to best use the information available to inform the estimation process. The proposed methods provide an excellent tool for the analysis of identifiability issues concerning hydraulic networks, and also the basis for the development of methods to be used in the real world.

The proposed methods provide ideal tools for the further, and deeper, analysis of identifiability issues of pipeline networks. From the examples presented, observations were made concerning the ease at which some parameters could be identified, and the difficulty associated with others. Future research could focus on formalising this work by a more detailed analysis aimed at understanding the correlation structures

between the parameters (*i.e. Rodriguez-Fernandez et al.* [2007]). This could lead to a better, more identifiable, parameterisation of the network.

The broad issue of sensor placement was not addressed within this work. However, the analytic nature of the network structure could facilitate in the analysis of the sensitivity of nodal states to parameter variations (as in *Nikolova et al.* [2004] with electrical circuits). Future research could investigate the interpretation and utility of Laplace-domain nodal sensitivity analysis for fluid line networks.

The fundamental limitation of all hydraulic network identification methods has to do with the model miss-match that exists between the idealised models and the observed behaviour of real pipelines within the field. Even for the most advanced turbulent-unsteady-friction (TUF) and viscoelastic (VE) pipeline models, much higher dissipation and dispersion rates are measured within some field pipelines [*Stephens*, 2008]. This issue of robustness to model miss-match is complicated and beyond the scope of this thesis, however, model miss-match must be directly addressed for the successful application of any identification methods to complex field pipeline networks.